

WEAR
PROCESSES IN
MANUFACTURING

*SHYAM BAHADUR AND
JOHN H. MAGEE, EDITORS*

STP 1362



STP 1362

***Wear Processes
in Manufacturing***

Shyam Bahadur and John Magee, editors

ASTM Stock #: STP1362



ASTM
100 Barr Harbor Drive
West Conshohocken, PA 19428-2959

Library of Congress Cataloging-in-Publication Data

Wear processes in manufacturing / Shyam Bahadur and John Magee, editors.

p. cm. -- (STP: 1362)

"ASTM Stock Number: STP1362 ."

Papers presented at a symposium held in Atlanta, GA, May 6, 1998.

Includes bibliographical references and index.

ISBN 0-8031-2603-4

1. Mechanical wear--Congresses. 2. Machining--Congresses. I.

Bahadur, Shyam, 1954- II. Magee, John, 1955 Sept 22- III. American Society for Testing and Materials.

TA418.4 .W42 1999

621.9--ddc21

99-11819

CIP

Copyright © 1998 AMERICAN SOCIETY FOR TESTING AND MATERIALS, West Conshohocken, PA. All rights reserved. This material may not be reproduced or copied, in whole or in part, in any printed, mechanical, electronic, film, or other distribution and storage media; without the written consent of the publisher.

Photocopy Rights

Authorization to photocopy items for internal, personal, or educational classroom use, or the internal, personal, or educational classroom use of specific clients, is granted by the American Society for Testing and Materials (ASTM) provided that the appropriate fee is paid to the Copyright Clearance Center, 222 Rosewood Drive, Danvers, MA 01923; Tel: 508-750-8400; online: <http://www.copyright.com/>.

Peer Review Policy

Each paper published in this volume was evaluated by two peer reviewers and at least one editor. The authors addressed all of the reviewers' comments to the satisfaction of both the technical editor(s) and the ASTM Committee on Publications.

To make technical information available as quickly as possible, the peer-reviewed papers in this publication were prepared "camera-ready" as submitted by the authors.

The quality of the papers in this publication reflects not only the obvious efforts of the authors and the technical editor(s), but also the work of the peer reviewers. In keeping with long standing publication practices, ASTM maintains the anonymity of the peer reviewers. The ASTM Committee on Publications acknowledges with appreciation their dedication and contribution of time and effort on behalf of ASTM.

Foreword

This publication, *Wear Processes in Manufacturing*, contains papers presented at the symposium of the same name held in Atlanta, Georgia on May 6, 1998. This symposium was also held in conjunction with the May 7–8 standards development meetings of Committee G-2 on Wear and Erosion, the symposium sponsor. The symposium was chaired by Professor Shyam Bahadur, Iowa State University; John H. Magee, Carpenter Technology, served as co-chairman. They also both served as STP editors of this publication.

Contents

Overview

vii

ABRASION IN CERAMIC GRINDING

- Use of a Two-Body Belt Abrasion Test to Measure the Grindability of Advanced Ceramic Materials—PETER J. BLAU AND ELMER S. ZANORIA** 3

- Observations on the Grinding of Alumina with Variations in Belt Speed, Load, Sample Rotation, and Grinding Fluids—CHRISTIAN J. SCHWARTZ AND SHYAM BAHADUR** 13

WEAR OF CUTTING TOOLS

- Wear Mechanisms of Milling Inserts: Dry and Wet Cutting—JIE GU, SIMON C. TUNG, AND GARY C. BARBER** 31

- Reducing Tool Wear When Machining Austenitic Stainless Steels—JOHN H. MAGEE AND TED KOSA** 48

- Machining Conditions and the Wear of TiC-Coated Carbide Tools—CHRISTINA Y. H. LIM, SEH-CHUN LIM, AND KIM-SENG LEE** 57

- Turning of High Strength Steel Alloy with PVD and CVD-Coated Inserts—ASHRAF JAWAID AND KABIRU A. OLAJIRE** 71

- Evaluation of Coating and Materials for Rotating Slitter Knives—MANFRED SCHLATTER** 86

- Tribology in Secondary Wood Machining—PAK L. KO, HOWARD M. HAWTHORNE, AND JASMIN ANDIAPPAN** 101

FRICITION IN VIBRATORY CONVEYOR

- Chaotic Behavior on In-Phase Vibratory Conveyors—JERRY Z. RASKI** 121

EROSION IN MANUFACTURING

Erosion and Corrosion Mechanisms in Pneumatic Conveying of Direct Reduced Iron Pellets—ALBERTO J. PÉREZ-UNZUETA, DORA MARTÍNEZ, MARCO A. FLORES, R. ARROYAVE, A. VELASCO, AND R. VIRAMONTES

137

Characterization of the Wear Processes due to the Material Erosion Mechanisms—LUCIEN H. CHINCHOLLE

150

Overview

The importance of tribological phenomena in engineering has long been recognized. The evidence for this lies in the extensive studies on tool wear performed over many decades. The same is the case with studies related to the friction and lubrication in deformation processing as evidenced by a number of conferences and related publications. In spite of this, the interaction between the tribologists and manufacturing researchers has not been great. The objective of this symposium was to provide a forum for these researchers for a mutually beneficial interaction.

There are many manufacturing processes in which wear and friction play dominant roles. In the present era of increased productivity, processing at high speeds contributes to the rapid wear of tools. The current emphasis on quality also demands tighter tolerances, which requires, among other things, the use of tools with less wear. In forming processes the wear of tools and dies occurs because of the stresses needed to deform material and the difficulty of lubrication in high contact stress situations. In processes performed at high temperatures, lubrication is a serious problem because of the lack of suitable lubricants and the difficulty of maintaining a lubricant film between the contacting surfaces. The absence of good lubrication results in adverse consequences such as rapid tool wear, surface damage such as galling, and increased power requirement. The recognition of tool wear as the limiting factor for high speed machining and as the factor contributing to the impairment of surface integrity has caused tool companies to invest heavily in the development of wear-resistant tools for machining. There are processes such as grinding which use two-body abrasion mechanism for material removal. Similarly, superfinishing operations use three-body abrasion for achieving the desired surface finish. Finally, minimizing erosive wear damage on critical components is often the key to a successful manufacturing process.

The collection of papers published in this volume may be grouped into the following categories. These categories are: abrasion in ceramic grinding, wear of cutting tools, friction in vibratory conveyers, and erosion in manufacturing. A brief summary of the papers in each category is provided below.

Abrasion in Ceramic Grinding

There were two papers presented in this category. One of the papers presented the two-body belt abrasion test for assessing quantitatively the grindability of new ceramic compositions. The test establishes a belt grindability index as the measure of grinding ease reported using the units of wear factor. A project funded by the US Department of Energy demonstrated that this test provided repeatable results which correlated well with the actual grinding behavior. The test is similar to one of the several abrasion testing geometries mentioned in the ASTM Standard G-132.

Using a similar test setup, another paper investigated the effect of variables such as belt speed, load, cutting fluid, and specimen rotation on the material removal rates in grinding. The cutting fluids investigated were mineral oil, water-glycol mixture, and biodegradable soybean oil. This paper presented the results of surface damage in grinding under different conditions and emphasized the detrimental effect of temperature rise in grinding.

Wear of Cutting Tools

In this category, a maximum number of papers were presented. One of the papers presented the tool life study for face milling inserts under various cutting conditions, with and without coolant. The material used for machining was 4140 steel and the milling inserts were C5 grade. One of the main conclusions of the study was that coolant does not always enhance the tool life. Optical and scanning electron micrographs showing the tool wear were presented and the wear mechanisms were identified.

Another paper presented tool wear results from the machining of austenitic 303 and 304 stainless steels with varying carbon, nitrogen, and copper contents. It was demonstrated that tool life increased by increasing the copper and nickel contents and by decreasing the carbon and nitrogen contents. The results of this study are important from a practical standpoint because machining of austenitic stainless steels poses special problems particularly in regards to early tool failure.

There are three papers in this section that deal with the effect of coatings and/or other treatments on cutting tools. One of these investigated the wear behavior of cemented carbide and TiC-coated cemented carbide tools in turning operations under different cutting conditions. The data from these tests together with the data from literature is used in constructing the wear maps. The latter are drawn with cutting speed and feed rate as the machining parameters. This kind of information is useful in selecting the cutting conditions for extended tool life. Another paper investigated the machining of a high strength steel alloy with grooved inserts, coated with plasma and chemical vapor deposition (PVD and CVD) processes, for different combinations of cutting speeds and feeds. Apart from the generation of machining data, the focus in this study was on the wear mechanisms, failure modes and tool lives of the inserts. The authors found that surface finish improved with a mixed carbide grade of insert (WC + TaC), and multilayered CVD coating produced a better surface finish. The third paper dealt with the investigation of coatings, substrates and substrate treatments that would increase the life of cemented carbide slitter knives used to slit magnetic media from wide rolls into narrow product form. The treatments tried in this work were ion implantation, implantation of boron, titanium nitride PVD and CVD coatings, and diamond-like carbon (DLC) coating. It was concluded that the coatings failed because of inadequate adhesion between the coating and the substrate. The plasma enhanced CVD titanium nitride coating gave good results but it was not considered economical.

A paper in this section deals with the tribology of wood machining such as tool wear, tool-wood frictional interactions, and wood surface characterization. The studies included the identification of friction and wear mechanisms and modeling, wear performance of surface-engineered tool materials, friction-induced vibration and cutting efficiency, and the influence of wear and friction on the finished surface. Various wood species were investigated from soft pine to hard maple and the results revealed significant variations in the coefficient of friction, an important parameter when modeling chip formation.

Friction in Vibratory Conveyor

In this paper, the problem of feeding connectors using vibratory conveyors to machines that assemble input/output (I/O) pins to the metallized ceramic substrate, as used in the computer industry, was studied. The motion of a single I/O pin on an in-phase, linearly oscillating conveyor using the classical model of friction was modeled and the results were compared with those from the experimental observations. The implications of these theoretical and experimental results are discussed in terms of the practical application of in-phase vibratory conveyors in manufacturing.

Erosion in Manufacturing

One of the papers studied the wear of pipe materials as used in a pilot plant which transports DRI (Direct-Reduced-Iron) pellets at high temperatures in the manufacture of steel. Included in this study were also the new candidate materials for pipes. The materials tested were 304 stainless steel, high chromium white castings, hard coatings based on high chromium-high carbon alloys, cobalt alloys and aluminum oxide. The samples from both the pilot plant and laboratory showed that erosion was the dominant mechanism of wear. The next paper introduced an electrochemical technique to assess erosion in aqueous and other systems that involve an electrolyte as the erosion fluid. The potential and the usefulness of this technique to measure slurry erosion, fretting corrosion and cavitation were also discussed.

Shyam Bahadur
Symposium Chairman and STP Editor
Iowa State University
Ames, IA 50011

John H. Magee
Symposium Co-Chairman and STP Editor
Carpenter Technology Cp.
Reading, PA 19612-4662

Abrasion in Ceramic Grinding

USE OF A TWO-BODY BELT ABRASION TEST TO MEASURE THE GRINDABILITY OF ADVANCED CERAMIC MATERIALS

REFERENCE: Blau, P.J. and Zanoria, E.S., "Use of a Two-Body Abrasion Test to Measure the Grindability of Advanced Ceramic Materials," *Wear Processes in Manufacturing, ASTM STP 1362*, S. Bahadur, J. Magee Eds., American Society for Testing and Materials, 1999.

ABSTRACT: The same properties that make engineering materials attractive for use on severe thermal and mechanical environments (e.g., high hardness, high temperature strength, high fracture toughness) generally tend to make those materials difficult to grind and finish. In the mid-1990's, a belt abrasion test was developed under subcontract to Oak Ridge National Laboratory to help to assess the grindability of structural ceramic materials. The procedure involves applying a 10 N normal force to the end face of a 3 x 4 mm cross-section test bar for 30 seconds which is rubbed against a wet, 220 grit diamond belt moving at 10 m/s. By measuring the change in the bar length after at least six 30-second tests, a belt grindability index is computed and expressed using the same units as a traditional wear factor (i.e., mm³/N-m). The test has shown an excellent capability to discriminate not only between ceramics of different basic compositions, e.g. Al₂O₃, SiC, and Si₃N₄, but also between different lots of the same basic ceramic. Test-to-test variability decreases if the belt is worn in on the material of interest. The surface roughness of the abraded ends of the test specimens does not correlate directly with the belt grindability index, but instead reflects another attribute of grindability; namely, the ability of a material to abrade smoothly without leaving excessive rough and pitted areas.

KEYWORDS: abrasion, abrasive wear, abrasive belts, ceramics, grinding, wear of ceramics

Structural materials, such as superalloys, intermetallic alloys and engineering ceramics, have been developed to achieve high hardness, high temperature strength, and high fracture toughness. However, these strong materials also tend to be difficult to grind and finish. In the 1990's, the U.S. Department of Energy supported a series of projects to help reduce the cost of machining advanced ceramics. One of these projects resulted in the development of a two-body belt abrasion test for quickly and quantitatively assessing the grindability of new ceramic compositions. Several publications describe this test method and the rationale behind its development [1-4]. This test was developed with a focus on simplicity, repeatability, ease of operator training, acquisition of rapid results, reduction of subjectivity, and the correlation of results with grinding behavior. It is similar to one

¹Senior research engineer, Metals and Ceramics Division, Oak Ridge National Laboratory, P.O. Box 2008, Oak Ridge, TN 37831-6063.

²Engineer, Caterpillar Inc., P.O. Box 1895, Peoria, IL 61656-1895.

of the several abrasion testing geometries mentioned in ASTM Standard Test Method for Pin Abrasion Testing (G-132-95) except that the path of the specimen repeats over the same portion of the belt instead of being constantly exposed to new abrasive. The belt abrasion test and its ability to distinguish between ceramic materials will be described in this paper.

Grindability means different things to different people. To some, it implies the relative ease by which stock can be removed from the surface of a particular workpiece material. To others, it refers to the ability of a material to be ground at high rates of material removal without adversely affecting the surface quality or ultimate function of the part. In the present work we will use the former definition. More formally stated:

grindability, n. - the relative ease by which material can be mechanically removed from the surface of a body by a relatively-moving, abrasive counterface applied to it under controlled conditions.

Grindability can be qualitatively assessed (e.g., "material A grinds more easily than material B"), or quantitatively assessed using a numerical value of some kind. Quantitative assessments require measurement of material removal under well-specified abrasive machining conditions.

There are many kinds of grinding (surface grinding, cylindrical grinding, belt grinding, creep-feed grinding, etc.), so it is entirely possible that any particular measure of a material's grindability may not correlate in the same way to all the different grinding processes. Thus, once a measure of grindability has been established, the user of the test must establish its correlation with the specific grinding process or processes of interest. Obviously, the closer the grindability test conditions approach of the grinding process of interest, the greater the likelihood that the grindability test results will be directly applicable. In the present case, we worked to develop a repeatable and quantitative grindability test which could be quickly, easily, and cost-effectively applied to small specimens of material with unknown grinding characteristics so as to provide initial guidance for selecting grinding parameters for that material. Structural ceramic materials are particularly difficult and costly to grind, and therefore were used as the focus of this work.

Test Method

Early in the development of the grindability concept, it was decided to use a belt abrasion test since it offered a cost-effective means to remove material compared with using a grinding wheel-based method. Grinding wheel-based methods have uncertainties arising from wheel-to-wheel variations as well as in the repeatability of dressing and truing operations. Grinding wheels can also develop lobes with prolonged use, and this introduces additional variations. Belts can be manufactured with extremely uniform dispersions of grits, and their low cost, relative to grinding wheels, means that a new belt can be used for each test series. This was particularly important in the case of ceramic grinding where diamond is usually the preferred abrasive.

The test method used a 220 grit diamond abrasive belt. This particular type of abrasive belt was seamless, which eliminated specimen bouncing over the typical end-to-end belt joint. The test specimen's cross-sectional dimensions were those of the "Type B specimen" in the ASTM Standard Test Method for Flexural Strength of Advanced Ceramics at Ambient Temperature (C-1161). This allowed the same lot of ceramic specimens to be tested for both flexure strength and grindability. Even broken flexure specimens provided sufficient material for the grindability testing since only the end face, not the center section, can be used.

The basic test geometry is shown in Fig. 1, and an exterior view of the testing machine is shown in Fig. 2. The 3.0 x 4.0 mm face of the test specimen was loaded against the belt (4.0 mm face parallel to the belt motion) under an 11.0 N normal force, calibrated using a compression load cell under the specimen tip with the belt motor turned

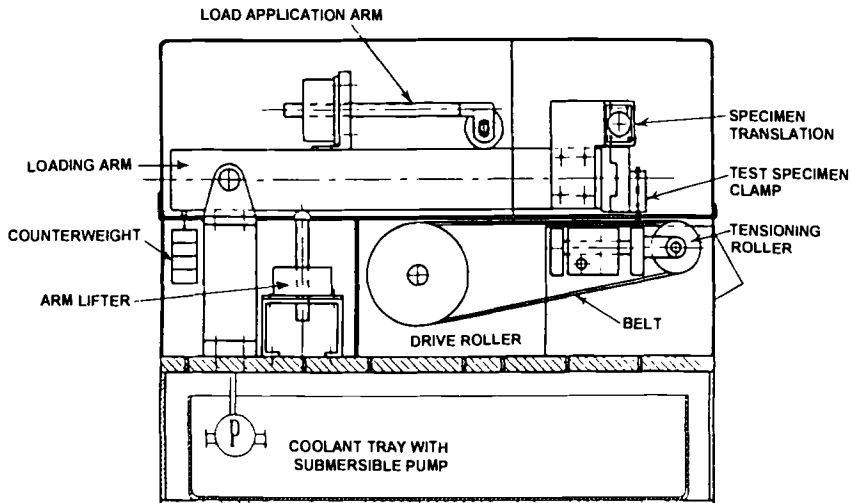


FIG. 1 — Diagram of the two-body abrasive wear testing machine used to assess the grindability of rectangular ceramic test bars.

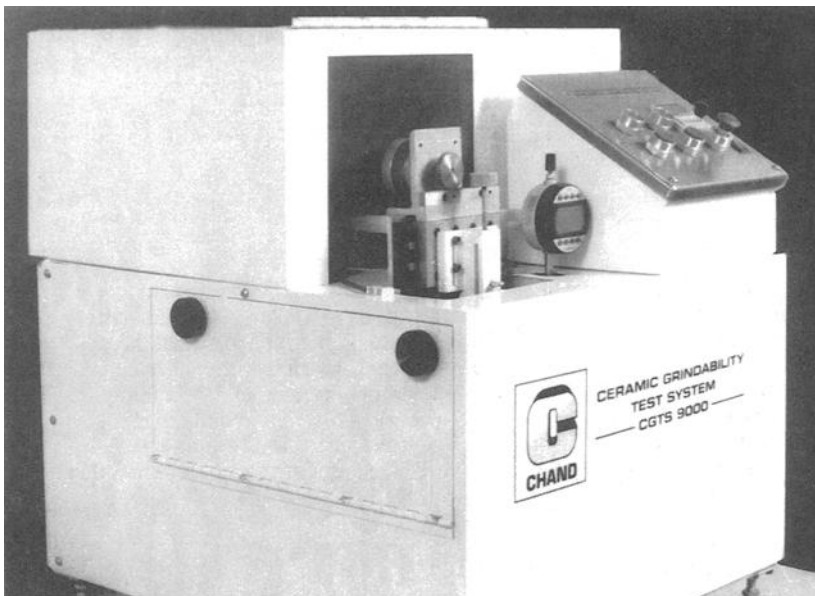


FIG. 2 — Grindability testing machine used in this investigation. Cycle controls are located on the panel at the upper right. The specimen is mounted in the holder near the center of the photograph and to the left of the dial of the electronic displacement gauge. A motor above the specimen holder moves the specimen to a new position after each test.

off. The belt speed was then adjusted to be 10.0 +/- 0.2 m/s. Test time is typically 30 seconds and is controlled automatically such that the specimen is lowered and raised at the proper time by a motorized mechanism. For highly-grindable materials, like alumina, the test time was reduced to only 5 seconds. A water-based commercial coolant, supplied by Chand Kare Technical Ceramics, Worcester, Massachusetts, was sprayed on the belt just ahead of the specimen using a deflector plate to spread the flow across the width of the belt.

Grindability is assessed through a quantity which we shall call the Belt Grindability Index (BGI). Units are volume loss of material per unit normal force per unit distance slid. For a 3.0 x 4.0 mm cross section specimen sliding at 10.0 m/s, the single test $BGI_{n=1}$ ($\text{mm}^3/\text{N}\cdot\text{m}$) is computed as follows:

$$BGI_{n=1} = 1.2 (\Delta l / P t) \quad (1)$$

where Δl is the specimen length change in mm, P is the normal force in N, and t is the test time in seconds. To account for any possible belt variabilities, and to improve repeatability of the results, several additional elements were added to the test procedure. At least six, and as many as eight, tests were performed per specimen, indexing the contact several millimeters to the side between subsequent tests. Thus, the reported BGI is as follows:

$$BGI = 1.2 (\Delta L / N P t) \quad (2)$$

where ΔL is the total length change after N tests, each one having a duration of t seconds.

It was found that the repeatability of the tests could be enhanced if the belt were first worn-in by running one complete test series across a new belt, and then repeating the series on the same locations a second and third time. The first set of readings on the new belt were therefore discarded, and the latter were reported here.

Surface roughness data used to evaluate the effects of grinding on the test specimen surface were obtained using a mechanical stylus profiling instrument (Rank Taylor Hobson, Talysurf 10, Leicester, UK) with a 2.5 μm tip radius.

Materials

One alumina ceramic and four silicon nitride ceramics were used in this study. Typical mechanical properties of these test materials are given in Table 1. As the results will show, the alumina represented a ceramic with relatively high grindability and the silicon nitride materials represented ceramics with relatively low grindability. We chose several grades of silicon nitride because we were particularly interested in determining whether the test was sensitive enough to discriminate between different members of the same ceramic family, and because silicon nitride is of current interest for rolling element bearings as well as for roller followers, valves, valve guides, fuel injector parts, and other components in heavy-duty diesel engines.

Results and Discussion

Considerations Related to the Test Method Itself — The ability of an abrasive wear test to discriminate between the wear performance of different materials is reflected by the repeatability of results obtained on the same specimen material. In order to account for possible variations in the characteristics of a given abrasive belt from one location to another, normal procedures call for using the total change in specimen length divided by the total sliding distance after at least six or more, side-by-side 30-second runs. However, in

one case we looked instead at the individual run-to-run variations across the belt. Data for seven sequential 30-second test increments (using an SN-1 silicon nitride test specimen) are shown in Fig. 3. The 4.8% coefficient of variation is excellent for a wear test.

TABLE 1—Typical mechanical properties of the test materials*

	AD-995	SN-1	GS-44	NT-154	NT-451	NT-551
Major constituents	Al ₂ O ₃	Si ₃ N ₄	Si ₃ N ₄	Si-Al-O-N	Si ₃ N ₄	Si ₃ N ₄
Density (Mg/m ³)	3.9	3.21	3.2	—	3.2	3.25
Modulus of elasticity (GPa)	372.-386.	—	310.	300.-310.	285.-295.	—
Mean 4-point flexure strength	380.	900.	1050.	750-907.	888.	994.
Fracture toughness (MPa√m)	3.0-4.5	7.0	8.2-8.6	4.7-5.0	5.0	5.5-6.0
Vickers indentation hardness at 98 N load (GPa)	14.7-15.0	14.0	14.6-15.8	—	19.8	—

* Sources of data:

Database on Properties of Ceramics, ORNL Report ORNL/M-3155, Oak Ridge National Laboratory (some NT-451 data)

Life Prediction Methodology for Ceramic Components of Advanced Heat Engines (Vol. 1), ORNL Report ORNL/Sub/89-SC674/1/V1 (NT-154 data)

A. Wereszczak, Oak Ridge National Lab., personal communication (NT-551 data)

Coors Ceramics Data Sheet on Ceramic Properties, Golden CO (AD 995 data).

Japan Fine Ceramics Center, Nagoya, SN-1 properties brochure (SN-1 data)

Allied Signal Ceramic Components Division, Torrance CA (some GS-44 data)

K. Breder, Oak Ridge National Lab., personal communication (some GS-44 data)

We also conducted an experiment in which the same specimen of SN-1 was used three times on the same belt. Results are shown in Table 2. While pre-conditioning the belt using multiple runs on the same position was shown to increase the repeatability of the measurement, it is not clear that one could consistently achieve the same degree of belt pre-conditioning with different specimen materials. Furthermore, the average BGI rises by about 15% with the first re-use. Belt loading with grinding swarf and the effects of the test material's hardness on the blunting of fresh cutting points would add other factors to what the test is actually measuring. In other words, a hard material of low abrasive wear rate would affect the belt pre-conditioning differently than a soft material. Therefore, adoption of pre-conditioning procedures might improve repeatability for a given material but it might also alter the relative grindability number from one material to another by including factors other than grindability alone. These issues remain for further study and test method refinement.

Test method ASTM G-132-95 recommends that the test specimen be moved continually across fresh, unused abrasive material during the tests. In contrast to this, the present method does not traverse the specimen until the test increment is completed (typically, 30 s; equivalent to 394 passes). Since actual production operations like surface

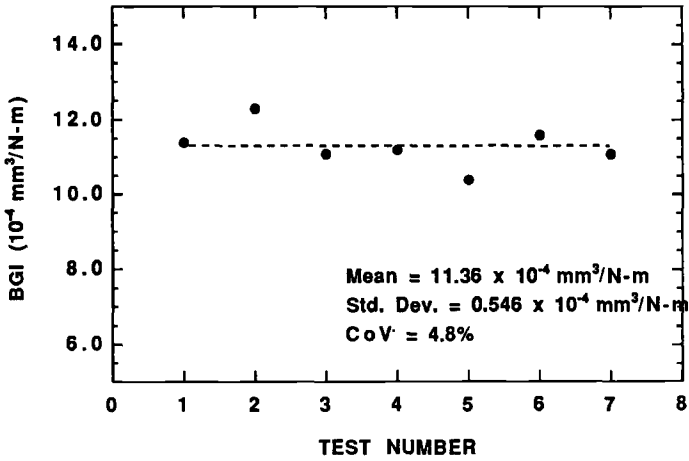


FIG. 3 — *BGI values calculated for seven sequential runs conducted several millimeters apart on the same belt . There appears to be no systematic variation in BGI with lateral position across the belt.*

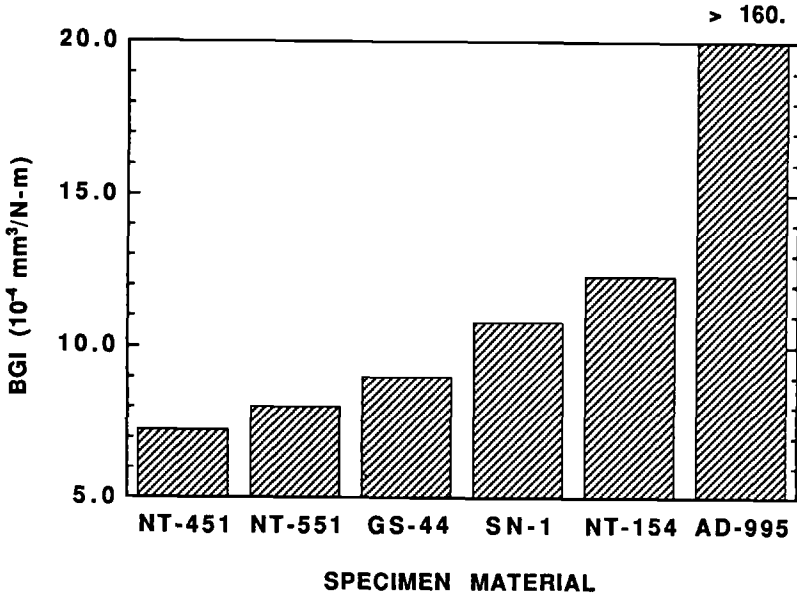


FIG. 4 — *BGI values for five silicon nitride materials and alumina.*

grinding use repeated passes with the same grinding medium (e.g., a grinding wheel), the use of repeated passes of the belt was felt to be justified in relating the two-body abrasion of surfaces to their relative grindabilities.

TABLE 2—*Effects of repeated use of the same belt.**

Belt Condition	Average BGI (mm ³ /N-m)	Standard Dev. in BGI (mm ³ /N-m)	CoV (%)
New	13.4 x 10 ⁻⁴	1.06 x 10 ⁻⁴	7.91
Used once	15.5 x 10 ⁻⁴	0.71 x 10 ⁻⁴	4.56
Used twice	15.5 x 10 ⁻⁴	0.44 x 10 ⁻⁴	2.84

*seven 30-second runs across the same belt for each series

Comparison of Belt Abrasion Data for Several Ceramic Materials.— Previous data for the grindability of various ceramic materials, calculated in the manner described above and obtained on a similar testing machine by Guo and Chand [5], are presented in Table 3. The alumina ceramic had the highest BGI (1.813 x 10⁻² mm³/N-m), silicon carbide had an average (for 3 materials) of 8.32 x 10⁻³ mm³/N-m, transformation-toughened zirconia (2 similar bars of material) had an average of 3.75 x 10⁻³ mm³/N-m, and the silicon nitride materials (12 varieties) averaged 2.04 x 10⁻³ mm³/N-m.

TABLE 3—*Selected BGI data from Guo and Chand (Ref [5]).*

Material	Commercial Designation	BGI*
Al ₂ O ₃	AD 995	181.3
Si ₃ N ₄	Allied Signal GS-44 (lot 1)	19.6
	Allied Signal GS-44 (lot 2)	21.2
	Allied Signal GN-10	18.2
	Norton NCX 5102	6.9
	Kyocera SN235P	15.5
	Kyocera SN220	24.3
	Kyocera SN 253	23.7
	Coors SRBSN	18.5
	Eaton SRBSN (lot 1)	22.2
	Eaton SRBSN (lot 2)	22.9
SiC	Ceraloy 147-3	34.3
	Carborundum HEXALOY	87.7
	Norton CVD SiC	70.2
ZrO ₂	Cercom PAD type B	91.8
	Coors TTZ (lot 1)	37.9
	Coors TTZ (lot 2)	37.0

* units of 10⁻⁴ mm³/N-m

Our current results on five silicon nitride materials and one alumina ceramic are presented in Fig. 4 in order of increasing grindability. For the rapidly-abraded alumina material, we shortened the incremental run time to 5 s and corrected for the distance slid in calculating the BGI. Each numerical value represents the average of at least six test increments. The most difficult materials to grind were NT-451 and NT-551, two high-performance ceramics with duplex grain-size microstructures optimized to provide toughness, high Weibull modulus in flexure, and high elevated temperature strength. The easiest silicon nitride material to grind was NT-154, a Si-Al-O-N-type ceramic.

In addition to measuring the material removal rate under two-body abrasive wear conditions, it was also of interest to examine the belt-ground test specimens' contact faces to determine whether their surface roughnesses correlated with their grindability. GS-44 had the lowest post-abrasion peak-to-valley roughness of the five silicon nitride ceramics. Using GS-44 as a reference material, Fig. 5 shows that relative BGI and P-V (peak-to-valley) roughness of the other ceramics relative to GS-44 did not correlate in the same way. Only for SN-1 was there a relative factor of 1.2 difference between both the BGI and the P-V roughness. In contrast, for NT-451 the BGI was about 0.8 of that for GS-44 while its P-V roughness was 1.3 times greater. These data indicate that surface quality and material removal rate do not in general correlate for silicon nitride materials. It is clear that identifying the detailed mechanisms by which material is abrasively removed from a surface is a different issue than measuring the quantity of that material removed per unit of exposure time to abrasive conditions.

Having established the repeatability and discriminating ability of the current test, there remains the task of correlating the BGI with the grinding characteristics of the same materials on different grinding operations. Since machining response, like wear, is a combined function of system characteristics and material properties, one might expect different correlations between the BGI values for a given series of materials and their grinding rates under, for example, cylindrical grinding, surface grinding, and creep-feed grinding. Such necessary correlations have yet to be performed. Nevertheless, the potential for establishing a viable ASTM standard test method using the test described herein seems to be excellent in light of the present results.

Conclusions

A two-body abrasive wear test was used to assess the belt grinding characteristics of a series of ceramics. Using a Belt Grindability Index, expressed as volume loss per unit applied force, per unit distance slid, the test was able to clearly differentiate between several types of ceramics as well as between several varieties within the same family of ceramic compositions. The repeatability of these results and the discriminatory capabilities of the current procedure were excellent. It would therefore seem to be a suitable candidate for a new ASTM abrasive wear testing method for hard-to-machine materials, like ceramics. Correlations of the BGI with tests on actual surface grinders are underway at this writing, because it is important to establish to what extent the differences in BGI between ceramic materials are reflected in their response to a range of commercial grinding conditions.

While the BGI seems to be a useful measure for material removal rate under controlled belt grinding conditions, it should not be used as a sole measure of grindability. Post-grinding factors such as the sub-surface residual stress state, the morphology of the final surface, and its flaw population, as it affects the initiation of fractures in service, must also be considered to complete the picture which defines the relationship between a material's machined-surface features and the surface's intended function. Additional work to establish the correlation between BGI values and specific grinding operations is needed before the method can be applied for selecting machining parameters to produce ceramic parts in a production environment. However, determining the belt abrasion wear rate of a material relative to others with known grinding characteristics can be a useful first step in that direction.

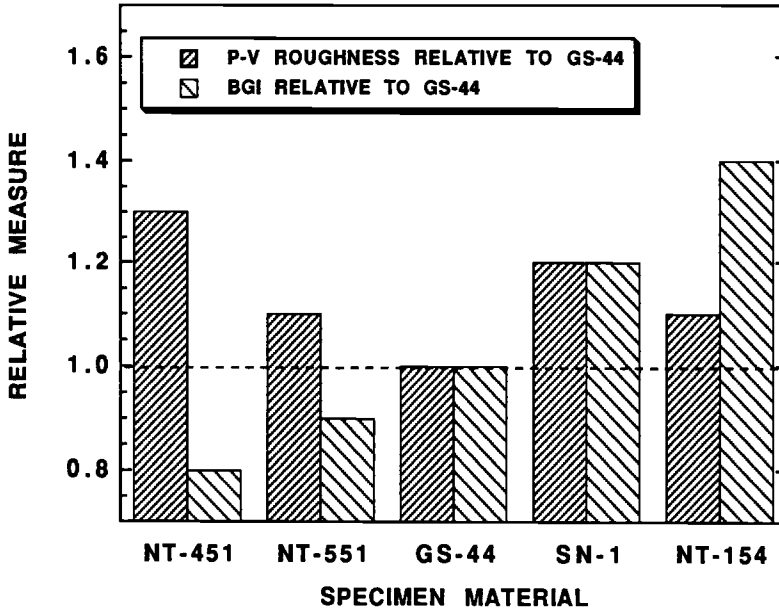


FIG. 5 — A comparison of the BGI values for five silicon nitride materials relative to their post-abraded peak-to-valley surface roughnesses. Data were normalized to this ratio for GS-44.

Acknowledgments

Discussions with and information from C. Guo, Chand Kare Technical Ceramics and the University of Massachusetts - Amherst, were helpful in preparing this paper. This research project was sponsored by the U.S. Department of Energy, Office of Transportation Technologies, Heavy Vehicle Propulsion Systems Materials Program, under contract DE-AC05-96OR-22464 with Lockheed Martin Energy Research Corporation.

References

- [1] Guo, C. and Chand, R. H. "Characterization of ceramic materials from the machining point-of-view," *Proceedings of Canadian Conference of Metallurgists, Symposium on Advanced Ceramics for Structural and Tribological Applications*, Vancouver, Canada, August, 1995.
- [2] Guo, C. and Chand, R. H., "Grindability of Ceramics," *Proceedings of the 1st International Machining and Grinding Conference*, Dearborn, MI September 12-14. Paper No. MR95-168. Society of Manufacturing Engineers, 1995.
- [3] Guo, C., "Grindability: the Basis for Cost-effective Ceramic Machining," *Ceramic Industry*, July 15, 1996, p. 196.
- [4] Chand, R. H and Guo, C., "A New Concept in Cost-Effective Machining," *The American Ceram. Society Bulletin*, Vol. 25 (7), 1996, pp. 58-59.
- [5] Guo, C. and Chand, R. H., "Cost-Effective Method for Determining the Grindability of Ceramics," Final Report, Subcontract Number 87X-SM036C, January 20, Oak Ridge National Laboratory, Oak Ridge, TN, 1996.

Christian J. Schwartz¹ and Shyam Bahadur²

OBSERVATIONS ON THE GRINDING OF ALUMINA WITH VARIATIONS IN BELT SPEED, LOAD, SAMPLE ROTATION, AND GRINDING FLUIDS

REFERENCES: Schwartz, C., and Bahadur, S., “**Observations on the Grinding of Alumina with Variations in Belt Speed, Load, Sample Rotation, and Grinding Fluids,**” *Wear Processes in Manufacturing, ASTM STP 1362*, S. Bahadur and J. Magee, Eds., American Society for Testing and Materials, 1999.

ABSTRACT: The volume of material removed in the grinding of alumina on a diamond-impregnated grinding belt was studied. Four grinding process parameters were tested: belt speed, normal load at the pin’s contact surface, sample rotation during grinding, and grinding fluid. The results showed that at low loads the belt speed did not have a significant effect on material removal rates; however, the material removal rate decreased at higher loads combined with higher speeds. It decreased, in particular, when the sample was also rotated. Of the fluids used, the 50% ethylene glycol - 50% water mixture produced the highest material removal rates while the lowest were produced by biodegradable soybean oil. The test conditions that produced high temperatures at the contact surface contributed to plowing as opposed to cutting and resulted in reduced material removal rates. The reasons for these variations were investigated by scanning electron microscopy of the surfaces, which revealed evidence of plastic deformation and temperature rise during grinding.

KEYWORDS: grinding, abrasion, abrasive machining, ceramic grinding, grinding variables

The field of ceramic grinding has grown steadily in recent years. With current demands on higher performance materials and close tolerances on manufactured parts, the grinding of ceramic materials is poised to become an even larger aspect of the production environment in the future. Ceramics offer good corrosion resistance, high heat tolerance, and surface durability unmatched by the metals and polymers; however, the fact that ceramics are different from other materials leads to many of the current problems in

¹ Graduate student, Mechanical Engineering Department, Iowa State University, Ames, IA 50011.

² Professor, Mechanical Engineering Department, Iowa State University, Ames, IA 50011.

production. These problems, in many cases, are caused by the above properties that make ceramics useful in applications.

Grinding of ceramics is important because it is a finish operation on many parts that can successfully be processed by other methods in the early stages of production. Sometimes, it is the only option available for configuring a part. For instance, the wire manufacture and biomedical industries commonly injection mold alumina to form a geometry and finish the parts by diamond grinding [1]. Approximately 80% of advanced ceramic grinding is performed using diamond cutting tools and practices [2], and similar practices were originally developed and optimized for use in grinding glasses and tungsten carbide [3]. Therefore, many of the variables in the grinding processes used on ceramics have never been rigorously tested and optimized. Allor and Jahanmir [2] have estimated that as much as 90% of the cost of a finished ceramic part is comprised of the machining costs due to very small material removal rates in grinding. In addition, there is a lack of knowledge of how fast a ceramic may be ground without damage.

Of late, much work has been done on studying the grinding process and how it relates to ceramics, models have been developed, and areas of further research have been identified. The mechanisms of material removal have been studied and an attempt has been made to pinpoint what aspects of the grinding process have led to problems when applied to ceramics. Of all the variables, temperature in the cutting zone seems to be one of the most important. Zarudi, Zhang, and Mai [4] showed that alumina deforms plastically at temperatures as low as 200 °C when it is exposed to a hydrostatic stress state, as when scratched with a blunt tool. This behavior becomes important in the context of cutting temperatures. Lavine and Jen [5] proposed a model to predict temperatures at the contact face during grinding. Their model considered heat transfer to the workpiece, the grinding fluid, and the grinding tool. It was indicated that even boiling of the grinding fluid was possible. Finite element modeling has been used by Li and Chen [6] to predict temperatures at the contact surface but determining the actual contact area has been a problem. The temperature problem is so complex that Hebbbar et al. [7] indicated that the thermal properties of the ceramic workpiece did not significantly affect the material removal rate during grinding.

Another aspect that has been studied has to do with the physical conditions of the ceramic before grinding, namely microstructural grain size. It has been shown by Xu et al. [8] that grinding force decreases with increasing grain size from 3 to 9 μm due to subsurface damage in the form of intergrain slip bands and intergranular microcracks. However, it is still apparent that there are no good criteria to ensure damage free grinding of ceramics.

There is another aspect to this field which has ties to the economic feasibility of ceramic grinding. It is the aspect of environmental issues surrounding the process. Legislative regulations can cause an otherwise promising approach to be cost prohibitive if it causes environmental harm. Statutes such as the Resource Conservation and Recovery Act (RCRA) [9] demonstrate the necessity of environmentally conscious manufacturing.

Although the grinding process is very complex, some estimates can be made to develop a starting point for research. In a simple way, grinding can be envisioned as a cutting process by a multitude of particles rubbing over the surface of a softer material. This process is predominantly abrasive but it becomes complicated because of the

hydrostatic stress state at particle contacts and the accompanying temperature rise. The size and shape of the hard abrasive particles affect the material removal rate in grinding. A simple relationship for abrasion is $Q=KW/H$, where Q is the volume of material removed per unit sliding distance, W the applied normal load, and H the indentation hardness of the abraded surface [10]. In this equation, K is a proportionality constant which depends upon other variables in the process, such as the geometry of the abrasive particles, dry or lubricated cutting, and two-body or three-body abrasion.

The removal of material in the case of ceramics would ordinarily be expected to take place by brittle fracture. This is not the case in practice because even brittle materials have shown the ability to deform plastically in asperity contact situations. A shallow plastic zone surrounding the rut left by the hard abrading particle over the ceramic surface is observed after scratching. The lateral cracks which originate in the plastic zone grow parallel to the surface and thereby contribute to the detachment of material during grinding. Wear surfaces thus show plastically deformed ruts, deep gouges from flaking, and removal of chips.

A model based on the above ideas and using the principles of fracture mechanics has been developed [10]. It gives the material removal per unit sliding distance, Q , as

$$Q = \alpha_4 N \frac{w^{5/4}}{K_c^{3/4} H^{1/2}}$$

where α_4 is a constant based on abrasive particle geometry, N the number of abrasive particles in contact with the surface, w the normal load supported by each particle, and K_c and H are the Mode I fracture toughness and indentation hardness of the abraded material, respectively. Similar to the earlier equation, this equation shows that material removal increases with increasing normal load but in addition to hardness, fracture toughness also emerges as a significant variable. What this model does not account for is the effect of temperature at the contact area.

Plastic deformation is influenced by temperature even for brittle materials such as alumina. With an increase in temperature, the volume of material removed will decrease because of more plastic flow and plowing rather than removal of material by abrasion. Therefore, lower temperatures should be advantageous in grinding for the sake of higher material removal rates. It is possible, then, that a cutting fluid with a high specific heat will lead to higher material removal rates due to better temperature control.

In light of these issues, this work was performed to determine the significance of several grinding variables in the material removal of alumina. Belt speed, normal load, rotation of the sample, and grinding fluid were varied to observe their effects on the material removal rate and to decide if there was an aspect of the grinding process that was dominant in governing the grinding behavior. This paper describes the details of the grinding experiments, presents and discusses the results, and gives final conclusions of the work.

Experimental Details

Sample Preparation

The samples used in the grinding tests were of alumina with 99.5% purity and were in the form of pins, 6 mm x 6 mm cross section and 12 mm long. Initially, 12 mm x 12 mm blocks were cut out of a 6 mm thick plate using a high speed water cooled diamond saw. The 12 mm square surface of each block was polished in succession with 50, 320, and 600 grit silicon carbide paper and then with 15, 6, and 0.5 μm diamond pastes. This surface was later used for scanning electron microscopy studies. These blocks were then cut on a low-speed diamond saw to provide pins of the dimensions 6 mm x 6mm x 12mm. The 6 mm x 6mm surface of the pin was polished by loading under a 5 N load against the diamond belt used in the test and moving at 0.5 m/s speed. It was this surface that was loaded against the belt in grinding tests. The four long edges of the pin were rounded by grinding on the belt to minimize belt damage when pins were rotated during the test. Before testing, the pin was ultrasonically cleaned in acetone and ethanol (to remove any film left by the evaporated acetone) and dried. The same preparation process was used for all alumina pins so as to provide approximately equal contact areas and surface roughnesses of the pin surfaces to be ground. This fact was checked qualitatively by naked eye and examination in a scanning electron microscope for several pins selected at random before testing.

Grinding Test

The equipment used for grinding was a belt sanding unit powered by a 0.186 kW (1/4 hp) DC motor as shown schematically in Fig. 1. The motor speed was regulated by a potentiometer. The belt was 1.2 m long and was supported by two rollers. It was of fabric composition with 20 μm diamond particles bonded to it by the belt manufacturer. A fixture was used to hold the alumina specimens under load against the belt during grinding. It had a platform to support weights. A 0.025 kW (1/30 hp) motor rotated this fixture by a chain and sprocket arrangement. This provided rotation to the alumina pin during grinding.

The rotational speed of the specimens was also regulated by a potentiometer. The entire unit was placed in a large plastic tub filled with the grinding fluid. The latter was maintained at a level high enough in the tub to allow the belt to carry some fluid to the grinding location during testing. The four parameters chosen for study were: grinding belt speed, contact pressure, superimposition of rotational motion, and the type of cooling fluid.

Whereas the abrasion equations given earlier do not include velocity as a dependent variable, it was considered to be an important variable in grinding because of the likelihood of higher temperatures with higher speeds. This could provide the conditions necessary for plastic deformation which would tend to reduce material removal. The speeds tested were 0.53, 1.04, and 1.50 m/s

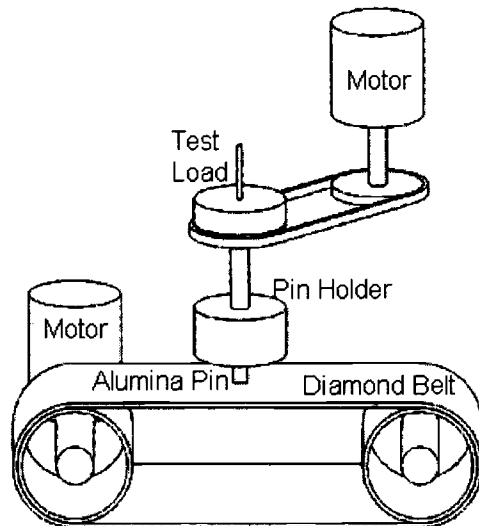


FIG. 1 -- Schematic diagram of test apparatus used. Belt and rollers were submerged in a tub filled with the chosen fluid during testing.

The normal load settings used were 7.3, 14.4, 30.7, 45.6, and 60.4 N. These loads resulted in variation of contact pressures from 0.2 to 1.7 MPa.

Sample rotation was used as another variable in the test. The basic premise was to add rotary motion to the linear motion at the contact surface. It was expected to increase the material removal rate without causing a significant increase in temperature rise. It was surmised that the change in orientation would cause new wear tracks to intersect the old tracks and thus make it easier for chips to separate from the surface.

In addition to preventing clogging of the belt, grinding fluids suppress the interface temperature rise which lowers the material removal because of plastic effects that dominate at the contact surface [11]. This implies that heat transfer properties of the grinding fluid are important in terms of both the material removal and surface integrity. With this in mind, three fluids were investigated as shown (Table 1). Their specific heat values are also presented in the table [12, 13].

The light mineral oil which is normally used in industry was used as the base fluid. It has a relatively low value of specific heat which indicates greater temperature rise for a given energy input. Water as a coolant is very efficient but reacts with alumina during the sliding process forming $\text{Al}(\text{OH})_3$ and thus damages the surface [14]. In view of this, a 50% ethylene glycol - 50% water mixture was used as the second grinding fluid. Its specific heat is much higher than that of the mineral oil which means that the fluid will undergo a lower temperature rise for the same energy input. Additionally, soybean oil was chosen as the third grinding fluid because it is biodegradable while the previous two are not. It thus has a great potential in terms of its future use.

TABLE 1-- *Grindings fluids used and their specific heats.*

Grinding Fluid	Specific heat, (kJ/kgK)
Soybean Oil	1.93
Mineral Oil	2.09
50% Ethylene Glycol - 50% Water	3.30

The pin was oriented in the specimen holder so that the finely polished 12 mm x 6 mm face served as the leading side. This was done so as to allow scanning electron microscopy of the edge of the polished surface to provide an indication of subsurface damage. Initially, the belt was activated and the pin was loaded on it after it reached the set speed. Each test was run for a duration of 60 s. After the test, the specimen was cleaned ultrasonically in acetone and ethanol, dried, and weighed in a precision balance. This provided the material removal rate. For each condition, three tests were performed and the mean data was plotted.

The ground surface as well as the subsurface damage were studied by scanning electron microscopy. For this purpose, the surfaces to be studied were gold sputter coated with a coat thickness of approximately 150 Å.

Results and Discussion

Mineral Oil

Figure 2 shows the material removal rate as a function of load when grinding was done in light mineral oil at three belt speeds. The larger the load, the greater is the material removal rate in all the cases. This would be expected because larger loads provide deeper embedment of the abrasive particles in the surface of the material being ground. The situation gets complicated because of heating at the interface which would be greater at larger loads and higher speeds. In the lower load regions, variation of material removal rate with load is practically linear and about the same for all speeds. At higher loads and at the highest speed of 1.50 m/s, the material removal rate for any load is lower than at lower speeds.

This was suspected to be because of the temperature rise. In order to verify this, the surface of the specimen abraded at 30.7 N and 1.50 m/s speed was examined by scanning electron microscopy and is shown in Figure 3. Compared to the surface abraded at the lowest speed and the lowest load (0.53 m/s and 7.3 N) and shown in Figure 4, it is obvious that the surface abraded at the higher speed and load has undergone considerable plastic deformation. The latter likely occurs because of a hydrostatic stress state at asperity contacts and would possibly be enhanced by the increase in temperature. The detachment of material from grooving action as involved in the abrasion process is retarded by plastic deformation. The direct evidence of heating in Fig. 4 is minimal.

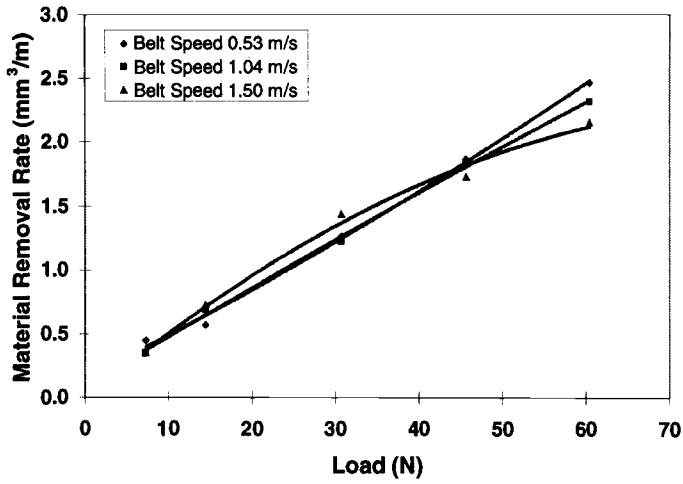


FIG. 2 -- Grinding response of alumina in mineral oil with no sample rotation.

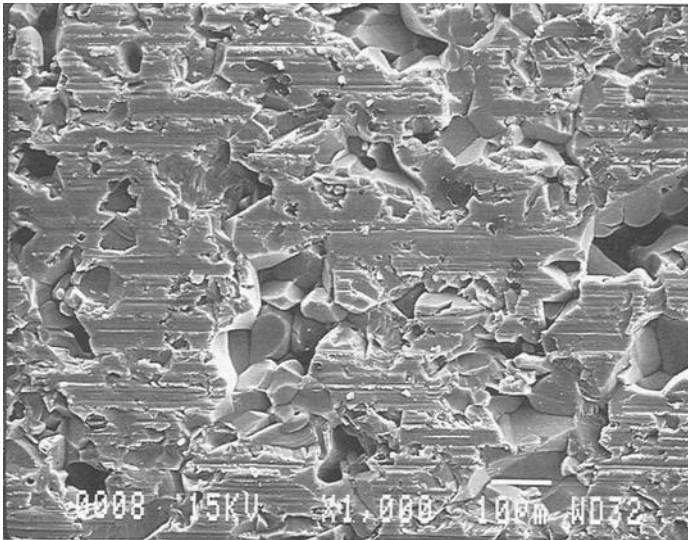


FIG. 3 -- Ground surface of a sample tested in mineral oil at 1.50 m/s belt speed and 60.4 N load with no rotation.

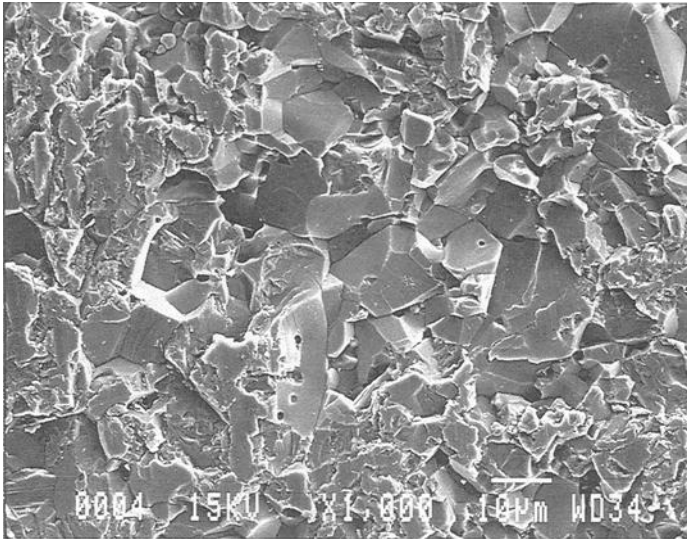


FIG. 4 -- *Micrograph of alumina pin tested in mineral oil at a belt speed of 0.53 m/s and load of 7.3 N with no sample rotation.*

The relative depth and width of furrows on a ground surface gives an indication of the plastic deformation experienced during grinding. This allows for qualitative judgement of the extent of plastic deformation based on the geometry of the furrows in a micrograph. With the superimposition of rotational motion of the pin at 5 rpm, the plowing action became predominant as shown in Fig. 5. The surface here exhibits deep, long, and continuous furrows. Contrast the severity of these furrows with Figs. 3 and 4 and it is apparent that the grinding conditions in this case were more severe. There is also the evidence of heating at locations which are featureless and are often interspersed with holes with smooth boundaries in Fig. 5. In this situation of plowing action, the material was often displaced rather than detached. Consequently, the material removal rate with motion of the pin was lower than when the pin was stationary, being in contact with the traversing belt in both cases. This is shown in Fig. 6. It should also be noted that the curves in this case are not linear in the high load region even at the low speeds of 0.53 and 1.04 m/s, and at the highest speed of 1.50 m/s the curve is almost flat. The effect of temperature rise is thus pronounced in the case of pin rotation and is in no way conducive to increased material removal rate.

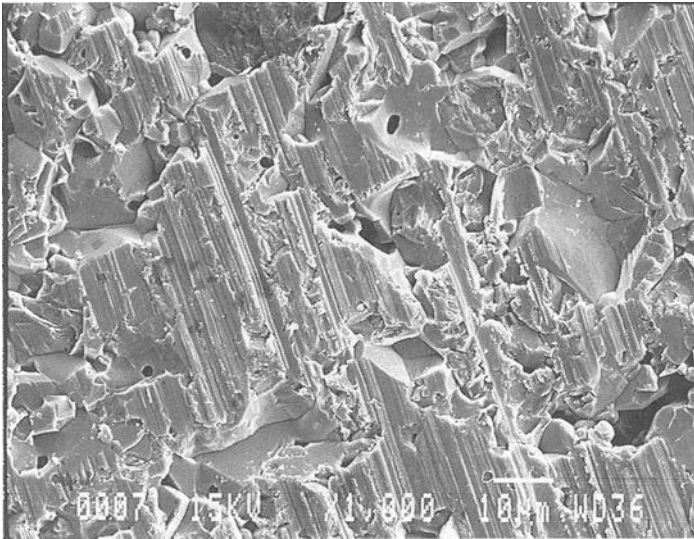


FIG. 5 -- Ground surface of a sample tested in mineral oil at 60.4 N, 1.50 m/s belt speed, and 5 rpm rotation. Wear tracks are deep and have a slight curvature.

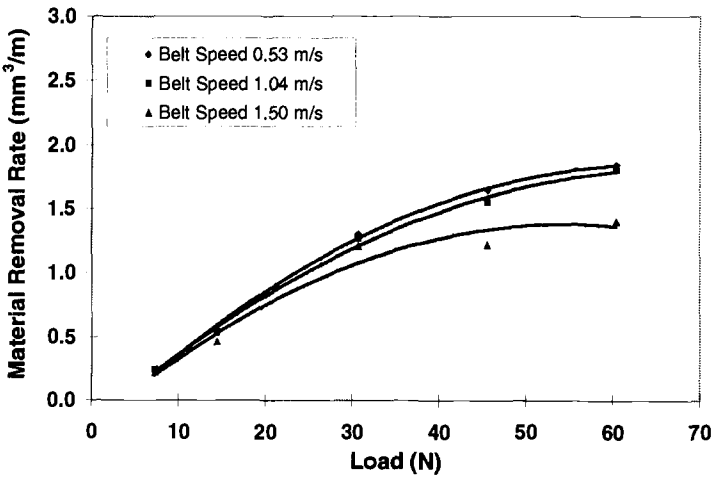


FIG. 6 -- Grinding response of alumina in mineral oil with sample rotation at 5 rpm.

Glycol and Water Mixture

To further investigate the possibility that temperature rise had a significant effect on material removal rate in mineral oil, a 50-50 mixture of water and ethylene glycol (which has a higher specific heat than mineral oil) was next tried. As shown in Fig. 7, the material removal rate for any speed and load was higher than in the case of mineral oil. This indicates that the glycol-water solution provided a better cooling action which is also justified because of its higher specific heat (Table 1). The shape of the curves with no pin rotation is the same in Figs. 2 and 7. The material removal rate at the higher speed of 1.50 m/s is lower for any load in the higher load region than that at the lower speed (Fig. 7). Figure 8 shows the scanning electron micrograph of the surface abraded at the highest load and speed in glycol solution. There is evidence of plastic deformation which accounts for lower material removal rate at the higher speed. The comparison of this to Fig. 3 (which is for the lower load of 45.6 N) shows that the amount of plastic deformation in the case of glycol solution is much less than that in mineral oil. This further attests to more efficient cooling in this case and accounts for higher material removal than in mineral oil for the corresponding conditions.

With the added effect of pin rotation, the material removal rate at 1.50 m/s belt speed and low loads was much higher than in the case of mineral oil. This should indeed be the case if thermal softening at the interface is not a factor. However, in the higher load range, pin rotation reduces the material removal rate because heating becomes a significant factor even in the case of glycol solution.

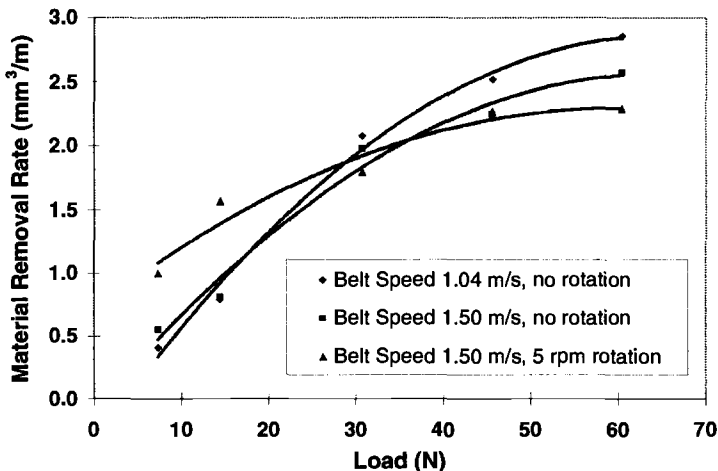


FIG. 7 -- Response of alumina in glycol mixture with and without rotation.

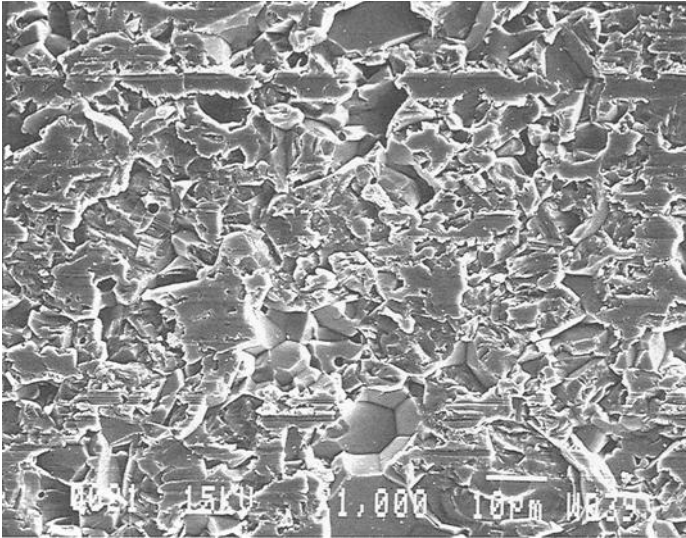


FIG. 8 -- *Ground surface of pin tested at 60.4 N in glycol mixture at 1.50 m/s belt speed with no rotation.*

Soybean Oil

The results from the grinding of alumina in soybean oil (Fig. 9) indicate that the material removal rate for any load and speed combination was the lowest of the three grinding fluid cases. In other respects, the results were similar. Considering first the case with no rotation of the pin, the material removal rate at the higher speed of 1.50 m/s is lower than that at 1.04 m/s specifically at higher loads. This indicates that heating effect is significant and it affects the material removal behavior. The scanning electron micrograph in Fig. 10 of the pin surface abraded in soybean oil at 1.50 m/s speed and 60.4 N load shows a much greater plowing effect due to localized heating than for the same test condition in mineral oil (Fig. 3). The plowing effect is even more pronounced in Fig. 11, as indicated by more severe furrows, showing the deformation features on the abraded surface for the same load and speed conditions but added rotational motion of the pin. This is reflected in the material removal as well because the material removal rate with pin rotation is much lower than with no pin rotation.

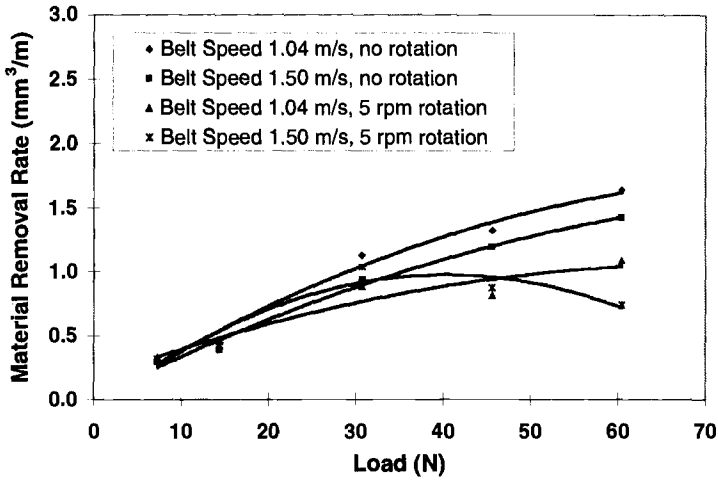


FIG. 9 -- Grinding response of alumina in soybean oil with and without sample rotation.

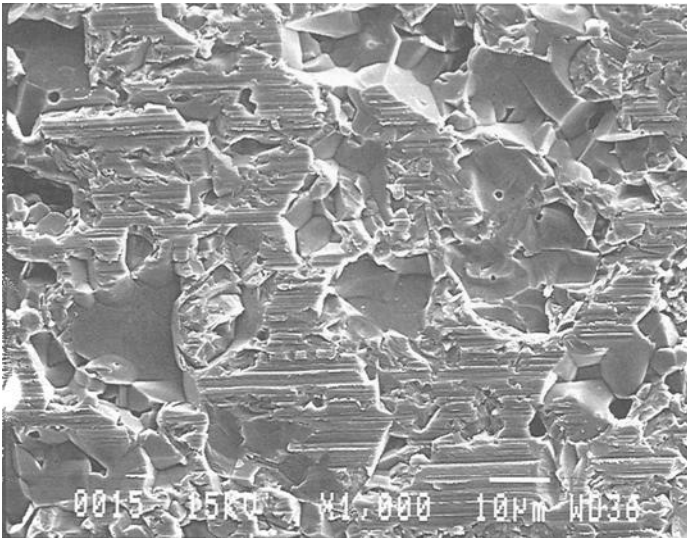


FIG. 10 -- Ground surface of pin tested in soybean oil at 60.4 N, 1.50 m/s belt speed, and no rotation.

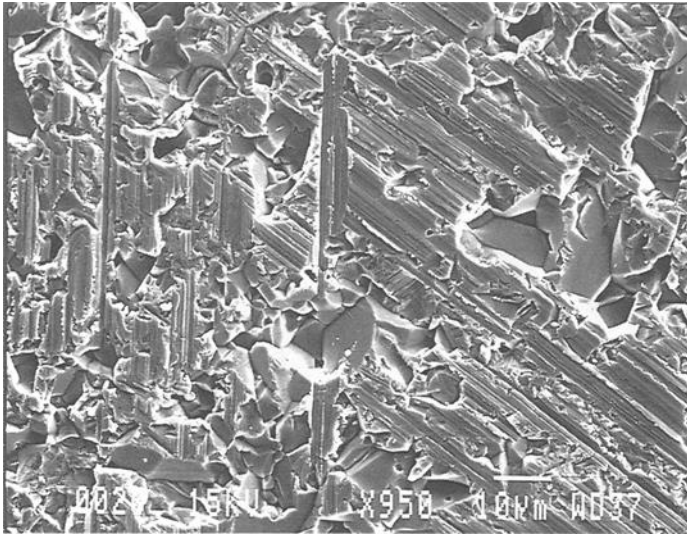


FIG. 11 -- Ground surface of pin tested in soybean oil at 60.4 N, 1.50 m/s belt speed, and 5 rpm rotation.

Figure 12 shows the vertical finely polished surface of the pin abraded in soybean oil at the highest load and speed combination. There is indication of the material removal occurring by ductile fracture mechanism as opposed to grain pullout that would be the case from brittle fracture mechanism. In view of the above discussion that would hardly be unexpected.

Abrasion Models

The above results indicated that the models of abrasion presented in the introduction section are not valid for abrasive grinding. According to the models, the material removal rate should increase with lower hardness and higher loads. The experimental results on grinding indicated that with the increase in load the temperature increased which should have lowered the hardness. But, contrary to the model prediction, the material removal decreased. The model also implies linear dependence between material removal and sliding distance. This was also not observed experimentally because with added sliding from pin rotation the material removal rate decreased. The reason for this effect was also temperature rise. Thus, more than any factor studied in this work, the temperature rise at the interface governed the material removal rate. This was also reflected in terms of the material removal results from three grinding fluids. The effectiveness of the grinding fluids in suppressing temperature rise in the cutting zone depends upon their specific heats as well as their lubrication ability. With glycol-water

solution as the grinding fluid, the temperature rise was the lowest because it had the highest specific heat. It is believed that the temperature rise in the case of soybean oil was higher than that in mineral oil for two reasons: lower specific heat, and lack of effective lubrication because of oxidation of the soybean oil at high temperature.

It is expected that the results reported above which are significant in terms of the grinding efficiency are valid for other ceramic materials as well.

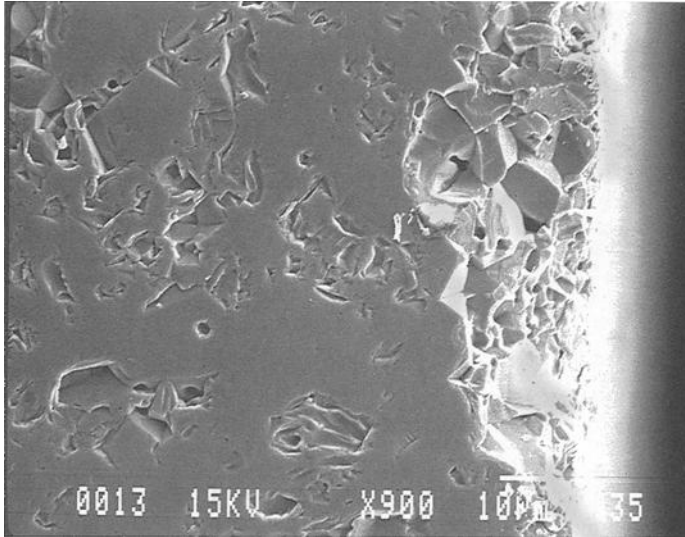


FIG. 12 -- Micrograph of polished side perpendicular to ground face of pin tested in soybean oil with a load of 60.4 N and a belt speed of 1.50 m/s.

Conclusions

1. Material removal in abrasive belt grinding increases with increasing load, almost linearly at lower loads but not so at higher loads because of the heating effects.
2. Heating, which is significant at higher loads and higher speeds, tends to cause considerable plastic deformation. This deformation appears to lead to the reduction in material removal rate.
3. With the addition of the rotational motion of the pin to the linear motion of the belt, material removal rate decreased at high loads and there was increased plowing of the surfaces as opposed to cutting. Most likely, this plowing was due

to significant plastic deformation of the ground surfaces because of heating involved under such severe conditions.

4. Of the three cooling fluids (mineral oil, glycol-water mixture, and soybean oil) used in this work, the material removal rate was the highest in the case of glycol-water mixture and the lowest for soybean oil. This was most likely due to the differences in specific heat among the fluids.
5. Scanning electron microscopy of the ground surfaces revealed that the material removal rate depended up the extent of plastic deformation of the surfaces, being lower with higher plowing effects.
6. The mathematical models proposed for abrasion are not applicable to grinding situations because of the complication from temperature rise.

References

- [1] Mason, F., "Making Tiny Ceramic Tools," *Manufacturing Engineering*, Vol. 118, January 1997, pp. 50-54.
- [2] Allor, R. and Jahanmir, S., "Current Problems and Future Directions for Ceramic Machining," *American Ceramic Society Bulletin*, Vol. 75, July 1996, pp. 40-43.
- [3] Chand, R. and Guo, C., "What's Happening with Machining of Ceramics?" *Manufacturing Engineering*, Vol. 117, October 1996, pp. 74-78.
- [4] Zarudi, I., Zhang, L., and Mai, Y.W., "Subsurface Damage in Alumina Induced by Single-Point Scratching," *Journal of Materials Science*, Vol. 31, February 15, 1996, pp. 905-914.
- [5] Lavine, A. S., and Jen, T. C., "Thermal Aspects of Grinding: Heat Transfer to Workpiece, Wheel, and Fluid," *Journal of Heat Transfer*, Vol. 113, May 1991, pp. 296-303.
- [6] Li, Y. Y., and Chen, Y., "Simulation of Surface Grinding," *Journal of Engineering Materials and Technology*, Vol. 111, January 1989, pp. 46-53.
- [7] Hebbar, R. R., Chandrasekar, S., and Farris, T. N., "Ceramic Grinding Temperatures," *Journal of the American Ceramic Society*, Vol. 75, October 1992, pp. 2742-2748.
- [8] Xu, H.H.K., Wei, L., and Jahanmir, S., "Influence of Grain Size on the Grinding Response of Alumina," *Journal of the American Ceramic Society*, Vol. 79, May 1996, pp. 1307-1313.

- [9] Miller, P. C., "Coolant Survey: A Flood of Fluid Choices," *Tooling & Production*, March 1986, pp. 37-43.
- [10] Hutchings, I. M., *Tribology, Friction and Wear of Engineering Materials*, CRC Press, Boca Raton, Ann Arbor, London, Tokyo, 1992, pp. 142-153.
- [11] König, W., Tönshoff, H. K., and Fromlowitz, J., "Belt Grinding," *CIRP Annals*, Vol. 35, February 1986, pp. 487-494.
- [12] Bailey, A. E., *Industrial Oil and Fat Products, Second Edition*, Interscience Publishers, Inc., London, 1951, p. 89.
- [13] *Specific Heat, Nonmetallic Liquids and Gases*, Y. S. Touloukian, C. Y. Ho, Eds., IFI/Plenum, New York, Washington, 1970, pp. 102, 192.
- [14] Gates, R. S., Hsu, S. M., and Klaus, E. E., "Tribochemical Mechanism of Alumina with Water," *Tribology Transactions*, Vol. 32, 1989, pp. 357-363.

Wear of Cutting Tools

Jie Gu,¹ Simon C. Tung,² and Gary C. Barber³

WEAR MECHANISMS OF MILLING INSERTS: DRY AND WET CUTTING

Reference: Gu, J., Tung, S. C., Barber, G. C., "Wear Mechanisms of Milling Inserts: Dry and Wet Cutting," *Wear Processes In Manufacturing, ASTM STP 1362*, S. Bahadur and J. Magee, Eds., American Society for Testing and Material, 1999.

ABSTRACT: There is less literature on wear of milling tools than on wear of turning tools because milling is one of the most complicated machining operations. The intermittent milling action creates mechanical and thermal surges that distinguish milling from single-point machining. A systematic tool life study for face milling inserts was conducted with and without coolant. Workpieces made of 4140 steel were cut by C5 grade carbide inserts under various cutting conditions. The comparison between dry and wet cutting shows that caution should be taken when applying a coolant for milling operations. Special tests should be carried out in evaluating potential coolant candidates. It is not always true that coolant enhances tool life for milling. Wear mechanisms are presented by means of wear maps. Identified wear mechanisms are: micro-attrition, micro-abrasion, mechanical fatigue, thermal fatigue, thermal pitting, and edge chipping.

KEYWORDS: cutting insert, tool life, wear mechanism, milling, SEM

Previous studies have been done to minimize tool wear and make the wear consistent and predictable. Many tool life equations have been proposed in the literature. The application ranges of the tool life equations[1-3] are limited to where the parameters of the equation are fitted. There are several handbooks[4-5] that recommend machining conditions. The information in these books is general and provides a starting point only.

Machining generally involves single-point or multi-point cutting tools. Most researchers focus on single-point cutting, trying to isolate many factors that affect the

¹ Sr. manufacturing engineer, GM Powertrain, Flint Component, 902 E. Hamilton, Flint, MI 48550

² Staff research scientist, GM R&D Center, MC:480-106-160, 30500 Mound Rd. Box 9055, Warren, MI 48090

³ Associate professor, Mechanical Engineering, Mech. Eng. Dept., Oakland University, Rochester, MI 48309

process[6-9]. Milling is one of the most versatile machining operations. Milling can be used to generate a flat surface, pocket, curved die, gear teeth, etc. A cutting edge in milling engages and disengages a workpiece periodically. This intermittent action creates mechanical and thermal surges that distinguish milling from single-point machining.

Tool wear is the result of load, friction, and high temperature between the cutting edge and the workpiece. The major causes of wear are mechanical, thermal, chemical, and abrasive. The cyclic mechanical forces cause fatigue on the tool cutting edge. The temperature of a tool increases as the cutting speed increases. In milling, thermal shock leads to different kinds of wear that are not encountered in turning. When a cutting edge of the mill cutter engages the workpiece, the temperature starts to rise. The temperature drops when the cutting edge leaves the workpiece. This thermal cycle can be worsened if improper coolant is applied. Several basic wear mechanisms which occur during metal cutting are adhesive wear, abrasive wear, diffusion wear, oxidation wear, and fatigue wear[10,11]. Adhesive wear, also known as attrition wear, occurs mainly at low temperature. This mechanism is usually accompanied by built up edge (BUE). Abrasive wear is mainly caused by the hard particles of the workpiece material. The ability of the cutting edge to resist abrasive wear is related to its hardness. Diffusion wear is more affected by chemical factors during the cutting process. The chemical properties of the tool material and affinity of the tool material to the workpiece material will determine the development of diffusion wear mechanisms.

Some researchers present the rates of flank wear as a map with an abscissa of cutting speed and an ordinate of feed rate. Maps of uncoated high speed steel (HSS) inserts and Titanium nitride (TiN) coated inserts for turning have been reported[12,13].

The current popular tool materials are high speed steel, carbide, ceramic, and diamond. Recently, carbide is gaining more and more popularity. Ceramic and diamond are used for high speed machining. While carbide is currently the dominant cutting tool material, there are no wear maps for carbide like those for HSS[12,13]. The need to understand the milling process is very important. The use of coolant adds one more dimension to the tool life study. Tool life tests are time consuming, costly and complicated. The combination of machining conditions, workpiece-tool combination, tool geometry, cutting fluid, machine capability, workpiece finish status, etc., makes tool life research formidable.

In this paper we report our wear study on carbide milling inserts. Tool life profile maps are constructed. Major wear mechanisms are identified and the effect of coolant is discussed based on the test data.

Materials and Cutting Conditions

C5 is a tool grade generally recommended for cutting steel. We used C5 carbide inserts to cut 4140 pre-heated steel. The hardness of C5 carbide and the 4140 steel are 52 Rockwell C (Rc) and 27 Rc respectively. The composition of 4140 steel is: C 0.38~0.43%, Mn 0.75~1.00%, P (max) 0.035%, S (max) 0.040%, Si 0.15~0.35%, Cr 0.8~1.10%, Mo 0.15~0.25%. The coolant used in the test has a commercial name "TRIM-SOL". It is a water based emulsion coolant used at a 5% concentration mixed

with water. Its composition includes petroleum oil (30-35%), sulfonate (20-30%), chlorinated alkene polymer (20-30%), nonionic surfactant (3-5%), aromatic alcohol (3-5%) and propylene glycol ether (3-5%).

The inserts used in the test have a standard geometry designation: TBE-222 with a 0° rake angle and 5° clearance angle. FIG 1 shows the face milling test set up. The mill cutter with only one insert turns at a certain RPM while the workpiece is fed from right to left horizontally by the table movement. After a new pass is completed, the workpiece is moved up one depth of cut (DOC) and a new pass is made. The cutting is controlled by a CNC program written in Bridgeport, EZ-TRACK language. After the insert is installed in the mill cutter, the radial rake angle is minus 9° , the axial rake angle 0° , and the relief angle 5° .

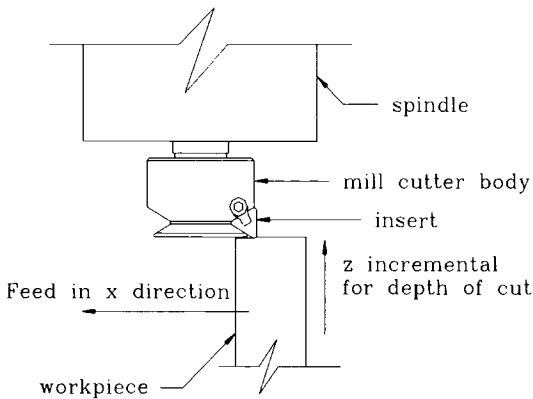


FIG 1 -- Vertical mill cutting of the specimen

The test is done at five cutting speeds: 60, 120, 180, 240, 360 m/min and four feed rates: 0.125, 0.200, 0.275, 0.315 mm/tooth. Depth of cut is 0.25 mm. The tool life criteria include flank wear, crater wear, and catastrophic tool failure. Recommendations for tool failure from ISO 8688-1:1989 [4-5] are flank wear: 0.35 mm, and crater wear: 0.10 mm. In the tests we chose the flank wear criteria to be 0.4 mm, slightly broader than the ISO recommendation. Crater wear in our tests never exceeds 0.05 mm, so the criterion does not apply.

Milling Test without Coolant

TABLE 1 shows the tool life expressed in cutting length. In the fourth row of the table, "c" stands for chipping. The cutting length shown before "c" is the length when the chipping first occurs. FIG 2 shows the 3-D view of the table (row four is not included).

From FIG 2, we see that feed rate has much less influence on tool life than cutting speed. When the speed is lower than 120 m/min, the tool life increases as the speed increases. In this speed range BUE has great influence on tool life. A BUE forms when

a small piece of workpiece material sticks to the insert, progressively increasing in size. When the BUE reaches a certain size, it breaks away from the insert. In our tests the built up material breaks at the interface of the insert and the BUE (FIG 3), a portion of insert material may be removed with the BUE material. This phenomenon accelerates the wear progress. When the cutting speed is low, BUE is heavy, and so the tool life is short. As the speed increases, BUE decreases, and the tool life increases. As the cutting speed increases further the tool temperature increases. Tool life reduces quickly because the hardness of the insert decreases at high temperature. The optimum cutting conditions in our tests are: speed 120 m/min and feed 0.125 mm/tooth.

TABLE 1 -- Tool life of dry cutting (meter)

		Cutting speed v (m/min)				
		60	120	180	240	360
feed per tooth mm/tooth	0.125	191m	1537m	829m	578m	461m
	0.20	341m	1450m	786m	497m	384m
	0.275	423m	1319m	673m	449m	262m
	0.315	24m/c	79m/c	30m/c	16m/c	n/a

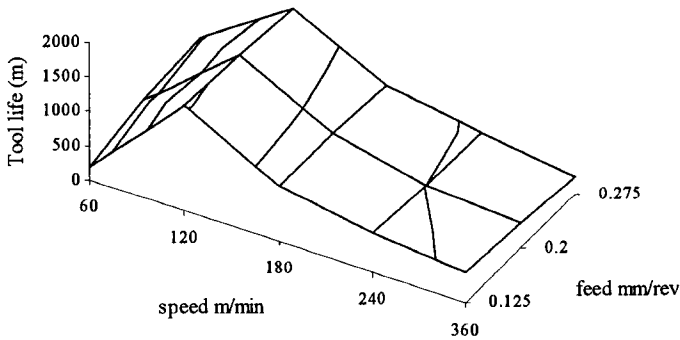


FIG 2 -- 3-D view of tool life (cutting length)

SEM pictures were taken to characterize the flank wear features on the inserts. Five wear mechanisms were identified: micro-attrition, micro-abrasion, mechanical fatigue, thermal fatigue, and edge chipping. FIG 4 shows the wear mechanism map, where the

dominant wear mechanism or combination of wear mechanisms is indicated in each region.

1). Micro-attrition. When the cutting speed is low, the flank surfaces have the appearance of a dull flat, FIG 5. The flat is created by segments of workpiece material smeared over the flank face. The carbide grains and the cobalt binder of the insert are worn at the same rate. So the carbide grains and cobalt binder are the same height during the wear process with no carbide grains protruding out of the flank face. As the BUE breaks from the insert, the flank face is worn by micro-attrition.

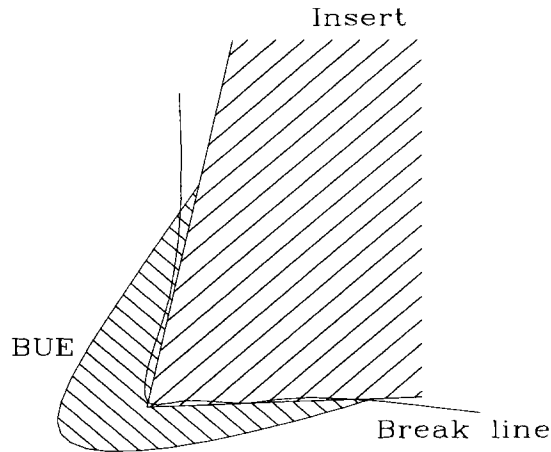


FIG 3 -- BUE breaks in the interface

2). Micro-abrasion. As the cutting speed increases, BUE gradually disappears. The hardness of the cutting edge decreases as the temperature increases with the speed. At high cutting speed the insert flank wear is caused by a micro-abrasion mechanism. The cobalt binder is worn faster than the carbide grains. So the carbide grains protrude out of the flank face (FIG 6).

However, in the middle cutting speed range BUE still exists, which activates a micro-attrition wear mode. On the other hand, the cutting speed is high enough to activate the abrasive wear mechanism. The flank face at middle cutting speeds has the appearance of small flats surrounded by protruding carbide grains (FIG 7). Therefore, the insert is worn by both micro-attrition and micro-abrasion.

3). Mechanical fatigue. When the mechanical impact increases as the speed and feed rate increased, the insert flank faces show micro cracks parallel to the cutting edges, see the horizontal crack in FIG 8. The crack is parallel to the cutting edge because the insert is subject to dynamic stresses in the direction normal to the cutting edge.

4). Thermal fatigue. At the highest cutting speeds, we observed cracks normal and parallel to the cutting edge (FIG 9). The temperature goes to extremes at high cutting speeds, and as the tool moves periodically in and out the workpiece, the temperature fluctuates. The tool-chip interface temperatures and temperature surges under the same

test conditions of this paper were calculated in reference [14]. A thermal cycle combined with thermal shock causes the thermal fatigue.

5). Edge chipping. At the feed rate of 0.315 mm/tooth or above, the inserts are chipped. When the mechanical load is large enough, the cutting edge undergoes micro chipping. This micro chipping changes the geometry of the cutting edge and makes the actual rake angle more negative. The micro chipping stage usually does not last long, and macro chipping will follow when enough micro chipping occurs.

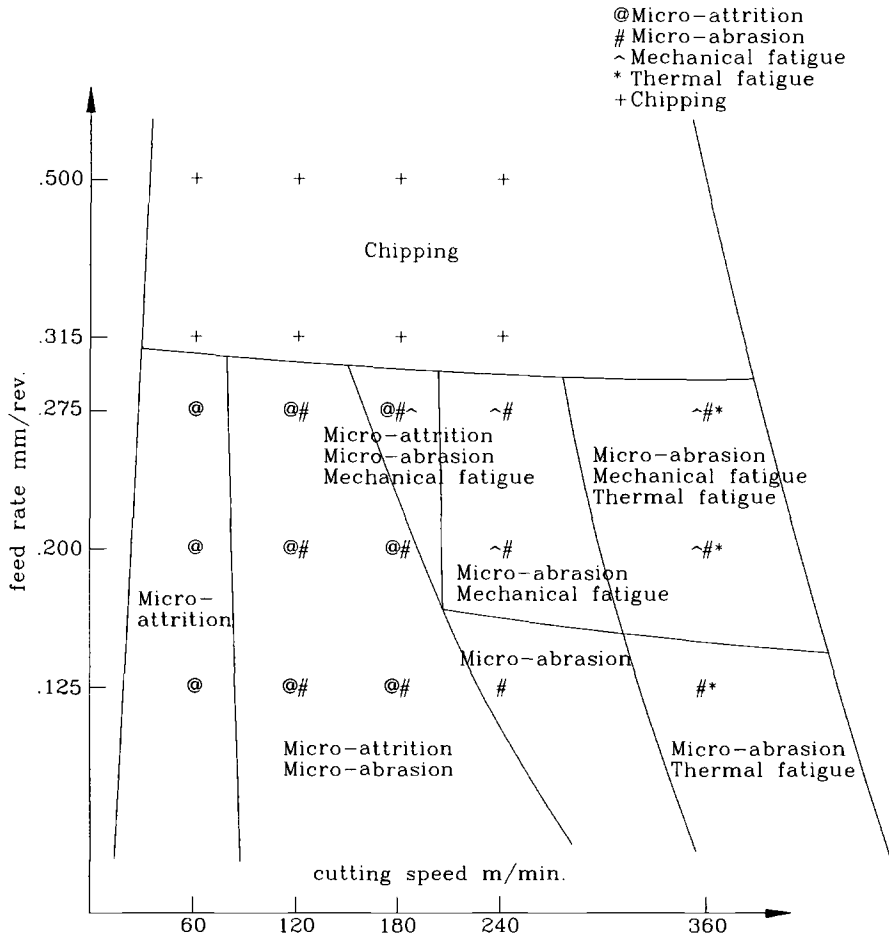


FIG 4 -- Wear mechanism map, C5 milling inserts, 4140 pre-heat treated steel, dry cutting.

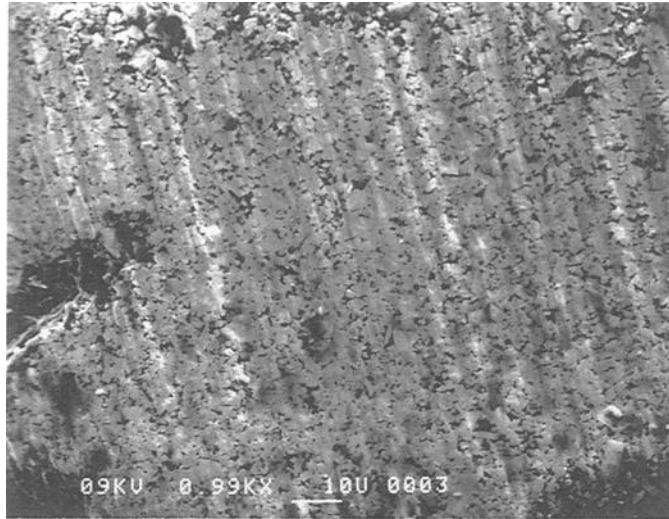


FIG 5 -- *Wear of flank face, X1000 magnification. Cutting speed 60 m/min, feed rate 0.125 mm/tooth, dry cutting. The flank face appears flat with carbide grains and the cobalt binder at the same height.*

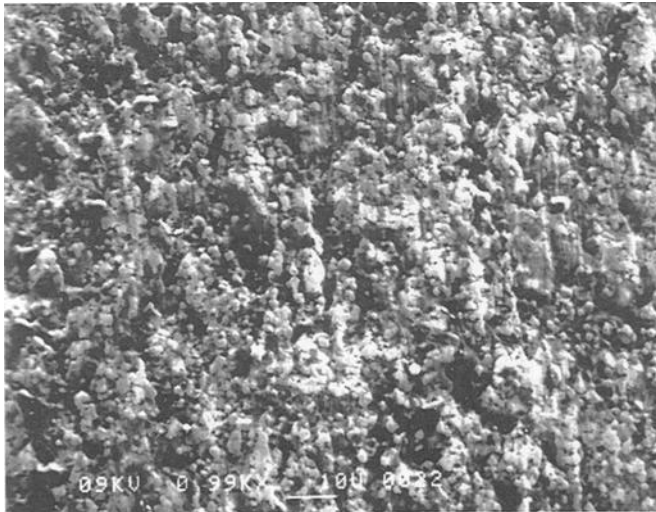


FIG 6 -- *Wear of flank face, X1000 magnification. Cutting speed 240 m/min, feed rate 0.125 mm/tooth., dry cutting. The carbide grains are shown protruding out of the flank face.*

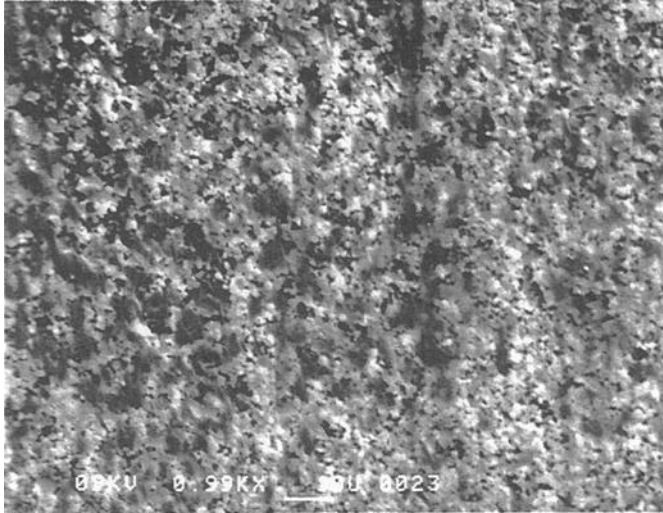


FIG 7 -- *Wear of flank face, X1000 magnification. Cutting speed 120 m/min, feed rate 0.125 mm/tooth, dry cutting. The face shows flats surrounded by protruding carbide grains.*

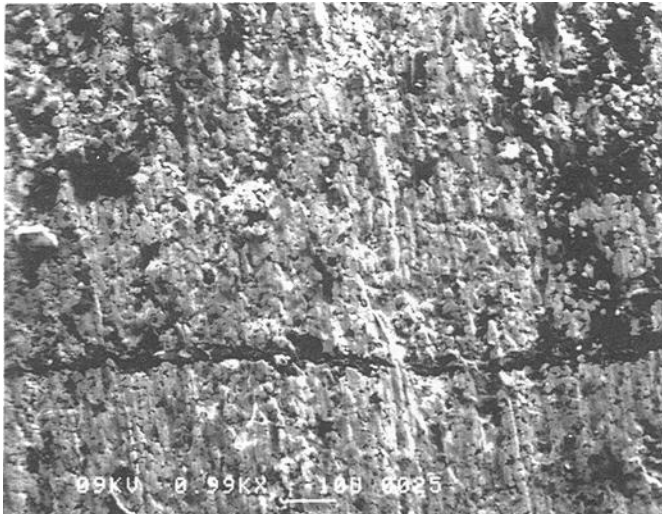


FIG 8 -- *Wear of flank face, X1000 magnification. Cutting speed 240 m/min, feed rate 0.275 mm/tooth, dry cutting. Mechanical fatigue cracks are parallel to the cutting edge.*



FIG 9 -- Wear of flank face, X1000 magnification. Cutting speed 360 m/min, feed rate 0.125 mm/tooth, dry cutting. Thermal fatigue cracks are perpendicular or normal to the cutting edge.

Milling Test with Coolant

The tool material, workpiece material, feed and speed matrix for tests with coolant were identical to those used without coolant. A copious flood of coolant (Trim Sol, 5% concentration) was applied to the cutter and cutting zone.

TABLE 2 shows the tool lives of inserts with coolant applied in the milling tests. Compared with TABLE 1 for dry cutting, it seems the inserts survive chipping better if coolant is used (see the last rows of both tables). Although there are temperature surges, the average temperature of the inserts is low in the presence of coolant. The lubricity introduced by the coolant reduces the cutting energy, which reduces the effect of the mechanical impact.

TABLE 2 -- Tool life of inserts with coolant on (cutting length, meter)

		cutting speed v (m/min)				
		60	120	180	240	360
feed per tooth mm/tooth	0.125	312m	978m	675m	606m	536m
	0.200	378m	815m	611m	524m	416m
	0.275	360m	730m	546m	487m	307m
	0.315	294m/c	226m/c	185m/c	10m/c	n/a

FIG 10 is the 3-D view of TABLE 2. The optimum conditions are at a cutting speed of 120 m/min, and feed rate of 0.125 mm/tooth, which coincides with the optimum conditions of dry cutting. The tool life profile map in FIG 10 has a similar shape as the one for dry cutting except the slope is less steep. To obtain a comparison between cutting with and without coolant, we calculated enhancement factors by dividing the tool life of wet cutting by the tool life of dry cutting. The results are shown in TABLE 3 and the table is plotted as a 3-D view in FIG 11.

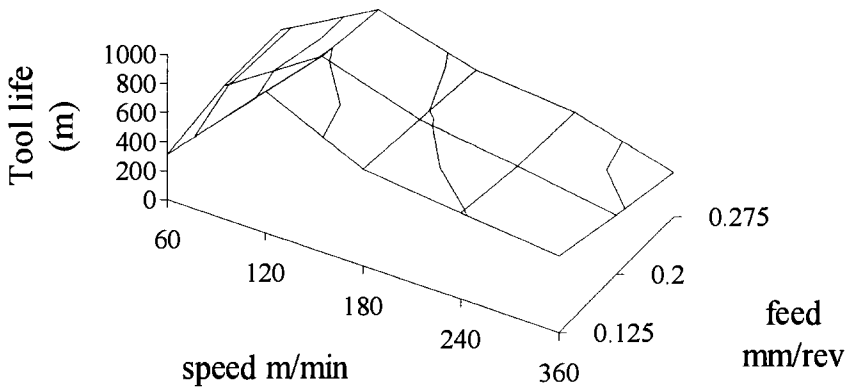


FIG 10 -- 3-D view of tool life of C5 insert when coolant is on

TABLE 3 -- Enhancement factors
(tool life wet/tool life dry) of wet cutting over dry cutting

		cutting speed v(m/min)				
		60	120	180	240	360
feed per tooth mm/tooth	0.125	1.63	0.64	0.81	1.05	1.16
	0.200	1.11	0.56	0.78	1.05	1.08
	0.275	0.85	0.55	0.81	1.08	1.17

The first column of TABLE 3 shows that at low speed the use of coolant helps the tool performance. When the feed is the lowest, the BUE is the heaviest for both dry and wet cutting. An enhancement factor of 1.63 on the top left corner of the table shows that coolant has a positive effect on reducing BUE and therefore increases tool life. We described before that BUE is primarily related to cutting speed. However,

BUE also depends on the feed rate. As the feed increases, the amount of BUE decreases. To understand this, we notice that the finished surface of a face milled part consists of a series of grooves cut by the insert nose radius. The formation of BUE is an interaction between the cutting edge and the workpiece material. This interaction is most likely to occur at the tip of the nose radius, which is the bottom of the machined groove valley, because the cutting force there is the highest. BUE is less likely to occur at the peak of the machined grooves. As feed rate increases, BUE at the peak of the groove gradually diminishes. Therefore, the amount of BUE for the entire cutting edge is reduced as the feed rate is increased [14]. Since the BUE is not as heavy at high feed rates, the benefit from using a coolant is reduced as feed rate increased, which is obvious in the first column in TABLE 3.

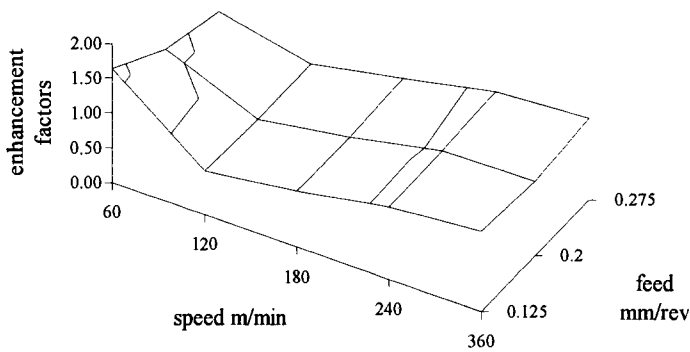


FIG 11 -- *Enhancement factor of milling with coolant over dry cutting*

The enhancement factor drops for the second and third rows in the first column of TABLE 3. In the mid range of cutting speed, the use of coolant has an obvious negative effect on tool life. The coolant introduces lubricity and antiwear properties, and lowers the average temperature. On the other hand, during the cutting period, the temperature of the cutting tool rises sharply due to the cutting energy. In the period when the tool is out of the cutting zone, the temperature is expected to drop quickly due to the application of the cutting fluid. These temperature surges subject the tool to thermal shock and fatigue which can reduce tool life. In the mid range of cutting speed, the negative effect of temperature surges surpasses the positive effects of the coolant and results in a reduction in tool life. As the cutting speed increases further, the enhancement factors exceed 1. The water based coolant in high speed cutting is effective in lowering the average temperature of the tool. This effect relieves the loss

of hot hardness and reduces the abrasive wear. However, the enhancement factors in the last two columns are barely over 1. There is no statistical significance to conclude that the use of coolant is better than dry cutting even in high speed cutting. The trend is clear that the tool performs better as the speed increases in wet cutting. In all of the cutting speed ranges, two effects are competing with each other: the negative effect of temperature surge and the positive effect of lowering average temperature. In the mid speed range, the negative effect predominates and results in an enhancement factor less than 1. As the speed increases, the positive effect predominates and leads to higher enhancement factors.

To summarize for machining with coolant, four wear mechanisms were identified for the flank wear: micro-attrition, micro-abrasion, thermal pitting, and edge chipping, as shown in FIG 12.

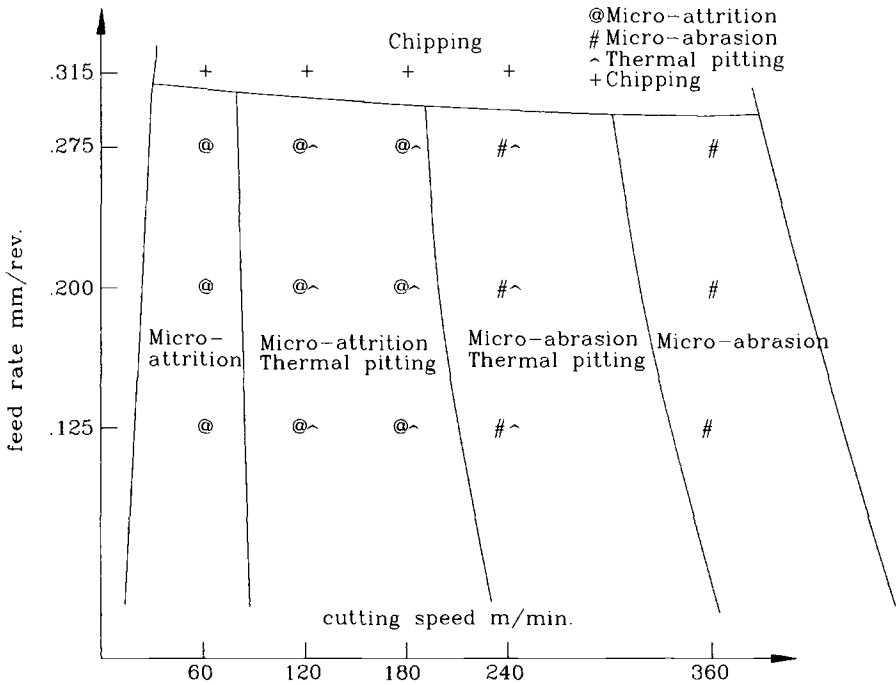


FIG 12 -- Wear mechanism map, C5 milling inserts, 4140 pre-heat treated steel, Trim-Sol coolant

1). Micro-attrition wear. When speed is low, BUE is still heavy even though the coolant reduces the BUE. The dominant wear mechanism is micro-attrition, (FIG 13). FIG 13 shows a dull flat of the worn flank face similar to FIG 5.

2) **Thermal Pitting.** Over the cutting speed range of 120-240 m/min, the flank faces of the inserts show pits of various sizes and depth, see Figs. 14-15. These pits are the result of thermal surges. The insert develops thermal cracks due to the thermal surges. These cracks are initiated over the whole flank face with shallow depth, and then lead to thermal pitting. The thermal fatigue in dry milling is different in nature. In dry milling the cracks caused by thermal fatigue are sparsely located and extended in depth. Thermal fatigue results in catastrophic failure in dry cutting instead of the thermal pitting seen in wet cutting.

3) **Micro-abrasion.** At high cutting speed, micro-abrasion dominates the flank wear, (FIG 16), where the carbide grains protrude out of the flank face. The coolant is effective in reducing the average temperature of the inserts. At lower temperature the inserts have higher strength which leads to higher resistance to mechanical fatigue.

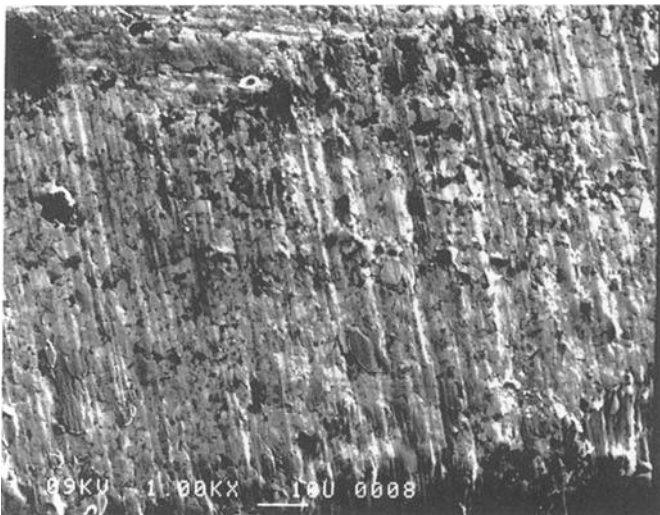


FIG 13 -- *Wear of flank face, X1000 magnification, micro-abrasion. Cutting speed 60 m/min, feed rate 0.125 mm/tooth, with coolant. The flank face appears flat with carbide grains and the cobalt binder at the same height.*

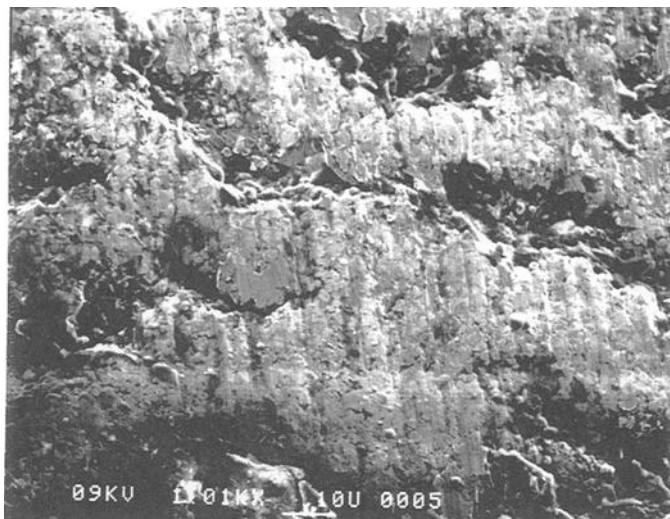


FIG 14 -- *Wear of flank face, X1000 magnification, thermal pitting. Cutting speed 120 m/min, feed rate 0.125 mm/tooth, with coolant. The dark areas are pits .*



FIG 15 -- *Wear of flank face, X1000 magnification, thermal pitting. Cutting speed 240 m/min, feed rate 0.200 mm/tooth, with coolant. The dark areas are pits.*

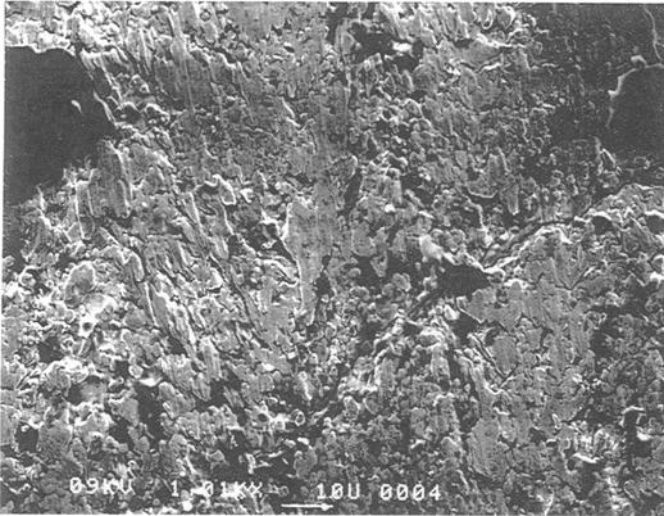


FIG 16 -- *Wear of flank face, X1000 magnification, micro-abrasion. Cutting speed 360 m/min, feed rate 0.200 mm/tooth, with coolant. The carbide grains are shown protruding out of the flank face.*

Discussion

The optimum cutting conditions based on tool life only were found to be a speed of 120 m/min and a feed rate of 0.125 mm/tooth, may not always be the best choice. In a production environment, optimization criteria involve more than just direct tooling cost. The production rate, labor cost, downtime, and equipment depreciation, all play a role in the final production net profit. A tool life curve such as the one shown in FIG 2 provides essential information for an overall optimization. One may want use a high feed rate in roughing. On the other hand, an engineer may want to use high cutting speed to achieve high production rate. A 3-D tool life profile map as the function of speed and feed over extended cutting condition range gives the engineer the liberty to balance the tool cost with other production parameters.

In this paper, the wear mechanisms of dry and wet cutting are presented by means of wear maps. These maps are useful for an engineer in trouble shooting. For example, if an abrasive mode is identified, the engineer may check the corresponding cutting speed. He may slow down the speed, but increase the feed rate to keep the material removal rate the same if the surface roughness is not critical.

An overall enhancement factor was calculated by dividing the average of all items in TABLE 2 by the average of TABLE 1. This enhancement factor of wet cutting over dry cutting is 0.81. Based on the tests described above, we recommend caution in applying coolant for milling. Special tests should be carried out in evaluating potential coolant candidates. It is not always true that coolant will enhance tool life for milling.

Summary and Conclusions

A systematic tool life study for face milling inserts was conducted with and without coolant. Workpiece specimens made of 4140 steel were cut by C5 grade carbide inserts under various cutting conditions. The comparison between dry and wet cutting shows that caution should be taken when applying a coolant for milling operations.

Wear mechanisms are presented by means of wear maps. Identified wear mechanisms are: micro-attrition, micro-abrasion, mechanical fatigue, thermal fatigue, thermal pitting, and edge chipping. The wear mechanisms observed in this paper reveal tool failure modes that help explain tool wear. At low cutting speeds, BUE prevails and accelerates wear. At medium speeds, micro attrition and abrasion are dominant wear mechanisms. At high speeds, the tool temperature is high and tool life is reduced.

The intermittent nature of milling produces temperature surges at the insert cutting edge. The application of coolant lowers the average temperature but increases the range of temperature surges (the temperature fluctuation as the insert disengages and engages the part). The test data show that the application of coolant may provide a negative effect on tool life.

Acknowledgments

The authors greatly appreciate the suggestions and comment of Dr. J. A. Spearot and Dr. D. J. Smolenski. Thanks to Curtis Wong for helping with the scanning electron microscopy analysis.

References

- [1] B.V. Niebel, A.B. Draper, R.A. Wysk, "Modern Machining Process Engineering," McGraw-Hill, New York, 1989, p.487.
- [2] E.G. Hoffman, "Fundamentals of Tool Design," 2nd ed., SME, Dearborn, MI, 1984, p. 83.
- [3] G. Boothroyd, W.A. Knight, "Fundamentals of Machining and Machine Tools," Marcel Dekker, New York, 1989, p.178.
- [4] "Machinery's Handbook," 24th edition, Industrial Press Inc. New York. 1992.
- [5] Drozda Wick, SME Handbook on Machining, Volume 1, SME Publisher, 1993.
- [6] B.H. El-Bialy, A.H. Redford, B. Mills, "Proposed Wear Mechanism for Titanium Nitride Coated High Speed Steel," *Surface Engineering*, Vol. 2, 1986, pp. 29-34.
- [7] F.A. Soliman, O.A. Abu-Zeid, M. Merdan, "On the Improvement of the Performance of High Speed Steel Turning Tool by TiN Coatings," *Wear*, Vol. 119, 1987, pp. 199-204.
- [8] G.R. Frenske, N. Kaufherr, R.H. Lee, B.M. Kremer, "Characterization of Cratering Wear

- Phenomenon in Nitride and Carbide Coated Tool Inserts," *Surface Coating Technology*, Vol. 36, 1988, pp. 791-800.
- [9] K.Y. Su, N.H. Cook, "Enhancement of High Speed Steel Tool Life by Titanium Nitride Super Coating," *5th North American Metalworking Res., Cnf*, 1977, pp. 297-302.
- [10] Sandvik Coromant, "Tool Wear, Optimizing Tool Performance Through Insert Wear Analysis," 1994.
- [11] P.K. Wright, E.M. Trent, "Metallurgical Appraisal of Wear Mechanisms and Processes on High-Speed-Steel Cutting Tools," *Metals Technology*, January, 1974, pp. 13-23.
- [12] S.C. Lim, S.H. Lee, Y.B. Liu, K.H. Seah, "Wear Maps for Uncoated High Speed Steel Cutting Tools," *Wear*, Vol. 170, 1993, pp. 137-144.
- [13] S.C. Lim, Y.B. Liu, S.H. Lee, K.H.W. Seah, "Mapping the Wear of Some Cutting Tool Materials," *Wear*, Vol. 162-164, 1993, pp. 971-974.
- [14] J. Gu, "Tribological behavior of cutting inserts used in face milling," Thesis, Oakland University, Rochester Michigan, 1997.

John H. Magee¹ and Ted Kosa¹

REDUCING TOOL WEAR WHEN MACHINING AUSTENITIC STAINLESS STEELS

Reference: Magee, J. H. and Kosa, T., "Reducing Tool Wear When Machining Austenitic Stainless Steels," *Wear Processes in Manufacturing, ASTM STP 1362*, S. Bahadur and J. Magee, Eds., American Society for Testing and Materials, 1999.

Abstract: Austenitic stainless steels are considered more difficult to machine than carbon steels due to their high work hardening rate, large spread between yield and ultimate tensile strength, high toughness and ductility, and low thermal conductivity. These characteristics can result in a built-up edge or excessive tool wear during machining, especially when the cutting speed is too high. The practical solution is to lower the cutting speed until tool life reaches an acceptable level. However, lower machining speed negatively impacts productivity. Thus, in order to overcome tool wear at relatively high machining speeds for these alloys, on-going research is being performed to improve cutting fluids, develop more wear-resistant tools, and to modify stainless steels to make them less likely to cause tool wear.

This paper discusses compositional modifications to the two most commonly machined austenitic stainless steels (Type 303 and 304) which reduced their susceptibility to tool wear, and allowed these grades to be machined at higher cutting speeds.

Keywords: screw machine test, tool wear, work-hardening rate, austenitic stainless steel

The significance of any scientific discovery does not become clear until several decades have passed. Clearly, a major metallurgical discovery of the twentieth century has been the addition of a critical amount of chromium to steel which dramatically improved corrosion resistance. Discovered around 1910[1], this new type of steel, dubbed stainless, has since developed into five distinct family of alloys and has a world-wide production of 1,000,000 tons annually. The most popular family of alloys is the austenitic that evolved from a basic steel composition of 18%Cr-8%Ni (commonly referred to as 18-8). They are known for their excellent corrosion resistance, strength, toughness and non-magnetic behavior. Austenitic stainless steels are commonly referenced as 300 series stainless per AISI (American Iron and Steel Institute) designation and, specifically, the steel containing 18%Cr, 8%Ni has been designated as Type 304.

¹Specialist and staff specialist, respectively Carpenter Specialty Alloy, 100 Bern St., Reading, PA 19612.

Upon their industrial use in the 1920's, machining difficulties were encountered, in comparison with carbon steel, due to their alloy content and austenitic structure. Specifically, at similar cutting speeds tools ran hotter with a tendency to produce a large built-up edge and excessive tool wear. By the early 1930's, it was discovered that an addition of sulfur (0.15% min.) to 18-8 greatly improved machinability[2]. This grade was designated as AISI Type 303. Sulfur in steels is present as discrete sulfide inclusions. The role of these inclusions in improving machining performance has been the basis of much study, and theories include lubrication, chip embrittlement, and stress-concentration effects as the mechanism for improving machinability. Whatever the reason, sulfides increase tool life, allow higher cutting rates, and benefit chip breakage/disposability. However, adverse effects can be seen in corrosion resistance, toughness, and formability.

Today after more than seventy years of use, Types 303 and 304 have become complementary alloys that still dominate the machining bar market. They have been thoroughly studied and continuously improved. A brief review of some key factors that influence tool wear and some recent compositional discoveries are discussed in this paper.

Machinability Test

In order to evaluate compositional and manufacturing effects on tool wear for Types 303 and 304, we developed a machinability test using an automatic screw machine, equipment typically used in production machine shops. The test procedure is based on ASTM E-618-Method for Evaluating Machining Performance of Ferrous Metals Using an Automated Screw/Bar Machine. Figure 1 is a schematic which shows the operations during the manufacture of the standard part on the screw machine. As the bar rotates, a high-speed-steel rough form tool shapes the part by feeding into the bar. Rough-form-tool feed is typically 0.002 ipr (inches per revolution). Drills generate heat and hollow out the part to ease cut-off by the cut-off blade. Heat from drilling simulates a key factor found in machining stainless steels in a production environment. Coolant used in this test is Microcut 540, a water-based cutting fluid used at a 5% concentration. A finish form tool shaves the surface of the larger diameter of the part. Finally, the cut-off blade severs the part. The bar is then indexed to the right for the next part.

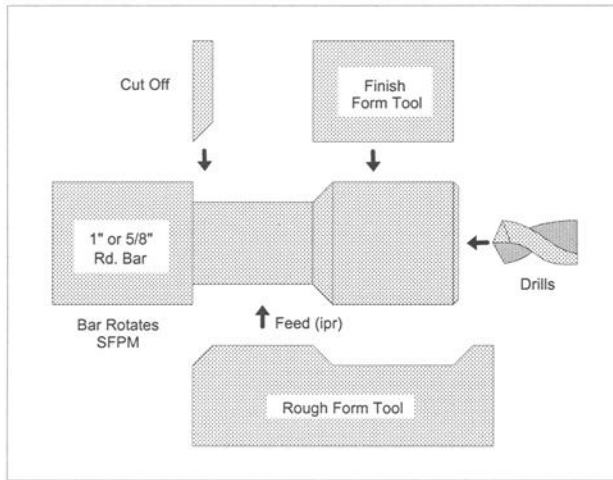


Figure 1 - *Schematic of Screw Machine Test*

This test does not provide an absolute number like a tensile test, but a relative comparison of one lot with another. The test speed (SFPM = surface feet per minute) is chosen so that the best material in the group to be evaluated can reach test termination within one shift, since our early experience with screw machine testing showed that interrupting a test overnight did not provide acceptable reproducibility of results. Normally, three tests are conducted per lot. The standard and desired test termination point is .003" growth of the rough-cut diameter of the test part, with part growth being a measure of the wear of the tool. However, in some cases, tool failure, i.e., burn out, will occur before part growth; therefore, tool failure is considered an alternate end point. In the case of austenitic stainless steel, the tool failure endpoint is quite common. Figure 2 depicts catastrophic tool failure of M2 rough-form tool.

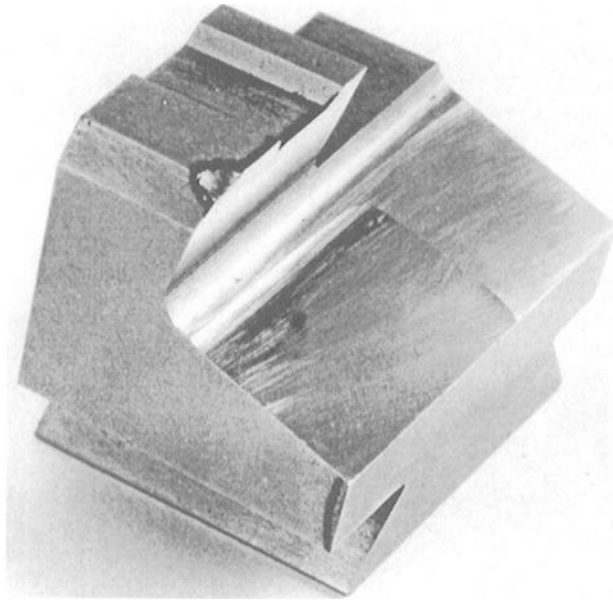


Figure 2 - Catastrophic M2 Rough-form Tool Failure

In some cases, particularly when there is a wide disparity in the machinability of materials, one alloy may not reach a termination point in a reasonable time frame, while the other comparative alloy reaches an endpoint in a very short time or small number of parts. In such cases, the "run-outs" are then used as the test results for the better lot, although this may preclude a statistical analysis using a t-test for significance. A large difference in the number of parts to test termination between materials or compositional modifications of the same alloy represents a significant difference in tool wear tendency. Secondary measures of machinability include the surface finish of the rough- and finish-cut surfaces of the part, measured using a profilometer, and a subjective characterization of the kind of chips being produced.

To confirm trends determined by laboratory screw machine tests, field trials at various production machine shops are performed whereby commercially-sold parts are manufactured. Large screw machine difference should correlate to increased productivity.

Effect of Residual Sulfur in Type 304

As previously discussed, it was known since the 1930's that the addition of sulfur (0.15% min.) dramatically reduces tool wear and increases machining speed in an 18-8 steel. In fact, our tests showed machining speed nearly doubles for Type 303 vs. Type 304[3]. However, this addition of sulfur is deleterious to corrosion, formability, and toughness; thus, many machined parts are manufactured from Type 304 bar and not Type

303. In the 1960's, machine shops observed that machinability varied from lot-to-lot for Type 304 bar. Eventually, it was postulated that machinability varied due to minor differences in sulfur content. Typically, sulfur content in Type 304 was <0.01%, but the maximum allowable sulfur per AISI is 0.03% max. Screw machine testing of controlled amount of sulfur determined that tool wear was improved with increasing amounts of residual sulfur. By having sulfur at the upper end of the allowable limit as shown in Figure 3[4], an enhanced- machining Type 304 was developed.

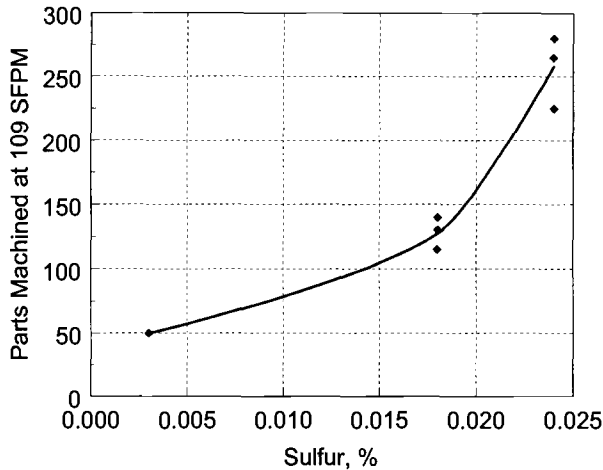


Figure 3 - *Effect of Sulfur Content on Type 304 Machinability*

C+N Content in Type 303

Carbon and nitrogen are critical elements in Type 303 and 304 since they help stabilize the austenitic structure at room temperature and minimize the potential for strain-induced martensite during machining operation. Typical C+N content in these steels has been 0.10%. This level balances known metallurgical concern with cost since lower C+N content generally requires an increased amount of expensive nickel. In austenite, C and N are strong interstitial strengtheners and increase the work hardening rate. These factors were believed to increase tool wear tendency and thus hurt machining productivity.

In the 1970's, a low C+N version of Type 303 was introduced for improved drilling characteristics. No significant difference in tool wear was observed in screw machine tests or machine shops. Studies[5,6] by others on lathe tests showed a slight improvement in tool life with decreasing C+N content; however, additional lathe studies performed on Type 303 with high Mn (outside alloy specification limits) revealed a more significant improvement in tool life. These tests measured the number of cuts, called wafers, by an M2 cut-off tool at a given machining speed prior to catastrophic tool wear. A greater number of cuts indicates less tool wear tendency for the material being

machined. Figure 4 depicts the effect with C+N content for Type 303 and high-Mn Type 303 on number of wafer cuts machined before excessive tool wear. It was postulated that an increased austenite stability due to the high Mn may have contributed to improved tool life[7]. Note, by reducing C+N, two elements which strongly increase austenite stability, other elements such as Mn, Ni and Cu need to be added to achieve equal or greater austenite stability[8].

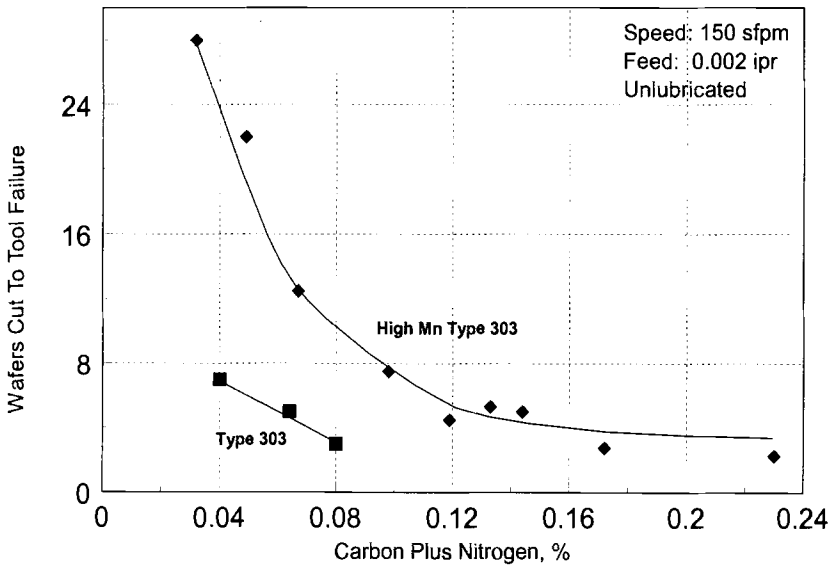


Figure 4 - Effect of C+N Content on Machinability Tool Failure for Type 303 and High Mn Type 303

Low C+N, Higher Ni+Cu in Type 303 and 304

Nickel content in both Type 303 and 304 has generally been between 8-9% for economic reason; however, to increase austenite stability, higher-nickel versions of Type 303 were investigated. Our screw machine results found in Table 1 reveal a significant improvement in machinability at 185 sfpm only in the low C+N, high nickel version of Type 303. Tool life was extended at this speed where a "run out" was declared for the low C+N, high Ni Type 303. Improved austenite stability due to higher Ni in combination with lower interstitial strengthening due to low C + N were both required to decrease tool wear. Work-hardening rate was also significantly reduced.

Table 1 - Effect of C+N and Nickel Content on Type 303 Machinability

Type 303 Parts Machined at 185 SFPM		
0.095 C+N 8.70 Ni	0.113 C+N 9.60 Ni	0.035 C+N 9.74 Ni
297	290	620+++

Additional work[9] was initiated on our screw machine to investigate the addition of Cu, an element known to reduce work-hardening rate and increase austenite stability. Results in Figure 5 show the dramatic improvement in parts machined due to reducing tool wear by the addition of 0.8% Cu to the low C+N high nickel Type 303. Field tests of this new version of Type 303 translated into a productivity gain of up to 50%. Unlike the screw machine test which measures the number of parts machined until significant tool wear or failure occurs, machine shops were decreasing cycle time by increasing speed and feed without negatively affecting tool life.

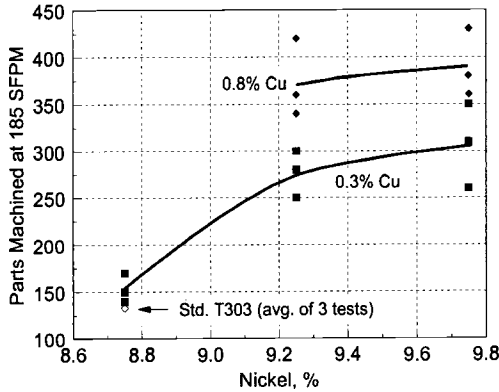


Figure 5 - Effect of Nickel & Copper Content on Low C+N Type 303 Machinability

Type 304 was the next steel to be evaluated on our screw machine for the effect of low C+N in combination with higher nickel content. Again, low C+N with 9.6% Ni dramatically improved machinability, see Table 2 below. Copper was then added to this low C+N, high nickel base and machinability was further improved, Figure 6. Little benefit was found when copper was increased beyond .77%. Additionally, this dramatic reduction in tool wear was observed in other austenitic stainless steels, like Type 316, which contains even higher nickel (10-14%) than Type 304 and an addition of 2% minimum Mo[10].

Overall, these screw machine studies and field trials dramatically demonstrated that the key to improve machinability in austenitic stainless steels is to fine-tune the austenite composition. These adjustments are aimed at reducing annealed hardness and lowering work hardening rate. These reduce tool wear and eliminate tool failure which are chronic problems in machining austenitic stainless steels. In production machine shops, these compositional adjustments mean higher machining speeds can be used.

Table 2 - Effect of C+N Content on High-Nickel Type 304 Machinability

Type 304 (9.6%Ni) Parts Machined at 117 SFPM	
0.098 C+N	0.038 C+N
203	533++

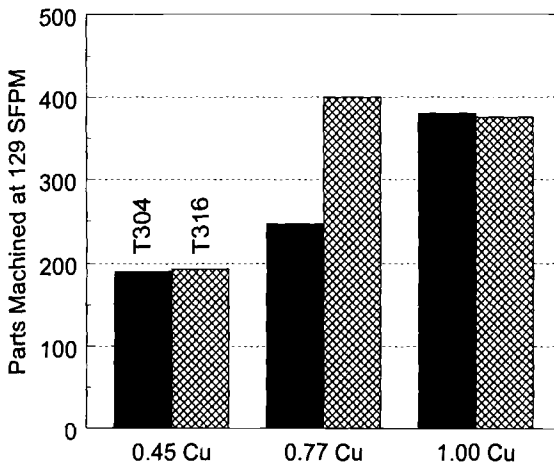


Figure 6 - Effect of Copper Content on Low C+N Type 304 & Type 316 Machinability

Summary

Tool wear has been the key limiting factor in machining austenitic stainless steels, largely due to high work hardening, large spread between yield and ultimate tensile strength, high toughness and ductility, and low thermal conductivity. A screw machine test based on ASTM E-618 has been used to evaluate compositional effects in austenitic stainless steels aimed at reducing tool wear. Earlier testing showed the benefit of high residual sulfur in Type 304 can affect tool life.

Recently, the emphasis has been on fine-tuning the composition of the austenite. Initial work on low C+N Type 303 resulted in insignificant effect on tool wear since any gain due to lower interstitial strengthening was offset by decreasing austenite stability. However, tool wear was dramatically improved when low C+N content was combined with high Ni+Cu content. This significant improvement was beneficial in high sulfur Type 303 as well as in low sulfur grades like Type 304 and 316.

References

- [1] Parr, J. G. and Hanson, A., "An Introduction to Stainless Steel," American Society of Metals, 1965, p. 12.
- [2] Palmer, F.R., "Ferrous Alloy," U.S. Patent 1,961,777, June 5, 1934.
- [3] Carpenter Guide to Machining Stainless Steels, Copyright 1985, p. 14.
- [4] Kosa, T., Ney Sr., R. P., "Machining of Stainless Steels," *Metals Handbook*, Volume 16, 9th Edition, pp. 681-707.
- [5] Eckenrod, et al, "Low Carbon Plus Nitrogen, Free-Machining Austenitic Stainless Steel," U.S. Patent 4,613,367, September 23, 1986.
- [6] Eckenrod, et al, "Low Carbon Plus Nitrogen, Free-Machining Stainless Steel," U.S. Patent 4,784,828, Nov. 15, 1988.
- [7] Rhodes, G. O., Eckenrod, J. J. and Pinnow, K. E., "A High Manganese Free-Machining Austenitic Stainless Steel," *Proceedings of High Manganese Austenitic Steels*, ASM International, 1987, pp. 53-61.
- [8] Novak, C. J., "Structure and Constitution of Wrought Austenitic Stainless Steels," *Handbook of Stainless Steels*, Chapter 4, pp. 4-29.
- [9] Kosa, et al, "Free-Machining Austenitic Stainless Steel," U.S. Patent 5,482,672, January 9, 1996.
- [10] Kosa, et al, "Free-Machining Austenitic Stainless Steel," U.S. Patent 5,512,238, April 30, 1996.

Christina Y. H. Lim,¹ Seh-Chun Lim,¹ and Kim-Seng Lee¹

MACHINING CONDITIONS AND THE WEAR OF TiC-COATED CARBIDE TOOLS

REFERENCE: Lim, C. Y. H., Lim, S.-C., and Lee, K.-S., “**Machining Conditions and the Wear of TiC-Coated Carbide Tools,**” *Wear Processes in Manufacturing, ASTM STP 1362*, S. Bahadur and J. Magee, Eds., American Society for Testing and Materials, 1999.

ABSTRACT: This paper examines the wear behavior of TiC-coated cemented carbide tools in turning. Experimental data from dry turning tests, together with similar data from the open literature, are used to construct wear maps depicting the flank and crater wear characteristics of these tools over a wide range of machining conditions. The maps show that both flank and crater wear rates vary according to the cutting speeds and feed rates used. An overall wear-damage map for this class of coated tools is also presented for the first time. The presence of the safety zone and the least-wear regime, within which the overall wear damage to the tools is low, suggests the possibility of selecting the machining conditions to achieve a compromise between the rates of material removal and tool wear.

KEYWORDS: flank wear, crater wear, overall wear damage, wear maps, safety zone, TiC coatings, cemented carbide tools

The wear of tools in metal cutting accounts for a sizeable portion of the manufacturing costs of products and components. Although tool wear is rarely catastrophic, it lowers the operating efficiency and increases the rate of tool replacement.

¹ Assistant professor and associate professors, respectively, Department of Mechanical and Production Engineering, National University of Singapore, 10 Kent Ridge Crescent, Singapore 119260, Republic of Singapore.

While wear can never be totally eliminated, it may be reduced by using tool materials that are more resistant to wear, or by operating under conditions that will result in less tool wear. One notable example of the first means of wear reduction is the proliferation of coated tools in the last three decades. Virtually all metal cutting tools today are coated with either single, or more usually, multiple, layers of hard, wear-resistant materials such as titanium nitride (TiN), titanium carbide (TiC) and aluminum oxide (Al_2O_3) [1]. Diamond, the hardest substance of all, has also been recently applied to cutting tools in coating form [2]. Besides reducing tool wear, such coatings also bring about significant improvements in cutting economies and tool performance through lower cutting forces and better surface finish of the workpiece [3].

The second approach towards tool wear reduction is manifested in the detailed recommended machining conditions for various combinations of tool and work material found in handbooks (see for example, [4-6]). While this wealth of data may assist the machinist in selecting the appropriate machining conditions, such information is not particularly useful to the engineer or tool designer in understanding the wear processes that take place during machining. It would be beneficial to have a global framework where the wear behavior of cutting tools could be understood in relation the operating conditions. This would contribute to a more informed and educated selection of the most suitable tool material and machining conditions for a particular application.

A previous investigation [7] showed that the application of TiN coatings onto high speed steel (HSS) tool inserts dramatically expands the range of machining conditions within which acceptable rates of flank wear may be experienced during dry turning operations. The findings suggested that the degree by which TiN coatings improve the wear performance of uncoated HSS tools is not uniform, but instead depends very much on the machining conditions used.

Having studied the wear of coated HSS inserts, the attention is now focused on coated carbide inserts, which are widely used in industry today. This work examines the flank and crater wear characteristics of TiC-coated cemented carbide tool inserts during dry turning of steel workpieces under a wide range of machining conditions. The methodology of wear maps from the earlier work is applied here to explore the ways in which these tools may be used in a more effective manner.

Experimental Details

A series of experiments was executed in accordance with the International Standard ISO 3685-1977 (E) test for single-point turning tools [8]. Commercially available TiC-coated tool inserts of geometry ISO SNMN 120408 from Sumitomo's AC720 coated grade were used in these tests. The cemented carbide substrates belonged to the ISO application group P20-P30 and these had been coated with TiC to an average thickness of $8.5 \mu\text{m}$. Knoop microhardness indentation testing on the TiC coating with a load of 50 gf indicated a mean hardness of 2678 kg/mm^2 . The workpiece material, a hot-

rolled medium carbon steel (AISI 1045 equivalent) with an average hardness of 89 HRB, was used in its as-received condition. A toolholder of designation ISO CSBNR 2525M12 was employed to achieve the specified cutting geometry listed in Table 1. The chipbreaker, which formed part the clamping mechanism of the toolholder, was fully wound back during the tests to prevent it from supporting the chip and shortening the contact length.

TABLE 1 – *Tool geometry for turning tests.*

Back rake angle	-6°
Side rake angle	-6°
End clearance angle	6°
Side clearance angle	6°
End cutting edge angle	15°
Side cutting edge angle	15°
Nose radius	0.8 mm

A total of 13 sets of various combinations of cutting speed and feed rate were selected for the tests, with the aim of adequately covering the recommended range of machining conditions for coated tools [4-6]. The choice of these 13 conditions was also influenced in part by the need to explore the wear behavior under certain machining conditions for which no wear data were available from the open literature. This was to ensure the proper construction of the wear maps later. The depth of cut was kept constant since it has been shown that this parameter has little effect on tool wear [9]. A value of 2 mm was chosen, based on the average depth of cut used in the machining tests of other researchers whose data were extracted for the wear maps. No cutting fluid was used in these experiments, as stipulated in ISO 3685-1977 (E) [8].

Results and Discussion

Tool Wear Data

According to ISO 3685-1977 (E) [8], flank and crater wear are measured by the width of the flank wear land, VB, and the depth of the crater, KT, respectively. These measurements are illustrated schematically in Fig. 1.

It has been shown previously [10] that the rates of flank and crater wear may be more meaningfully portrayed by the dimensionless parameters of VB and KT per unit

cutting distance respectively. These quantities are more conveniently represented by $\log(VB \text{ or } KT / \text{cutting distance})$, and they are used in the present study to describe the wear behavior of these coated carbide tools.

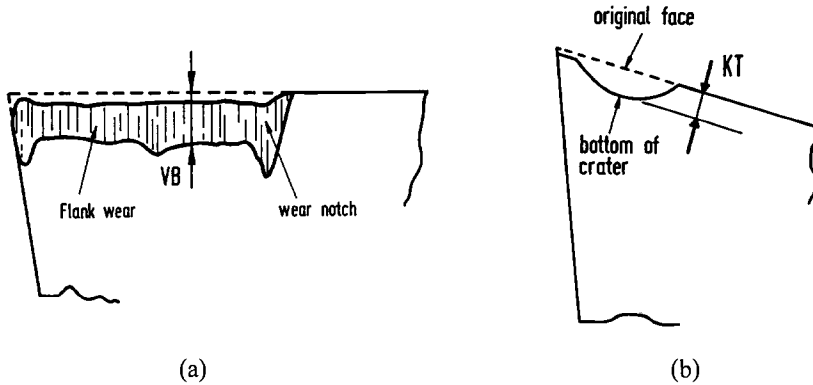


FIG. 1 – Measurement of (a) flank, and (b) crater wear (after ISO 3685-1977 (E) [8]).

Wear Maps for TiC-Coated Carbide Tools

Wear maps are useful tools for presenting the overall behavior of wearing systems in a more complete and meaningful fashion [11-13]. Research on metals [14-17], ceramics (see for example, [18]), and some cutting tools [7,10,19] has shown that such maps facilitate the study and understanding of the relationships between measured wear rates and the dominant wear mechanisms over a wide range of operating conditions. The wear-map approach is adopted in this work to examine the wear characteristics of the TiC-coated carbide tools.

The construction of a wear map first requires the extensive gathering of wear data from the technical literature for the particular wear system of interest. In this case, information relating to flank and crater wear of TiC-coated carbide tools during dry turning of steel workpieces was collected. The axes of the map are then decided: usually two (sometimes three) operating parameters of the system are selected to form a plane (or space) within which empirical wear data are presented. Here, the same axes as those employed previously [7,10,19]; namely, cutting speed (in m/min) and feed rate (in mm/rev), are used.

The results of the present cutting tests, together with similar data from 35 other sources, are used to construct the wear-rate maps for flank and crater wear of TiC-coated carbide tools, shown in Figs. 2 and 3 respectively. The map for flank wear in Fig. 2 is somewhat different from that presented earlier [20]; it has been revised in accordance with

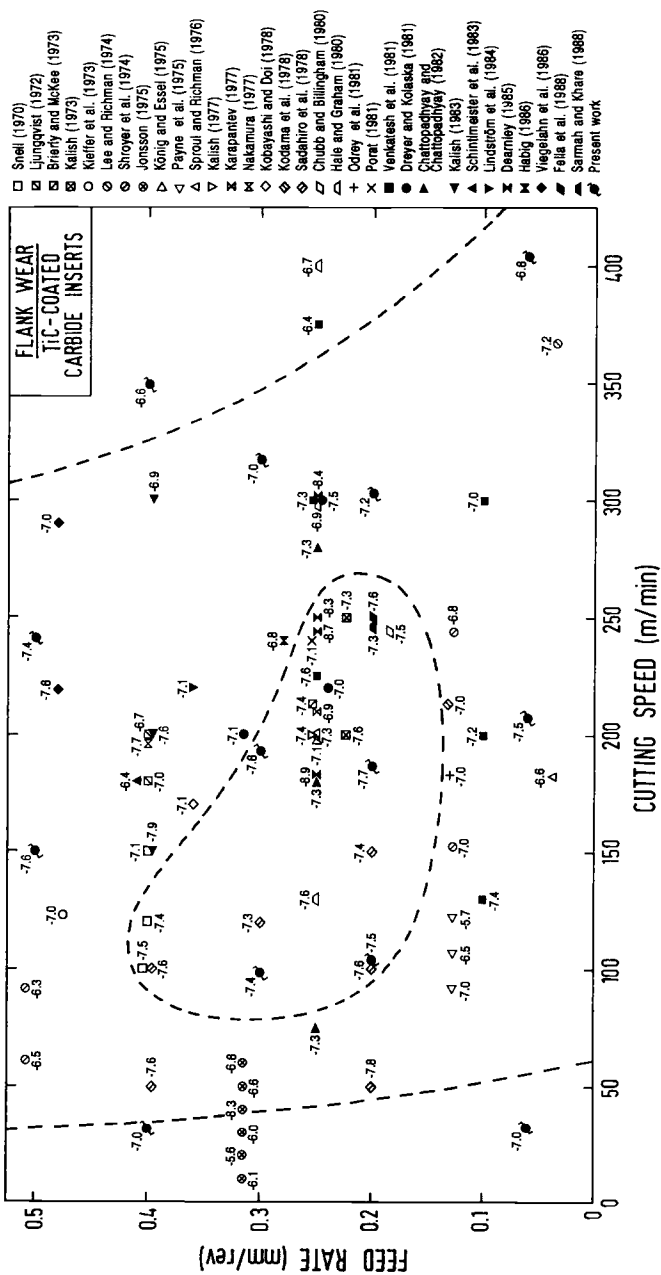


FIG. 2 – Map showing the flank wear rates of TiC-coated carbide tools during turning.

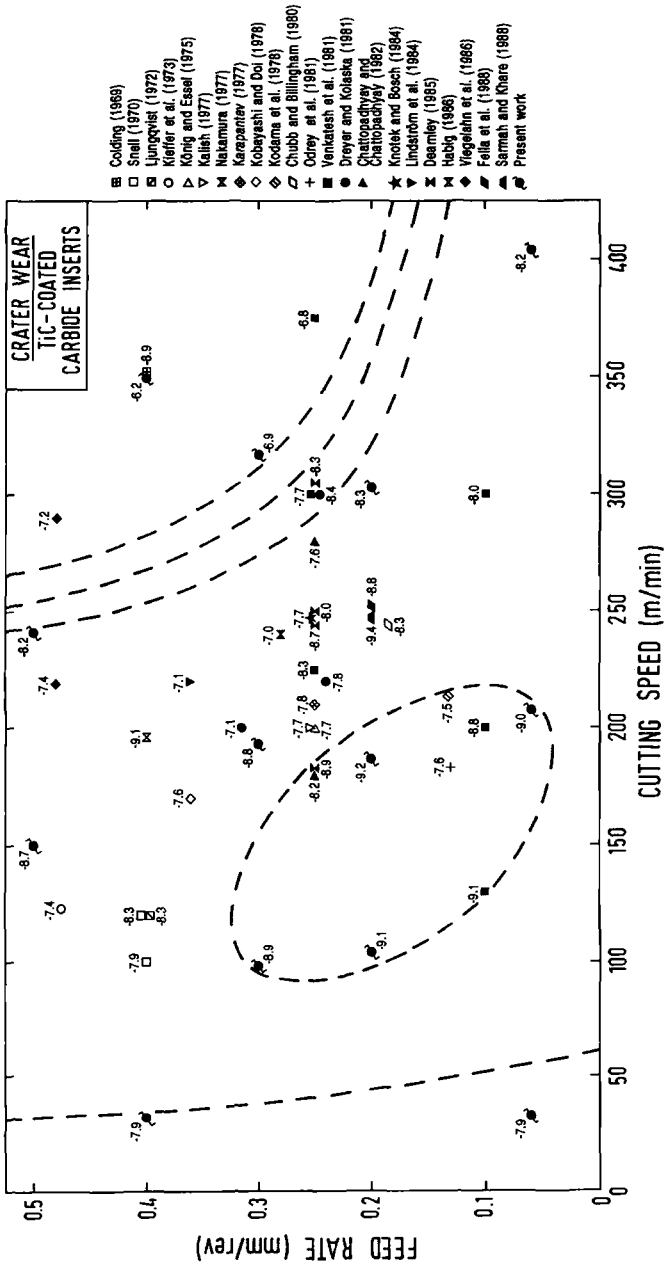


FIG. 3 - Map showing the crater wear rates of TiC-coated carbide tools during turning.

new data acquired after completing the earlier map. The crater wear map is presented for the first time. Each point on the maps represents a unique machining condition defined by cutting speed and feed rate. The number found next to the point is the flank or crater wear rate measured under that particular condition; the more negative the value, the smaller the wear rate (for example, a wear rate of -7.5 is one order of magnitude lower than -6.5).

Close inspection of the wear rates on these maps reveal some scatter: this is inevitable when comparing data produced by different people over a period of nearly 30 years. However, in spite of these local variations and apparent “conflicts” in the wear rates, an overall trend still emerges, and it is possible to define different regions on each map within which wear rates of a similar range of values are contained. These areas are delineated by the dashed boundaries on the maps. Three major wear regions are demarcated on the flank wear map; these are: the safety zone (wear rates < -7.5), the moderate-wear region (-7.0 to -7.4), and the high-wear zone (> -6.9). On the crater wear map, the wear rates span a wider range than in the case of flank wear, and these are divided into five regimes: the safety zone (< -8.5), a least-wear zone (-8.0 to -8.4), and three other higher-wear regions (> -7.9).

To obtain a clearer picture, the dashed boundaries are replotted in Figs. 4 and 5 with the data points removed and a unique shading applied to each of the different areas. The boundaries on the wear maps reflect the influence of cutting speed and feed rate on the wear of the inserts. Tool wear does not increase in a linear nor uniform manner with increasing speed and feed: at low cutting speeds, the wear rate is fairly high, but this decreases as speed and feed increases, reaching a minimum under moderate cutting conditions before rising again when speed and feed are increased further.

The safety zones and least-wear regimes on the maps for both flank and crater wear coincide with much of the range of cutting speeds and feed rates recommended for normal machining with this class of tools, typically between 80 to 250 m/min and 0.1 to 0.6 mm/rev respectively. With the use of this map, it is possible to optimize the machining operation by adjusting the cutting conditions such that a fairly low level of flank or crater wear can be maintained without too much compromise on the desired rate of material removal.

Overall Wear Damage

In practice, it is not possible to isolate a tool from wear at its flank face or rake face, as these processes occur simultaneously during machining. It may therefore be more useful to consider the total amount of wear damage due to both flank and crater wear. This concept was first proposed when studying the wear of uncoated HSS tools [10]. Since flank and crater wear have no direct relationship with each other, it is not possible to merge the measured flank and crater wear rates in a meaningful manner. However, by defining an arbitrary unit that describes the “degree of wear damage” sustained by the tool, the two wear-rate maps may be usefully combined. The overall wear-damage map is

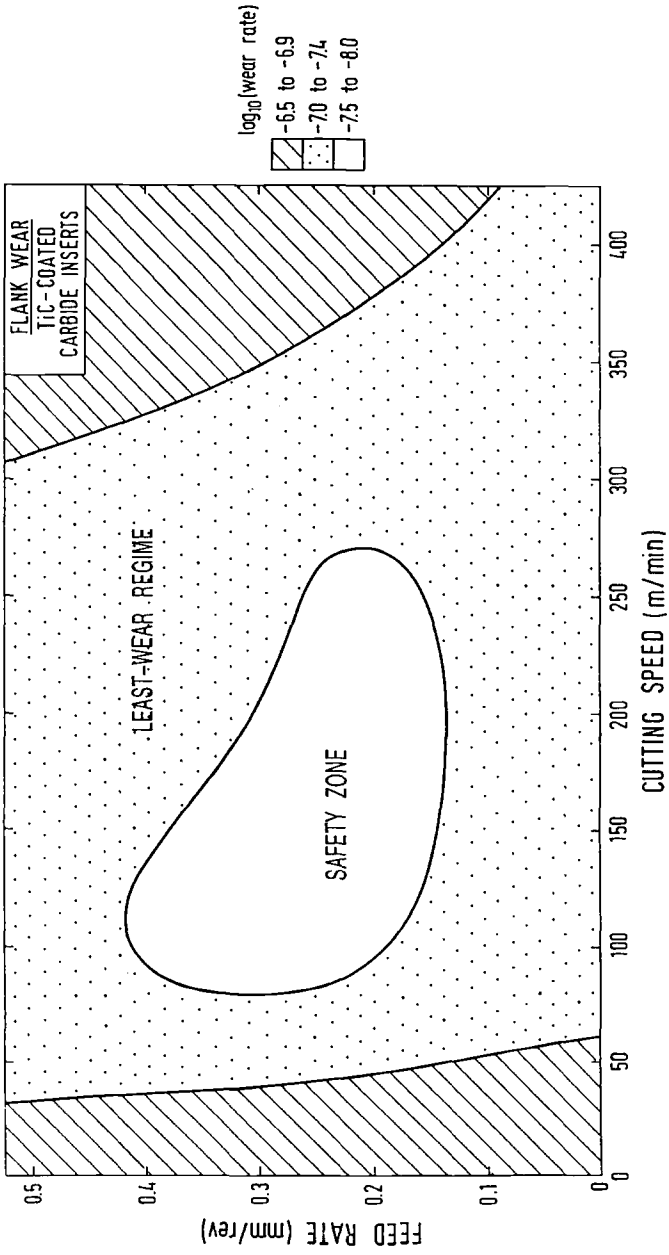


FIG. 4 – Map for flank wear of TiC-coated carbide tools during turning.

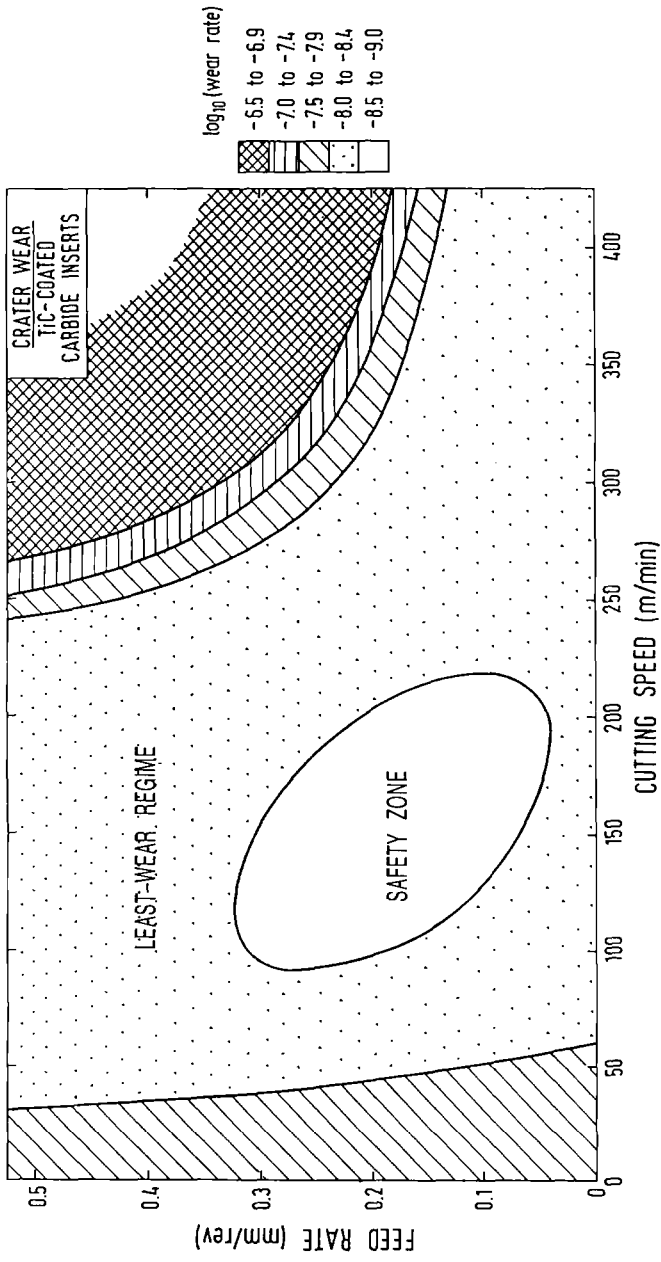


FIG. 5 – Map for crater wear of TiC-coated carbide tools during turning.

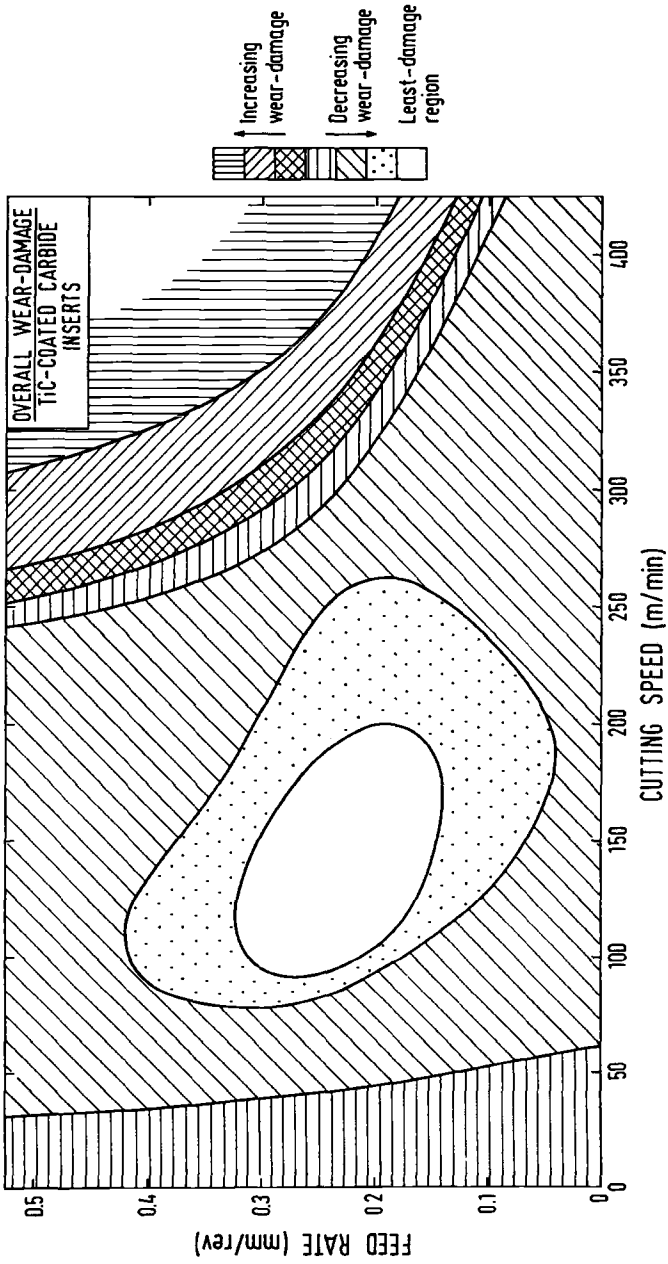


FIG. 6 – Overall wear-damage map for TiC-coated carbide tools during turning.

constructed by superimposing the maps for flank and crater wear, and combining the two safety zones to give a region with the least overall wear damage; the overlap of one safety zone with the next least-wear region of the other map would give the next least-wear-damage region, and so on, with a certain amount of liberty taken to smooth out some of the boundaries. The final map is shown in Fig. 6.

The least-damage zone in Fig. 6 is the range of machining conditions where the tool will sustain the least amount of both flank and crater wear. This region is smaller than either of the safety zones on the flank and crater wear-rate maps. At the low-speed end of the map, the contours are identical to those on both flank and crater maps; this suggests that similar wear processes may be operating at the flank and rake faces in that speed range. At high speeds and feeds however, the boundaries are similar to those on the crater wear map, indicating the dominance of crater wear under those conditions.

Similar observations have also been made by other workers previously. Stjernberg and Thelin [21], as well as Lindström et al. [22], found that tool life was limited by crater wear when they performed tests at cutting speeds ranging from 180 to 240 m/min with a feed rate of 0.36 mm/rev. Similarly, Viegelahn et al. [23] observed deep craters forming at 379 m/min and 0.48 mm/rev that eventually led to catastrophic failure of the tool. Chubb and Billingham [24] reported that wear on the flank face was slower than at the crater when testing at 244 m/min and 0.185 mm/rev feed. Their machining condition lies within the safety zone of the flank map but outside that of the crater map, thus supporting their observation of a lower flank wear rate. In another study, Colding [25] found that crater wear was between 5 to 10 times greater than flank wear when cutting between 220 to 352 m/min and 0.4 mm/rev. Finally, Dearnley [26] also noted that the flank wear rate became less than the crater wear rate as the cutting speed was raised. The fact that the overall wear-damage map correctly reflects all these observations lends support to the viability of this map as a meaningful description of the wear suffered by TiC-coated carbide tools under different machining conditions.

Concluding Remarks

This study has demonstrated that flank and crater wear rates for TiC-coated carbide tools vary with cutting speed and feed rate. They are highest at high speeds and feeds, but they also show a modest increase at very low speeds; the lowest wear rates are obtained under moderate cutting conditions. It has also been shown that the lives of these tools are limited by crater wear at high speeds and feeds, while flank wear becomes the controlling factor at lower speeds and feeds. A wear map may be seen as a useful depiction of the overall wear behavior of these tools, in much the same spirit as an equilibrium phase diagram is of an alloy. Wear maps could become ideal complements to the detailed recommendations found in machining handbooks in helping the machinist select the appropriate conditions where a maximum metal removal rate may be coupled to an optimum interval between tool changes in order to attain the highest productivity. The

wear maps also provide valuable global frameworks by which future, more detailed investigations of the wear of these tools may be related.

References

- [1] Clavel, A., "Coated Tools: Two Decades of Improving Productivity," *Cutting Tool Engineering*, Vol. 41, No. 1, February 1989, pp. 68-73.
- [2] Inspektor, A., Bauer, C. E., and Oles, E. J., "Superhard Coatings for Metal Cutting Applications," *Surface and Coatings Technology*, Vol. 68/69, 1994, pp. 359-368.
- [3] Wick, C., "Coatings Improve Tool Life, Increase Productivity," *Manufacturing Engineering*, Vol. 97, 1986, pp. 26-31.
- [4] Machining Data Center, *Machining Data Handbook*, Vol. 1 and 2, Metcut Associates Inc., Cincinnati, OH, 1980, 3rd ed.
- [5] Davis, J. R. (ed.), *Metals Handbook, Vol. 16: Machining*, ASM International, Metals Park, OH, 1989, 9th ed.
- [6] Drozda, T. J. (editor-in-chief), *Tool and Manufacturing Engineers Handbook, Vol. 1: Machining*, Society of Manufacturing Engineers, Dearborn, MI, 1983, 4th ed.
- [7] Lim, S. C., Lim, C. Y. H., and Lee, K. S., "The Effects of Machining Conditions on the Flank Wear of TiN-Coated High-Speed-Steel Tool Inserts," *Wear*, Vol. 181-183, 1995, pp. 901-912.
- [8] "Tool-Life Testing with Single-Point Turning Tools," *International Standards, ISO 3685-1977(E)*, International Organization for Standardization, Geneva, 1977.
- [9] Tipnis, V. A., "Cutting Tool Wear," in Peterson, M. B. and Winer, W. O. (eds.), *Wear Control Handbook*, American Society of Mechanical Engineers, 1980, pp. 891-930.
- [10] Lim, S. C., Lee, S. H., Liu, Y. B., and Seah, K. H. W., "Wear Maps for Uncoated High-Speed Steel Cutting Tools," *Wear*, Vol. 170, 1993, pp. 137-144.
- [11] Ruff, A. W., *Eurotrib 89 – Proceedings of the 5th International Congress on Tribology*, Helsinki, 1989, Vol. 4, Finnish Society for Tribology, pp. 26-31.

- [12] Czichos, H., "Presentation of Friction and Wear Data," in Blau, P. J. (ed.), *Metals Handbook*, Vol. 18, ASM International, Metals Park, OH, 1992, 10th ed., pp. 489-492.
- [13] Kendall, K. A., "Friction and Wear of Cutting Tools and Cutting Tool Materials," in Blau, P. J. (ed.), *Metals Handbook*, Vol. 18, ASM International, Metals Park, OH, 1992, 10th ed., pp. 609-619.
- [14] Lim, S. C. and Ashby, M. F., "Wear-Mechanism Maps," *Acta Metallurgica et Materialia*, Vol. 35, 1987, pp. 1-24.
- [15] Lim, S. C., Ashby, M. F., and Brunton, J. H., "Wear-Rate Transitions and Their Relationship to Wear Mechanisms," *Acta Metallurgica et Materialia*, Vol. 35, 1987, pp. 1343-1348.
- [16] Antoniou, R. and Subramanian, C., "Wear Mechanism Map for Aluminum Alloys," *Scripta Metallurgica*, Vol. 22, 1988, pp. 809-814.
- [17] Liu, Y., Asthana, R., and Rohatgi, P., "A Map for Wear Mechanisms in Aluminum Alloys," *Journal of Materials Science*, Vol. 26, 1991, pp. 99-102.
- [18] Ramsey, P. M. and Page, T. F., "A New Approach to Predicting the Wear Behavior of Ceramic Surfaces," *British Ceramic Transactions Journal*, Vol. 87, 1988, pp. 74-80.
- [19] Lim, S. C., Liu, Y. B., Lee, S. H., and Seah, K. H. W., "Mapping the Wear of Some Cutting-Tool Materials," *Wear*, Vol. 162-164, 1993, pp. 971-974.
- [20] Lim, S. C., Lim, C. Y. H., and Lee, K. S., "Wear of TiC-Coated Carbide Tool Inserts," in Nishimura, M., et al. (eds.), *Proceedings of the International Tribology Conference, ITC' 95*, 28 Oct to 2 Nov 1995, Yokohama, Japan, Japanese Society of Tribologists, Tokyo, pp. 603-608.
- [21] Stjernberg, K. and Thelin, A., "Wear Mechanisms of Coated Carbide Tools in Machining of Steel," *Proceedings of the International Conference on High Productivity Machining, Materials and Processes*, ASM International, 1985, pp. 95-104.
- [22] Lindström, J., Collin, M., and Thelin, A., "Preparation and Machining Properties of CVD Al₂O₃ Coated Cemented Carbide Tools with Various Intermediate Layers," *Proceedings of the 9th International Conference on Chemical Vapor Deposition*, 1984, The Electrochemical Society, pp. 689-708.

70 WEAR PROCESSES IN MANUFACTURING

- [23] Viegelahn, G. L., Mamalis, A. G., and Zavaliangos, A. J., "A Note on Machining with a Single-Coated Tungsten-Carbide Tool of 5° Negative Rake Angle," *Journal of Mechanical Working Technology*, Vol. 13, 1986, pp. 163-174.
- [24] Chubb, J. P. and Billingham, J., "Coated Cutting Tools – A Study of Wear Mechanisms in High Speed Machining," *Wear*, Vol. 61, 1980, pp. 283-293.
- [25] Colding, B., "Wear Characteristics of Coated Carbide," *International Cutting Tool Day*, Sandviken, 1969, pp. 1-15.
- [26] Dearnley, P. A., "Rake and Flank Wear Mechanisms of Coated and Uncoated Cemented Carbides," *Transactions of the ASME: Journal of Engineering Materials and Technology*, Vol. 107, 1985, pp. 63-82.

Ashraf Jawaid¹ and Kabiru A. Olajire^{2,*}

TURNING OF HIGH STRENGTH STEEL ALLOY WITH PVD- AND CVD-COATED INSERTS

REFERENCE: Jawaid, A. and Olajire, K.A., "Turning of High Strength Steel Alloy with PVD- and CVD-coated Inserts," *Wear Processes in Manufacturing, ASTM STP 1362*, S. Bahadur and J. Magee, Eds., American Society for Testing and Materials, 1999.

ABSTRACT: PVD TiN-coated(T1) and CVD Ti(C,N)/TiC/Al₂O₃-coated(T2) inserts were used to machine a high strength low-alloy(HSLA) steel to assess their performance. The single-layer PVD-coated insert gave comparable tool life results to the triple-layer CVD-coated insert due to better coating adhesion, finer grain size and lower cobalt content. Observed active failure modes at high cutting speeds and feed rate were mainly chipping/fracture on the minor cutting edge for T1 and excessive nose wear for T2. The wear mechanisms on the former were interfacial sliding, dissolution/diffusion, and attrition wear mechanisms, while the latter wore principally by interfacial sliding and plastic deformation.

KEYWORDS: wear rate, wear mechanism, coated insert, steel alloy, failure mode

Steel alloy accounts for about 10% by weight in transport aircraft manufacture [1], and it is mostly used for landing gear components whose designs are based on ultimate bending strength. The strength requirement places a limitation on cutting speed as a result of temperature-dependent properties of cutting tools. Thus, high speed machining of such alloys require cutting tools of high temperature mechanical properties and adequate inertness.

¹Professor, Associate Dean of Engineering, Coventry University, Coventry CV1 5FB, England.

²Research student, Manufacturing Engineering Division, Coventry University, Coventry CV1 5FB, England.

*Corresponding Author; on study leave from the department of Industrial & Production Engineering, University of Ibadan, Nigeria.

Though existing ceramic tools meet these requirements, their fracture toughness is remarkably lower than that of conventional cutting tools, e.g cemented carbides.

Cemented carbide represents a significant proportion of the cutting tools and it has been mostly used for machining steel alloys due to its excellent cutting performance, i.e., reasonable wear rate. The current state of cutting tool technology involves the synthesis of hard ceramic materials (TiN, Al₂O₃, TiC, e.t.c) as coatings; through either chemical vapor deposition (CVD) or physical vapor deposition (PVD) coating techniques, on cemented carbide substrate to enhance the productivity of machining. The synthesised tools (i.e. coated carbides) have been observed to have reduced wear rates and extended tool lives [2-3]. PVD coatings have lessened the need for high coating thickness, and in addition, improve tool life and surface finish due to high adhesion strength, compressive stress and elimination of η -phase [4]. In contrast to the CVD techniques (deposition temperatures: 600-1100°C), PVD employs relatively low deposition temperatures, i.e 300-600°C [5]. An excellent review of the development and performance of PVD- and CVD-coated inserts, and the strengths and weaknesses of the coating techniques have been documented [6-8]. Many research workers have reported on the active failure and wear mechanisms of cemented carbides [3-4, 9]. Smoothly worn grains (dissolution/diffusion wear) and mechanical detachment of fragments of tool material (attrition wear) have been observed on cemented carbides at relatively high and low cutting speeds respectively [3]. However, there is still limited amount of similar data on coated cemented carbides. Research and industrial activities have shown the significant change in machinability parameters, i.e. cutting forces, wear rate and wear mechanisms, surface finish/integrity, e.t.c when machining with same insert of different coating layers. Dearnley [3] has also observed that the relative rake and flank face wear resistance of coatings on coated tools is dependent on the workpiece being machined and not necessarily in accordance with their solubility product rankings. All these findings suggest a varying wear rate at the cutting edge for different cutting tools, and the need for a continual effort to investigate the cutting performances of newly introduced inserts as they become available, for any meaningful improvement in the productivity of machining and cutting tool technology. This work has therefore concentrated on two differently ceramic-coated carbides in machining a high strength low-alloy (HSLA) steel. The objective is to investigate the effects of coatings, coating techniques, and cutting conditions on tool life, active failure modes and wear mechanisms of the inserts. In the following sections, details of the experimental techniques, obtained results and discussion are given. The final section is on the observed conclusions from the work.

Experimental Procedures

The steel alloy is a cylindrical bar in conformance with the ISO requirement for test pieces of length to diameter ratio to be ≤ 10 [ISO 3685]. It was turned without the use of coolant or lubricant on a Cincinnati Milacron CNC lathe (Cinturn

10). Up to 6 mm of material was removed from the outside surface of the cast skin to minimize any effect of inhomogeneity on the experimental results, and a chamfer was created on the workpiece with a different insert to avoid any damage to the tested insert by entry shock through the workpiece edge. The observation and recording of wear parameters were made at some chosen intervals on an optical microscope. Crater wear was not measured due to the groove profile on the tool rake face which would make such measurement inaccurate. The cutting tools were rigidly clamped in the tool post of the lathe during machining to have the following geometry: back rake angle: -6° , cutting rake angle: -6° , and approach angle: 95° . Machining was stopped on reaching either the twentieth minute of cut when low wear rate was experienced, or chipping/fracture of cutting edge, average flank wear = 0.4 mm, maximum flank wear = 0.7 mm, notch wear = 1.0 mm, nose wear = 0.5 mm, and surface roughness = 6.0 μm . Information on the inserts and workpiece is given on Tables 1, 2 and 3.

TABLE 1-- Tools' technical details and cutting conditions.

Tool Code	Substrate	Others
T1	Grade: M05-M20 Substrate: Co-6.0%, Cr-0.4%, Traces of Ta, Ti, & Nb. Hardness: 93.0 Rockwell A Density: 14.9 gm/cm ³ Grain size (μm): 1-5	Chip geometry: Medium finishing Coating material (μm): TiN-2 Coating Technology: PVD
T2	Grade: M20-M35 Substrate: Co-6.3%, Ta-3.5%, Ti-2.0% & Nb-1.5%. Hardness: 91.0 Rockwell A Density: 13.95 gm/cm ³ Grain size (μm): 1-7	Chip geometry: Roughing Coating materials (μm): Ti(C,N)-2 + TiC-4 + Al ₂ O ₃ -1.5 Coating Technology: CVD
Cutting speed (m/min): 100-150 (low) and 200-250 (high) Feed rate (mm/rev): 0.2 (low) and 0.4 (high) Depth of Cut (mm): 2.0		

TABLE 2-- Properties of tungsten carbide and coating materials.

Coating material	Hardness(HV)		Chemical stability	Dissolution rate		Free formation energy	
	25°C	1000°C		100°C	1100°C	100°C	1000°C
W ₂ C	1500	-	-	1.1×10^{10}	3.2×10^2	-10	-7.5
TiC	3200	300	44	1.0	1.0	-45	-40
TiN	2450	250	80	1.0×10^{-8}	2.2×10^{-1}	-72	-55
Al ₂ O ₃	2500	900	399	1.1×10^{-24}	4.1×10^{-5}	-115	-100

The selection of cutting conditions was made to observe the effect of cutting temperature (i.e. cutting speed) on the tool life/wear rate and wear mechanisms of the inserts. Feed rate and depth of cut have much lesser influence on cutting temperature [10]. Though the inserts have cemented carbide substrate of different grades, their mechanical properties, as shown in Table 1, do not significantly differ. Ultrasonic cleaning of the inserts was done with alcohol before gold-coating for examination on the scanning electron microscopy (SEM) and energy dispersive X-ray analysis (EDAX). SEM and EDAX were used to identify the wear mechanisms.

TABLE 3-- *Chemical composition of high strength low-alloy steel.*

Element	% composition	Element	% composition	Element	% composition
C	0.375	Cr	1.79	Al	0.008
Si	0.22	Mo	0.47	N	0.004
Mn	0.45	Ni	3.99	Ti	0.004
P	0.003	Cu	0.020	Ca	<0.0005
S	0.003	Sn	0.005	Pb	<0.0005
Supplied condition: Normalized + Annealed				Hardness: 274 BHN	

Experimental Results and Discussions

Tool Life and Failure Mode

The tool life and associated dominant failure or wear modes observed on the inserts are represented in Figure 1. None of the inserts reached the set failure criteria at the cutting speed of 100 m/min for both feed rates due to low wear rates; hence machining was stopped at the twentieth minute of cutting. Similar low wear rate was achieved at the higher cutting speeds of 150 and 200 m/min for the low feed rate. However, the measurement of wearlands indicated the dominant wear to have occurred mostly on the flank. At other cutting conditions T2 presented longer tool lives with significant nose wear as the active failure mode. Macro-chipping/fracture on the minor cutting edge and plastic deformation respectively were observed as additional failure modes to the nose wear at low and high feed rates (Figures 2 and 3). Chipping/fracture phenomenon also limited the cutting life of T1 at the speed of 250 m/min for the low feed rate without any significant wear on the main flank and nose, and at high feed rate beyond the cutting speed of 150 m/min (Figure 4). The groove wear on the minor flank of both inserts was due to the entrapment of hard chipped carbide particles between the minor flank and the rigidly supported rotating workpiece. The hardness values of the substrates of T1 and T2 are 93 and 91 Rockwell A, as compared to the hardness of the coatings (i.e. 61.7 and 85 Rockwell A, equivalent of 300 and 900 HV respectively for TiN and Al₂O₃ coatings, at the cutting temperature of about 1000°C obtainable at the cutting speed [3]).

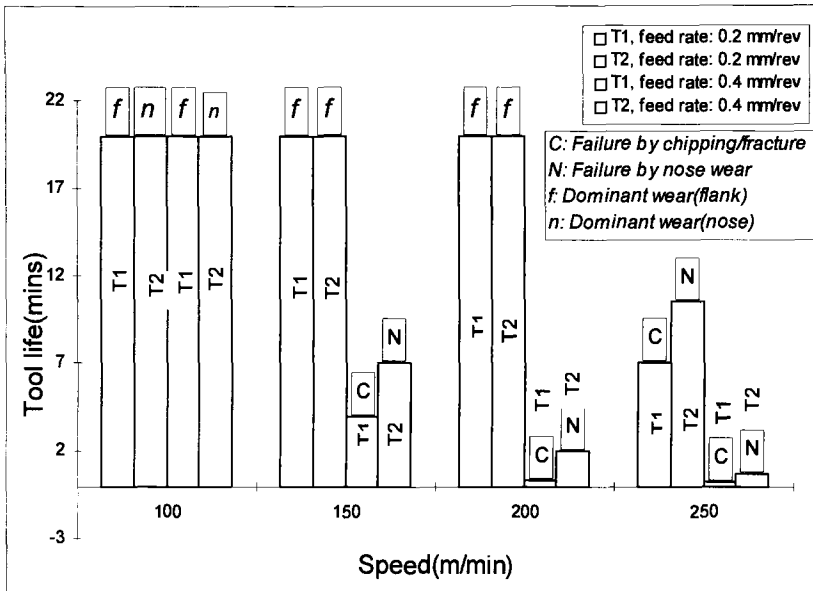


FIG. 1-- Tool life and failure mode in turning HSLA with coated carbides at depth of cut of 2.0 mm.

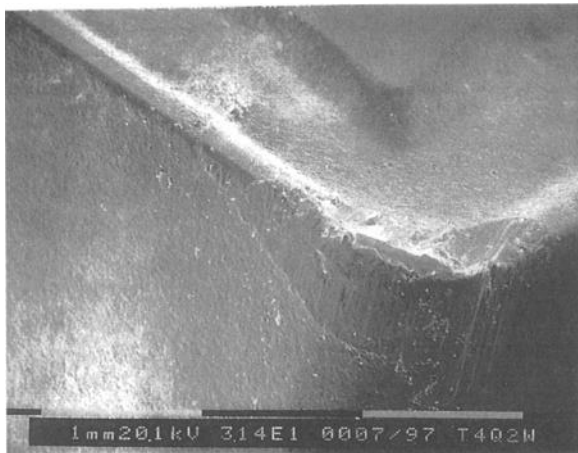


FIG. 2-- Typical wear and chipping/fracture on T2 at high cutting speeds.

The chipping/fracture at the occurred position is capable of causing damage to the finish/integrity of the machined surface. It is a phenomenon influenced by tool geometry. The development of crater wear increases the effective rake angle, which thus reduces the strength of the cutting edge [11]. Because the maximum compressive force occurs on the cutting edge [3], this may result in microcracks and

eventual chipping/fracture. The phenomenon is delayed when plastic deformation is experienced, as in the case of T2.

A closer observation revealed that the chipped region on T1 is characterised by peaks with sharp edges, thus suggesting a brittle fracture. The effect of these sharp and hard chipped particles is more evident by the obvious groove depth and width on the minor flank. In the contrary, a view of the chipped region on T2 shows a ductile fracture by the shining and smooth appearance of the uneven surface (Figure 2); with shallow grooves created on the minor flank.



FIG. 3-- Excessive nose wear and plastic deformation on T2 at high cutting speeds and feed rate.

Effect of Coating and Cutting Condition on Tool Life

A review of the tool lives shows very obvious sensitivity of the inserts to change in the cutting conditions, which was higher for T1. Figure 1 shows the drastic fall in tool life with the increase in cutting speed at high feed rate. There is no doubt the fact that cutting speed (i.e. cutting temperature) influenced the rake and flank face wear of T1 and T2 (Table 4), but its effect on tool life was secondary as the inserts mainly failed at high feed rate (i.e. high cutting stress) through chipping/fracture, nose wear and plastic deformation. Because the magnitude and distribution of rake face temperature is proportional to the chip/tool contact length [12], and the fact that coated tools have similar chip/tool contact lengths regardless of coating materials [3], it thus appears that the magnitude and distribution of rake face temperatures of the inserts generally did not differ remarkably. It is then logical to suggest the better tool life performance of T2 (CVD-Ti(C,N)/TiC/Al₂O₃) to be due to the combined excellent thermomechanical and chemical properties of the coating layers. Alumina on T2 protects the underneath coatings for a long machining time,

being the most stable of all ceramic coatings at high cutting temperature, from dissolution/diffusion wear (Table 2).



FIG. 4-- Excessive nose wear and chipping/fracture on T1 at high cutting speeds.

The free energy of formation (Kcal/gm.atom) gives the ability of each coating material to dissociate into atomic elements and chemically combine with another atomic element in the adjacent material [7].

TABLE 4-- Observed nose and flank wear rate(m/min) on the inserts.

Feed rate	0.2 mm/rev		0.4 mm/rev	
	T1	T2	T1	T2
Low	0.00605	0.01155	0.0291	0.0939
High	0.02075	0.0413	3.354	1.326

High adhesion strength and improved microhardness of TiN coating, made possible by the PVD coating technique, enhanced wear and tool life performance of T1, as compared with T2. There is minimal nose and flank wear, and no evidence of either pitting or flaking, as observed on the latter (Figure 3). In addition unlike the flank and nose wear on T2, wear started a little below the cutting edge on T1. This thus protects the cutting edge for a long machining time.

Wear Mechanism Studies

An investigation of the wear mechanisms leads to the understanding of workpiece/cutting tool interaction, and thus clarifies the phenomenon of wear or

failure modes. A detailed study of the failure/wear modes on all the faces of the tool suggested the following wear mechanisms:

- (a) dissolution/diffusion;
- (b) attrition;
- (c) sliding; and
- (d) plastic deformation

These wear mechanisms shall be considered for their roles in the wear/failure phenomenon taken place on each face of the inserts.

Rake face wear-- There was no serious wear of TiN and Al₂O₃ coatings respectively at low cutting speeds. The wear mechanism was a combination of interfacial sliding and deformation of the coating asperities along the direction of chip flow as given in Figures 5a-b [3]. The deformed coating breaks, after the yield strength is exceeded, to be carried away by the flowing chip (Final stage, Figure 5a). A careful examination of the rake face of T1 shows that it experienced brittle deformation of TiN coating (Figure 5b). Plastic deformation, resulting in ductile fracture, has been observed as the wear phenomenon on alumina coating [3]. At high cutting speeds some voids were observed, very close to the cutting edge, on the rake face of T1 (Figure 6). The deformation of coating asperities was in the opposite direction to chip flow, which made it easier for the chip to pluck the tool rake face under the high compressive stress and temperature obtainable at the cutting speed. The examination of the chip underside on EDAX shows an evidence of seizure (a secondary shear process) and adhering tungsten carbide particles (Figure 7). This is an indication of an attrition wear mechanism. Though the phenomenon of void formation may lead to crater wear in the manner shown in Figure 8, the intimate contact at the tool/chip interface under high compressive stress and temperature of about 1115 °C [12] is a pre-requisite for dissolution/diffusion wear of the atomic elements of the TiN coating or tungsten carbide to the adjacent workpiece, or vice versa. This thus aided the severe crater observed at high cutting conditions on T1 (Figure 4). The smooth rake face wear on T1 at high cutting conditions, a phenomenon of dissolution/diffusion wear [3], suggests the effect of attrition may have been limited only to the first few minutes of cutting. A general dissolution/diffusion model for carbide inserts in machining HSLA is represented in Figure 9. Information on the dissolution rate and free energy of formation of ceramic coatings and tungsten carbide is given in Table 2. It is possible to have substitutional diffusion of Ni in the workpiece and Co in the cutting tool because of their similar crystal structure and close lattice values. Also, Mo has similar ability to form carbide as W and thus can diffuse into the tool substrate to partially replace W in the carbides at high cutting temperature [13].

In addition to the wear phenomena of sliding and plastic deformation of alumina on T2, there is the evidence of seizure at the onset of chip flow manifested by plucking of the tool rake face (Figure 10). At high cutting conditions the phenomena of seizure and plastic deformation were still observed in a higher

degree(Figure 11). It was particularly observed that high feed rate encouraged the decohesion of alumina from the underneath TiC coating (Figure 12).

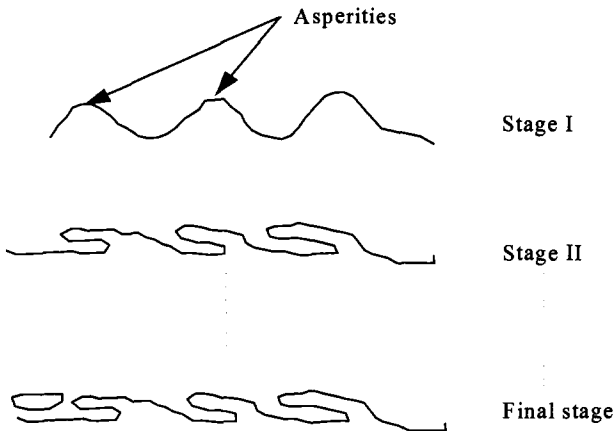


FIG. 5a-- Phenomena of sliding wear and deformation of coating asperities.

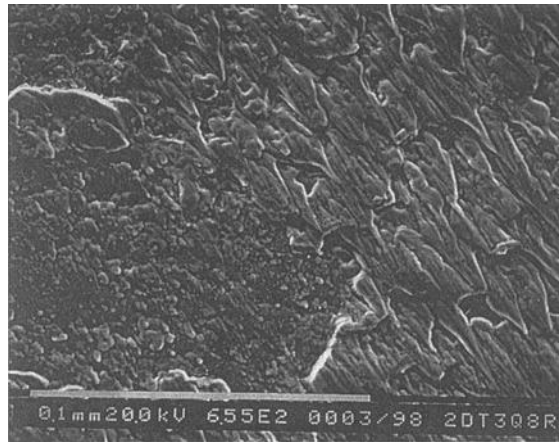


FIG. 5b-- Brittle deformation of TiN coating along chip flow direction.

The difference in the thermal expansion coefficients of the coatings because of the localized interface temperature (Al_2O_3 : $8.4 \times 10^{-6}/^\circ\text{C}$, TiC: $7.7 \times 10^{-6}/^\circ\text{C}$), and the consistent sudden impact and shear force in the direction of chip flow could weaken the interfacial adhering strength. This thus led to decohesion of alumina. Because alumina coating is the least soluble in steel of all the coating materials (Table 2), the effect of dissolution/diffusion wear may not have been as significant as the effect of sliding wear and plastic deformation.

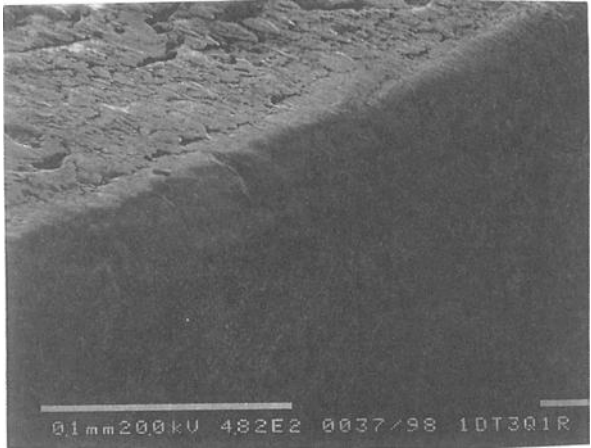


FIG. 6-- Sliding wear and void formation on T1 at high cutting speeds after 2 minutes of cut.

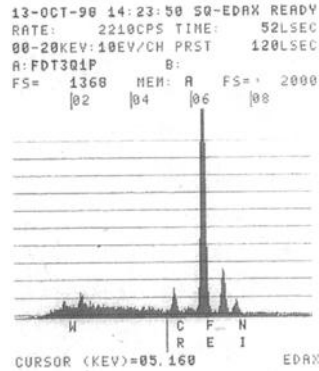


FIG. 7-- Evidence of seizure observed on T1 showing sticking of tungsten carbide to the underside of chip.

The absence of significant crater wear and presence of plastic deformation on the nose of T2 are evidence of this proposition. Thus the effect of dissolution/diffusion wear was not to the same degree on the rake face of the two inserts even though they both experienced similar magnitude and distribution of cutting temperatures. However there is no doubt the possibility of slight dissolution/diffusion wear taking place, either on alumina or any of the exposed underneath coating layers and substrate.

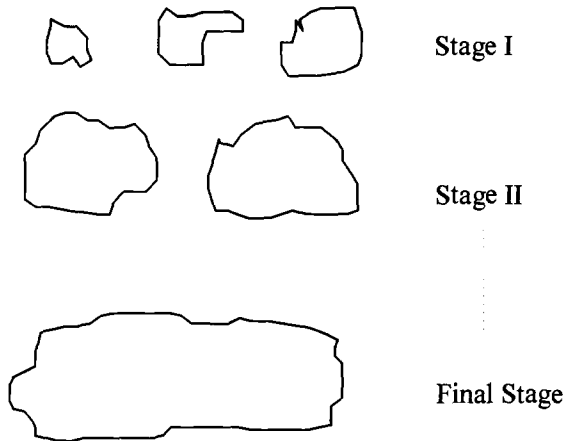


FIG. 8-- Stages in crater development through void formation.

Flank and nose wear-- The two inserts experienced low wear on both the flank and nose regions between the cutting speeds of 100 and 200 m/min at low feed rate. This was generally the case for T1 except at high cutting conditions. However an increase in either feed rate or cutting speed worsened the degree of wear on T2 (Figures 2 and 3). Table 4 summarises the wear rates of the inserts after some predetermined cutting times. The cutting times took into consideration the sudden failure of T1 at high cutting conditions.

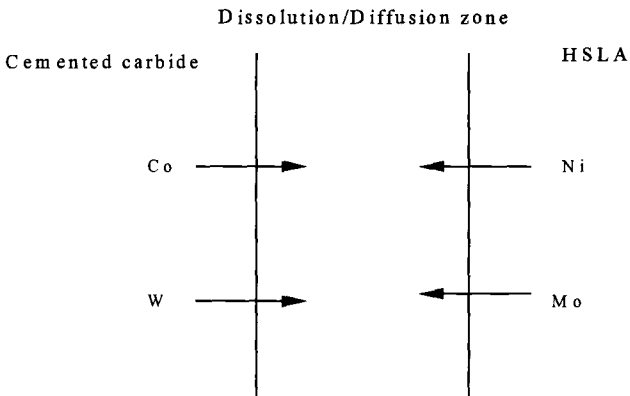


FIG. 9-- Basic dissolution/diffusion model

Wear rate is given by the division of the sum of wearlands on the nose and flank by the cutting time. The TiN (on insert T1) generally presented lower wear rate, except at high cutting conditions whereby the superiority of the thermomechanical properties and chemical stability of alumina (on insert T2) became obvious. At the highest cutting conditions (i.e. speed: 250 m/min, feed: 0.4 mm/rev), the nature of vertical grooves (ridges) created on the main flank and nose of the two inserts is different from that on their minor flanks (Figures 3 and 4). This seems unlikely to have been caused by abrasion because of the relatively higher hardness of the coatings as compared to the workpiece. Unlike the minor flank wear, such directional shallow grooves on the main flank depict an interfacial sliding between the workpiece chamfer and flank/nose of the inserts. A sufficient constraint at the flank/workpiece interface must have encouraged the development of shear forces of significant magnitude which caused the obvious signs of surface plastic flow of the coatings. The magnitude of the flank and nose shear stress is many times greater than the rake face shear stress due to the active compressive forces of the latter being highest on the cutting edge [3]. The evidence of sheared workpiece on the nose and flank region of T2 suggests an unrapid interfacial movement between the workpiece and cutting tool. This is sufficient to allow diffusion/dissolution wear to take place. Owing to very insignificant flank and nose wear on T1, the intimate contact only became evident at the highest cutting speed and high feed rate. Thus the flank and nose wear on T2 at the highest cutting speed for low feed rate, and between the cutting speeds of 150 and 250 m/min at high feed rate, suggest the possibility of dissolution/diffusion wear. This thus corroborates the ability of PVD coatings to reduce dissolution/diffusion wear, but on the flank and nose as observed in this case.

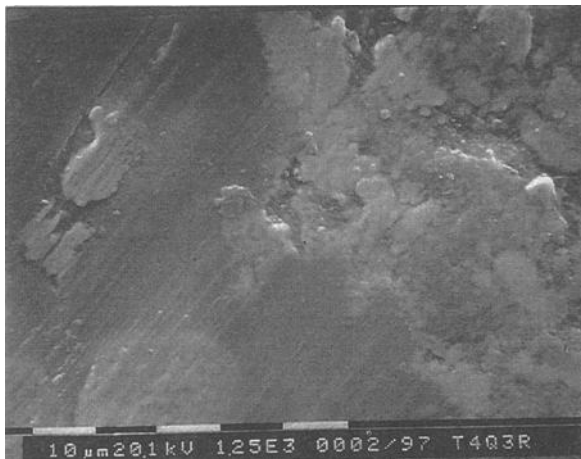


FIG. 10-- *Typical pattern of sliding wear and plastic deformation of alumina coating along chip flow direction at low cutting speeds.*

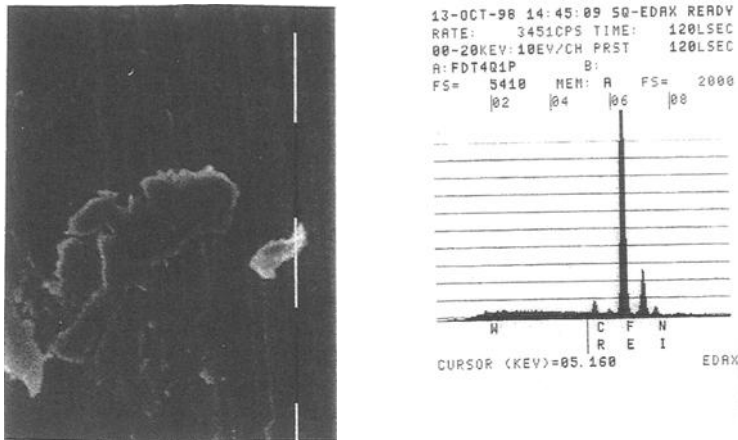


FIG. 11-- Evidence of seizure on T2 showing tungsten carbide sticking to underside of chip at high cutting speeds.

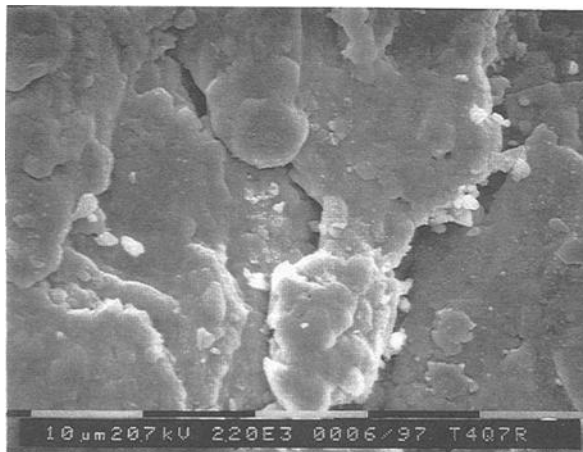


FIG. 12-- Evidence of loose and plastically deformed alumina coating, suggesting decohesion mechanism.

The wear rates, given in Table 4, also support the degree of dissolution/diffusion wear on the flank and nose of the two inserts. Because the flank face temperature of T1 is lower than T2 (lower flank wear), in addition to lower shear stress, plastic deformation of TiN coating may not be too obvious. However, it could appear smooth on alumina due to very small plastic strains and limited resolution capability of SEM [3].

Conclusion

A high strength low-alloy (HSLA) steel was machined with two ceramic-coated inserts, each of PVD and CVD. The conclusions are:

- (a) PVD-TiN (T1) presented better nose and flank wear rate than CVD-Ti(C,N)/TiC/Al₂O₃ (T2), except at the highest cutting conditions. While the latter failed mainly through excessive nose wear and plastic deformation, it was chipping/fracture that resulted in tool failure for the former. The wear mechanism is a combination of sliding, attrition, plastic deformation and dissolution/diffusion wear. However, the ability of PVD coatings to reduce dissolution/diffusion wear on the flank and nose was observed.
- (b) Higher adhesion strength, metastable structure, improved microhardness and finer grain size, enabled by PVD coating technique, enhanced the tool life performance of insert T1 when compared to T2.
- (c) Insert T2 presented longer tool lives than T1 because of the thermally and chemically stable top layer alumina coating, and higher content of the cubic carbides: (Ta, Ti, Nb)C, which both resist abrasion and rake face diffusion wear mechanisms.

Acknowledgement

The authors wish to express their gratitude for the support of Rolls Royce Plc, SECO Tools (UK) Ltd and Kennametal Hertel (UK) Ltd. The valuable technical assistance of Mr Richard Pheasy and Ms Chris Lovering on the CNC turning centre and Scanning Electron Microscope is also appreciated.

6.0 References

- [1] Flower, H. M.; *High Performance in Aerospace Materials*, Chapman & Hall, Lond. SE1 8HN, U.K., 1995.
- [2] Sundquist, H. A.; Sirvio, E. H. and Kurkinen, M. T.; 1983, "Wear of metal-working tools in plated titanium nitride," *Metals Technology*, Vol. 10, pp. 130-134.
- [3] Dearnley P. A.; January 1985, "Rake and Flank Wear Mechanisms of Coated and Uncoated Cemented Carbides," *Journal of Engineering Materials and Technology (Trans ASME)*, Vol. 107, pp. 68-82.
- [4] Venkatesh (1), V. C.; Ye, C. T.; Quinto, D. T. and Hoy, D. E. P.; 1991, "Performance studies of Uncoated, CVD-coated and PVD-coated carbides in turning and milling," *Annals of the CIRP*, Vol. 40, No 1, pp. 545-550.
- [5] Prengel, H. G.; Pfouts, W. R. and Santhanam, A. T.; 1998, "State of the art in hard coatings for carbide cutting tools," *Surface and Coatings Technology*, Vol. 102, pp. 183-190.
- [6] Santhanam, A. T. and Tierney, P.; "Cemented Carbides," *Metals Handbook: Machining*, Vol. 16, 9th Edition, A.S.M. International, U.S.A., 1989, pp. 71-89.

- [7] Hunt, J. L. and Santhanam, A. T.; "Coated Carbide Metalcutting Tools: Development and Applications," *Fundamental Issues in Machining*, ASME Publications, PED-Vol. 43, editors: Barney E. Klamecki and Klaus J. Weinmann, presented at the Winter Annual Meeting of the American Society of Mechanical Engineers, Dallas, Texas, November 25-30, 1990, pp. 139-155.
- [8] Dini, J. W.; 1997, "Properties of Coatings: Comparisons of Electroplated, Physical Vapour Deposited, Chemical Vapour Deposited, and Plasma Sprayed Coatings," *Materials and Manufacturing Processes*, Vol. 12, No 3, pp437- 472.
- [9] Cho, S. S. and Komvopoulos, K.; January 1997, "Wear Mechanisms of Multi-layer Coated Cemented Carbide Cutting Tools," *Transactions of the ASME(Journal of Tribology)*, Vol. 119, pp. 8-17.
- [10] Thomas, J. D.(Editor-In-Chief); "Chapter 1: Principles of Metalcutting and Machinability," *Tool and Manufacturing Engineers Handbook: Machining*, Vol. 1, 4th Edition, S.M.E., U.S.A., 1983, pp. 1:1-1:66.
- [11] Trent, E. M.; *Metal Cutting*, 3rd Edition, Butterworth-Heinemann Ltd, Oxford, 1991.
- [12] Dearnley, P A and Trent, E M; 1982, "Wear mechanisms of coated carbide tools," *Metals Technology*, Vol. 9, pp. 60-75.
- [13] Jiang, L; Hanninen, H; Paro, J and Kauppinen, V; 1996, "Active Wear and Failure Mechanisms of TiN-coated High Speed Steel and TiN-coated Cemented Carbide Tools When Machining Powder Metallurgically Made Stainless Steels," *Metallurgical and Materials Transactions A*, Vol. 27A, pp. 2796-2808.

Manfred Schlatter¹

EVALUATION OF COATINGS AND MATERIALS FOR ROTATING SLITTER KNIVES

REFERENCE: Schlatter, M., "Evaluation of Coatings and Materials for Rotating Slitter Knives," *Wear Processes in Manufacturing, ASTM STP 1362*, S. Bahadur and J. Magee, Eds., American Society for Testing and Materials, 1999.

ABSTRACT: Magnetic tapes are manufactured in broad webs of large length. The single tapes are cut from this with rotating slitter knives. Because of the extremely high quality requirements to the tape edges, the endurance of the slitter knives is limited. Among other things, experiments were carried out with knives made from ceramics and cermets, with coatings of PVD-TiN, TiAlN and DLC and with ion implantation on cemented carbide knives. Most experiments were not successful, only a plasma enhanced CVD titanium nitride coating brought a technical, if not economic success.

KEYWORDS: magnetic tapes, slitter knives, tool wear, coatings, titanium nitride, titanium carbide, tungsten carbide, diamond like carbon, ionimplantation

Subject of the Investigations

In spite of the introduction of optical systems like CD or DVD [1, 2] and the constantly increasing storage capacity of hard disks, magnetic tapes continue to play an important role for data storage purposes because of their proliferation, simple handling and favorable prices per stored amount of data. Modern systems also use tape technologies for digital video camcorders (DVC) or as a computer backup system (data cartridges, DLT) [2]. There is a visible trend towards smaller tapes or smaller numbers of cassettes with high packing density. In 1997, 49% of all storage media were tapes with worldwide sales in excess of 7.5 billion US dollars [2].

Magnetic Tape

Tapes for magnetic data storage are made of thermoplastic polyester film and magnetic coating [3-5] with a total thickness between 6 and 25 μm . The quality of the write and read process depends, among other things, on the close contact between magnetic head and tape. Therefore, especially high demands on tape edge quality are made. The edges

¹ Senior manager, R & D Slitting and Assembling, EMTEC Magnetics GmbH, Industriestr. 1, D-77731 Willstätt, Germany.

must above all be free of ridges and may show no bulges, so that no gap occurs between tape and head [4]. Very clean cuts are also necessary in order to guarantee that no fluff or dust particles, which would contaminate the write and playback equipment in use, are found at the edges [5].

Manufacturing of Magnetic Tape

Magnetic tapes with length up to 30 kilometers and a width of 0.3 to 1.5 meters are coated with a magnetic coating and then wound up to large rolls with a diameter of approximately 1 meter. The rolls are then cut in slitting machines into the strips about 3.8 to 50 mm in width known as magnetic tape and they are individually coiled [3, 4]. Thus, each roll can yield up to 170 parallel tapes. Slitting is done by rotating slitter knives [3-6]. In order to limit manufacturing costs, the knives are pre-assembled on an upper and a lower shaft in a so-called knife box and can be changed as a unit if the knives need to be re-ground.

Parameters for the Slitting of Magnetic Tape

Slitting with rotating slitter knives (Fig. 1) has been known for a long time and the optimal parameters for good quality and an economical manufacturing process were examined more than 25 years ago [8]. The geometrical preconditions for slitting are penetration and axial dislocation in order to press the bottom knives against the upper ones [8, 9]. Other parameters are tilt and overspeed [8-10]. The type of the magnetic tape itself also influences the quality of the tape edges [11].

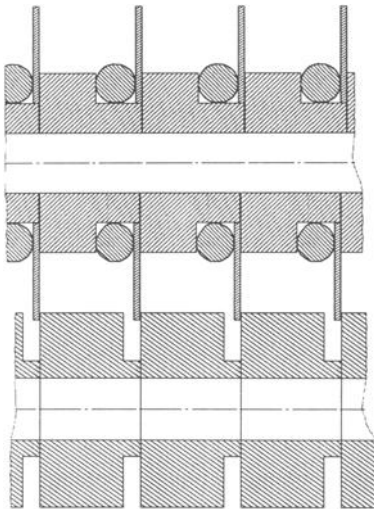


FIG. 1--Cross section of slitting with slitter knives with broad lower blades and the narrow, suspended top blades.

Adjustment of penetration and pressing of top and bottom blades allows the blades to touch, so that the tape is cut but not squeezed between the knives. Wear results from this contact and the relative velocity of the knives and the knife edges become blunt. Therefore, the values for the penetration and the axial pressure must be as small as possible. The tilt could be realised easily by displacing one of the shafts from the parallel direction. With the tilt, the knife edges only touch at one point. This results in an especially "sharp" cut, but causes more wear. The overspeed is the difference in rotation speed between top and bottom blades, with the upper blade rotating faster, giving a "pulling" cut. This value can be optimized for each tape material as a compromise between high tape edge quality and low wear [8].

Wear of the Slitter Knives

Due to the contact pressure of the knives, which are pressed against each other by a spring [6], the relative movement of the knives against each other and the abrasive magnetic particles in the magnetic coating or other hard components of the tapes, the slitter knives wear and must be reground regularly. The wear on upper and bottom blades was examined and the results published in 1975 [12] and differs because of the magnetic coating only being on one surface of the tape and because of the different encompassment angles.

Knife wear is normally higher on the surface with the magnetic coating (Fig. 2) and more strongly influenced by tape quality than the knife wear on the "reverse side" of the tapes. Serious errors, such as knives [13] turning eccentrically or falling, are not be discussed here, as these must be prevented for accurate slitting. With the introduction of cemented tungsten carbide as a slitting knife material more than 20 years ago [12], economical use of such knives became possible. However, it would be desirable to further lower the costs for procurement and post-treatment. Therefore, the task in question was to modify the knives in such a way that the procedure became more economical.

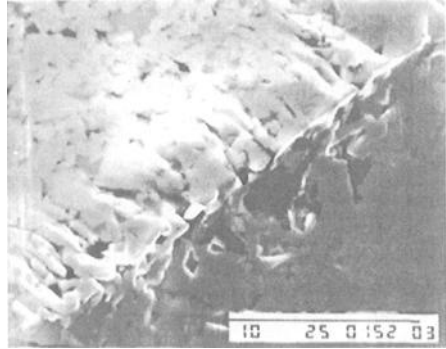


FIG. 2--Typical wear on a cemented carbide top blade: Flat surface with radial striation wear (left) and volume face with wear and tear along the edge (right).

Description of the Modified Tools

In addition to the optimization of geometry and adjusting parameters, there are principally three different means to extend knife life: the use of wear resistant materials, surface modification and coating of known materials.

Alternative Materials

Of course the endurance of cemented tungsten carbide knife materials (Table 1, no. 1 and 2) has been improved by finer grain size [14], but completely new solutions cannot be excluded. An important factor for a material's wear resistance is its hardness. Therefore, materials that are used to reduce wear in other fields (Table 1, experiments 3 to 6) and/or harder than cemented tungsten carbide (Table 1, experiments 7 and 8) were examined. It is known from other fields of technology that through use of new materials such as ceramics, including cubic boron nitride [15-19] or cermets [18-20], new technological ways were opened in metal machining. We found that knives can be made virtually from all materials; in some cases, such applications have already been published [15, 17]. For the time being, it is impossible to produce carbon nitride C_3N_4 [21] knives.

TABLE 1A--Experiments with new slitting materials:
types and numbers of samples.

no.	name of specimen	remark	top blade	bottom blade	combination with		color
			pieces	pieces	tungst.c.	itself	
1	tungsten carbide	standard for comparison	>1 000	>100	yes	yes	grey
2	tungsten carbide	standard for comparison	>100	>1 000	yes	yes	grey
3	ZrO ₂	Y ₂ O ₃ -stabilized	10	130	yes	yes	white
4	ZrO ₂	MgO-stabilized	5	no	yes	no	yellow
5	Cermet 1	TiC+TiN	9	no	yes	no	grey
6	Cermet 2	TiC+TiN	10	no	yes	no	grey
7	SiC	...	12/6	no	no	no	grey
8	B ₄ C	with Ti ₂ B	no	10	no	no	grey

bold mean application

> 100 several hundred pieces per year

> 1 000 several thousand pieces per year

TABLE 1B--Experiments with new slitting materials: properties.

no.	name of specimen	binder	grain size	density	hardness	bending strength	Young's modulus	porosity
		type [%]	µm	kg/dm ³	MPa	MPa	GPa	[%]
1	tungsten carbide	Co 3-10	0.5-1.0	14.5*	Vickers HV30: 1700*	3100*	610	0
2	tungsten carbide	Co 10-15	0.5-1.0	14.0*	Vickers HV30: 1400*	3000*	590	0
3	ZrO ₂	no	0.5	6.0	Knoop: 18000	800	200	0
4	ZrO ₂	no	?	5.74	Vickers HV0.5: 1250	520	210	> 0
5	Cermet 1	CoNi 13.5	> 1	7.0	Vickers HV30: 1600	2300	450	0
6	Cermet 2	CoNi 16.7	> 1	7.0	Vickers HV30: 1450	2500	440	0
7	SiC	no	?	3.1	Knoop: 27000	350	370	0
8	B ₄ C	?	?	3.3	Vickers HV0.5: 3500	730	480	< 0.1

all numbers.... from supplier

bold mean application

* averages

Knives made of titanium boride Ti_2B [22] were not available and specimens of the material titanium carbide in steel binder were too expensive. The examined knives shown in Table 1 consists in each case of around 5 to 10 technical specimens, which were made by machining the not yet cemented workpiece and not by pressing as in mass-production.

Coatings

In the case of tools for machining metals like drilling, turning or milling, the coatings have prevailed in recent years and were constantly improved [18, 19, 23]. Titanium aluminum nitride coatings (TiAlN; Table 2, experiment 13) as well as the classic titanium nitrides, titanium carbide coatings and combinations of both are currently introduced. Coatings, which contain chromic nitride (CrN; Table 2, experiment 18 and 19) [24] or made of diamond-like carbon (DLC; Table 2, experiment 14 to 17) [25-31] were also examined in this work for knives. All coatings of 10 or 60 knives according to Table 2 were carried out similar to the procedures used in metal machining tool mass-production. Knives with DLC coating were again technical specimens of 10 pieces for each experiment. The coatings DLC2 to DLC4 (Table 2, experiments 15 to 17) were a series of experiments aimed at improving the adhesion of the coating, which succeeded: the DLC4 coating was considerably better than the DLC2. As with the manufacturing of the new materials, standard procedures were used for the manufacturing of the coatings and no development of coatings was carried out. The plasma enhanced CVD coating technique yielded very good and regular coatings with only few pits (Fig. 3) (P-CVD), as described in [32-35].

TABLE 2--Experiments with knife coatings.

no.	name of specimen	remark	top blade	bottom blade	color	coating thickn.	roughness R_z	hardness
			pieces	pieces		μm	μm	MPa
1/2	tungst.car.	for. compar.	> 1 000	> 1 000	grey	...	0.1	HV30: 1 700*
9	TiN	P-CVD	60	60	yellow	2.3	0.3	HV: 2 400
10	TiN	CVD	3	...	yellow	0.04	0.1	...
11	TiN	PVD	60	...	yellow	0.27	0.2	HV0.05: 2 300
12	Ti(CN)	PVD	60	...	blue-grey	0.5	0.5	HV0.05: 2 900
13	TiAlN	P-PVD	10	...	grey	3	0.2	HV0.05: 3 000
14	DLC 1	supplier 1	10	...	black	0.2	0.2	HV0.05: 4 000
15	DLC 2**	supplier 2	10	...	black	2	0.1	HV0.01: 3 000
16	DLC 3**	supplier 2	10	...	black	2	0.1	HV0.01: 3 000
17	DLC 4**	supplier 2	10	...	black	2	0.1	HV0.01: 3 000
18	CrN	CVD	3	...	grey	0.03	0.1	...
19	CrN	...	60	...	grey	2	1.0	HV0.03: 1 400

Information on layer thickness and hardness is the manufacturers;

*...average;

**...3 optimization experiments in sequence with coating liability corrected in each case

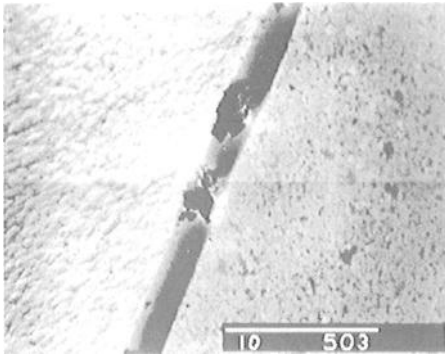


FIG. 3--2.3 μm thick titanic nitride coating on a knife edge flat surface made with plasma CVD; left: coating surface, to the right: ground outer face with free pit in the coating).

Laser enhanced surface coating of the knives with cemented carbide as described in [36-38] were examined on a single steel specimen, with the intention of not having to make the whole knife out of cemented tungsten carbide. The coatings were partly porous or the knives became uneven during coating so that they were not tested in use. Polycrystalline diamond coatings as described in [39] were not available for tools of the size used in the present study.

Using individual top and bottom knives with a 200 nm-thick aluminum nitride (AlN) coating, a 100 nm-pure carbon (C) coating and a 10 nm chrome (Cr) coating as a primer and following it with a 100 nm carbon (C) coating, experiments with very thin coatings were performed (not included in the Table). However, all these

coatings showed obvious coating defects during investigation with the interference microscope, the experiments were aborted.

Implantation of Material Corpuscles

Hardening procedures are mainly used for steel materials. However, it is also possible with special procedures to insert material particles to "harden" cemented tungsten carbides. Of these procedures, the implantation of boron [40] and ion implantation [41-52] seemed promising and were examined (Table 3).

TABLE 3--*Experiments with procedures for insertion of material corpuscles.*

no.	name of specimen	remark	top blade	coating thickness	roughness r_z	radiation doses
			pieces	μm	μm	10^{17} ions per cm^2
20	borizing	...	10	0.3
21	ionimplantation 1	supplier 1	60	0.01	...	1.3
22	ionimplantation 2	supplier 1	120	0.01	...	2.5
23	ionimplantation 3	at outer diameter*	180**	0.01	0.4	2.5
24	ionimplantation 4	supplier 2	120	0.01	...	4
25	ionimplantation 5	supplier 3	60	0.01	...	1.7
26	thermal implantation	ionbeam-cvd	60	1

Layer thicknesses and radiation doses are manufacturer's specifications,

*...all other knives were implanted at the flat surface,

**...knives with ions of boron, titanium as well as titanium and carbon

In the case of ion implantation, different procedures parameters such as the implantation dose and the implantation of different ions, such as boron and titanium [41, 46], were employed, in larger series of 420 knives treated in total. The nitrogen ion dose was varied in accordance with different references between approximately 1.3 and $4 \cdot 10^{17}$ cm^2 . As opposed to ion implantation coatings not only the flat surfaces were treated but also alternatively the outer diameter of the knives (Table 3, experiment 23), since wear occurs on both sides neighboring the slitting edge. In this way it was to be examined, whether it would be sensible to implant before every usage or after every regrinding.

It should be emphasized, that the knives with ion implantation of all variants behaved like untreated knives, e.g. while grinding. Neither chipping during grinding or usage, nor increased fracturability was observed.

Test Conditions and Experimental Results

In the case of the experiments concerning the suitability of the knives for the slitting of magnetic tape, a multistage procedure was used. On account of special conditions of use and cost structure, regrinding knives is indispensable today. It is possible to regrind such knives more than 100 times, so that their entire service life amounts to several years. Therefore, one of the conditions was that both new and varied or coated materials must be regrindable. If this condition was to be met, the kind of test would depend on the number of specimens available: small series of 2 knives were normally tested by slitting of only one tape on a laboratory slitting machine, larger series in a manufacturing environment. In this case, the experimental result is more significant since the cut on the laboratory slitting machine with only 2 top blades under optimal conditions would stress the knives less; chipping by possible machine oscillations are rare in this case. The procedure of combining the knives was different: occasionally, only top or only bottom blades were available, in other cases both. A standard cemented tungsten carbide knife was usually used as a counter knife; if both knives were available as pilot samples, identical materials or coatings were tested against each other.

Only videotape of the VHS standard grade with a chromium dioxide coating and a total thickness of 16 or 19 μm was cut. For each experiment and operation, 300 to $1\,000$ km of tape were cut using slitting speeds ranged from 300 to 720 m/min (5 to 12 m/s) and with well-slitting knives.

The special problem also lies in the assumption of regrinding possibility for coatings and the implantation of material corpuscles: on account of economical considerations, virtually only the face of the knife near the slitting edge, that is not re-ground, can be treated, so that the coating or the processing also remains effective after the regrinding operation. Since the outer diameter of the knives is normally re-ground, only the flat surface can be treated, which is not the main wear surface. On the other hand, this procedure is known from drills because the coating at transition of

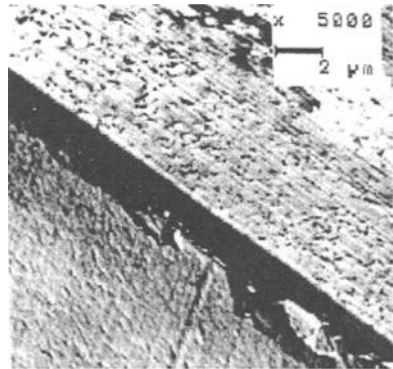


FIG. 4--Coating flaking while grinding of knives with a DLC coating.

the side face into the reground face on the end of a drill increases the resistance to wear.

Chipping Due to Grinding

Several knives and coatings were not usable at all, because no chipping-free edge could be achieved, not even after many regrinding experiments (Table 4). This above all applies for the superhard materials with small bending strength and for especially hard coatings which chip off near the edge due to grinding wheel pressure. Figure 4 shows the chipping of a DLC coating as an example (Table 2, experiment 16).

Chipping Due to Use

Other materials and coatings also proved to be impractical, although they were regrindable, but during use the slitting edges were broken down (Table 4). Especially while using knives employing coatings without optimal adhesive strength, large areas of the coating peeled off immediately after the knives touched, and the knife edges were destroyed. As an example, Fig. 5 shows the complete detachment of the DLC coating after only a few revolutions with the knives touching (Table 2, experiment 14).

Wear Measurement

Usually the assessment of the knives proceeded through the length of the cut of magnetic tape until the knives were blunt. In some cases single blades were tested by use in production together with cemented tungsten carbide serial knives, if it was safe to assume that the wear on the test specimens would be lower. An experimental evaluation was then possible by measurement and comparison of the wear marks of neighboring knives. In addition to ion implantation, the



FIG. 5--Slitting edge of a top blade with completely flaked off DLC coating after use.

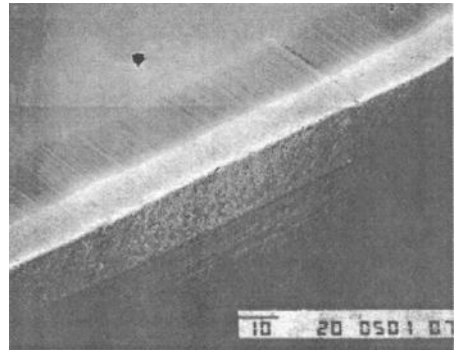


FIG. 6--Top blade with titanic nitride coating according to experiment 9; left: flat surface with worn-out coating and base material wear, right: volume face.

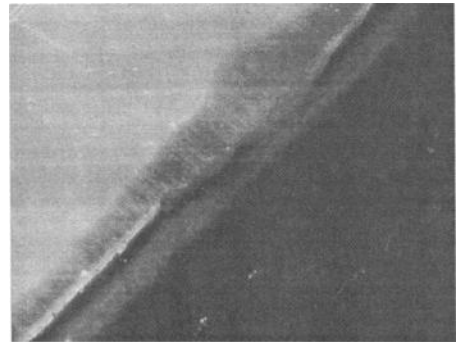


FIG. 7--Slitting edge of a ceramic top blade; left: flat surface; right: volume face.

best results were achieved with plasma CVD titanium nitride (Table 2, experiment 9). Both top and bottom blades never showed chipping, which would have prevented a good cut. Tool endurance was also still good after several years. Wear always affected the coating first, then continues on to the cemented carbide base material (Fig. 6), though normally later than with uncoated knives. However, the wear on other knives was severe (Fig. 7), e.g. with the ceramic top blades (Table 1, experiment 3) and with thermo-implantation (Table 3, experiment 26), that the tape edges were very poor under the same slitting operation conditions. A summary of all the experiments with the most important conditions of use is shown in Table 4, an evaluation of all of the usable knives is shown in Fig. 8.

TABLE 4--List of the conditions of use and of the qualitative size of wear.

no.	specimen	use in	chipping during		wear after		fig.	remark
			grinding	usage	first usages	20 usages		
1	tungst. carb.	production	no	no	low	low	2	top blade
2	tungst. carb.	production	no	no	low	low	...	bottom bl.
materials								
3.1	ZrO ₂	production	no	no	high	high	7	top blade
3.2	ZrO ₂	production	no	no	low	low	...	bottom bl.
4	ZrO ₂	laboratory	no	no	high
5	Cermet 1	production	no	no	high
6	Cermet 2	production	no	no	high
7	Sic	...	yes
8	B ₄ C	...	yes
coatings								
9.1	TiN	production	no	no	low	low	6	top blade
9.2	TiN	production	no	no	low	low	...	bottom bl.
10	TiN	laboratory	no	yes
11	TiN	production	no	yes
12	Ti(CN)	production	no	yes
13	TiAlN	production	no	yes
14	DLC 1	laboratory	no	yes	5	...
15	DLC 2	...	yes
16	DLC 3	...	yes	4	...
17	DLC 4	...	yes
18	CrN	laboratory	no	yes
19	CrN	...	yes
implantation of material corpuscles								
20	borizing	laboratory	no	no	indifferent	indifferent
21	ionimplant. 1	production	no	no	low	high
22	ionimplant. 2	production	no	no	low	high
23	ionimplant. 3	production	no	no	low	high
24	ionimplant. 4	production	no	no	low	high
25	ionimplant. 5	production	no	no	low	high
26	thermal impl.	production	no	no	high

The utility value for each knife was calculated using the doubled number of achieved kilometers of slit magnetic tape, divided by the achieved edge quality (deformation in μm), divided by the size of the wear marks (μm) and divided by the price for the knife or knife treatment. It could be recognized, that after frequent usage of the knives the

untreated cemented carbides have the greatest utility value. Ion implantation is only the best method to decrease knife wear for a limited period or for the first usages after treatment.

For the new materials, publications concerning comparable applications are too few, so that no correlation can be set up in detail. Only in the case of ceramics, above all with zirconium oxide, there are several references concerning the suitability for knives, e.g. [15], albeit for materials like paper or films are to be slit. These statements obviously do not apply if the films contain abrasive materials such as magnetic pigment.

In the case of coatings, references can be found in [26, 28], that single layer or multiple TiAlN coatings are indeed suitable for tools for machining operation, however not for knives, as the experiments also show. According to [28], knives should show very good results with CrN-coatings, which could not be confirmed with the present experiments (Table 4).

In the case of ion implantation, there are extensive studies for the implantation of nitrogen in steel or cemented tungsten carbide which predominantly report a positive effect. According to [54], there are no improvements to be expected: it was determined empirically by means of indexable cutting tools for turning and milling tools made of different cemented carbides that no improvement in endurance is attainable. In conclusion, it is also said in [54] that the ion implantation in the case of sliding friction with high surface pressure shows an improvement, but not in the case of "...tools with slitting, scraping and grinding load in the contact zone...". These corresponding results first became known after our own experiments.

Ion-implanted knives showed a special feature: in the first usages after implantation, they were very much better than all comparing tests and they caused endurance prolongation of up to 50 %. However, they fell below the average after longer use. [49] reports that after an abrasive wear of 5 μm , which is several times the usual implantation

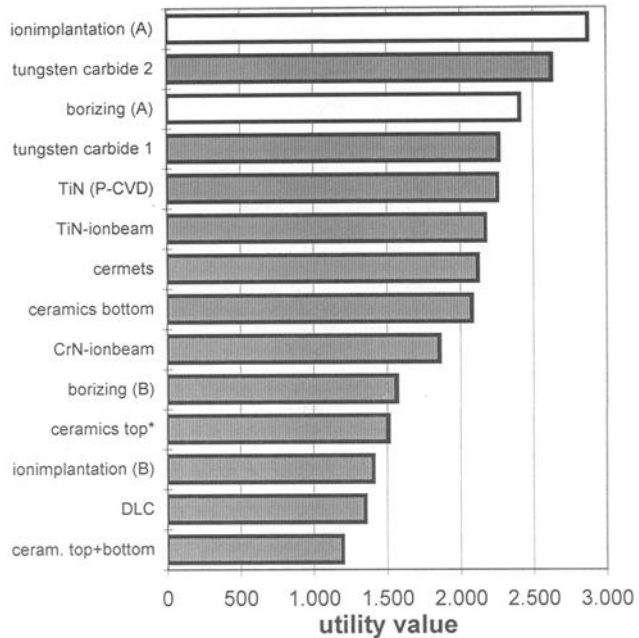


FIG. 8--Utility value analysis for the most important experiments; endurance, wear size, band edge quality and price were evaluated; A.... meaning during initial use, B.... after approximately 20 employments and later, *.... with cemented carbide counter knife.

depth, 20 % of the implanted ions can still be found. This means that the ions diffuse inwards into the material in case of abrasive wear and the changes in the surface caused initially are no longer effective. A further reason for failure of the knives after several usages could be the corrosion of the material, because in [54], it was found that the corrosion resistance initially is larger, however after prolonged influence of the corrosive medium was less than was observed on untreated comparable specimens. It is presumed that both effects occurred together and therefore the knives failed after few weeks.

Evaluation of the Experimental Results

The results show that the production of good quality knives and coatings of hard layers, after some unfavourable pilot experiments, was always possible. The results also show, as generally expected, that very hard and brittle materials would not be well suitable for the sharp edges, which must be reground. In actual fact, the problems both while shaping the knives and while making the edges (grinding), were proportional to specified hardness. Grinding was essentially done as with cemented carbide; in some cases advance and feed rate were decreased, which was successful in the case of ceramics or special DLC coatings (experiment 14), but not in the case of boron carbide (experiment 8) or the other DLC coatings (experiments 15 to 17).

The use of the knives occurred carefully under conditions that could be realized in series too. Maybe certain materials or coatings would have been able to perform successfully if parameters had been modified substantially; however, it was seen to be important that the conditions of use had to be comparable with current practice.

Measurement and assessment of wear occurred quantitatively provided that a measurement was possible. The measured values are averages, partially of highly scattering values, especially if there are only single numbers of measurements and therefore, are should be regarded as tendencies. However, a distinction of the tested materials and of the coatings in "better" or "worse" was always unambiguous and was included in the utility value analysis in Fig. 8.

Conclusions

In general, it must be said that almost all hard coatings like PVD-TiN, TiAlN-, CrN- and DLC coatings failed because of the inadequate adhesive strength of the coatings on the substrate or for lack of inner cohesion during tool regrinding when an extremely good edge quality was required. The evolution of useful primers and the further development of the coatings towards more ductility in combination with high permanence against abrasive wear would extend the possible applications of such integrated tools considerably. In the same way modified hard materials which show a high resistance against wear and a very good edge stability simultaneously would be desirable. These qualities were only observed in the knives with the plasma enhanced CVD titanium nitride coating which unfortunately were too expensive for mass use.

Ion implantation showed very good improvements, but only for a relatively short time during the first usages. The best results were achieved with the implantation of nitrogen and of titanium.

Alternative slitting procedures with laser or water jet were, up to now, not suitable, because they damaged the tape edges too much due to melting effects or fray outs. Cutting

slots as well as the removing of material are not desired. Fixed knives or razor blades of steel, coated steel, cemented carbide or diamond fail in the case of slitting magnetic tape because of the high relative speed during the usage and the quick destruction of the blade. A technically reasonable alternative would be the use of knives which are only employed once and which are not to be reground. However, this was not possible presently for economic reasons.

References

- [1] Snape, C. A. et al., "DVD Special Report II," *One to One - The International Media Manufacturing Magazine*. London, September 1997.
- [2] Lueck, L. B. et al., *Magnetic Media International Newsletter*. Honolulu, HI, USA, 16 Sep. 1997.
- [3] Jorgensen, F., *The Complete Handbook of Magnetic Recording*. 3rd ed. Blue Ridge Summit, PA, 1988.
- [4] Bhushan, B., *Tribology and Mechanics of Magnetic Storage Devices*. New York, 1990.
- [5] Hack, J. u. a., *Magnetische Informationsspeicher in der Daten-, Audio- und Videotechnik*. Expert Verlag, Ehningen, 1990.
- [6] Baumann, M., Birkmann, J., Bott, K., Scholtysik, B., "Vorrichtung zum Schneiden von Folienbahnen," DE 42 12 541 A1, 21 Oct. 1993.
- [7] Gaiser, D., Huber, M., Guenther, F., Kamm, E., "Schneidvorrichtung zum Längsschneiden von Materialbahnen," DE 26 19 085, 3 May 1976.
- [8] Feiler, M., *Ein Beitrag zur Klärung der Vorgänge beim Schneiden dünner flächiger Materialien*. Dissertation, Universität Stuttgart, 1970.
- [9] Klein, H., "Der Kreismesser-Scherenschnitt und seine optimale Einstellung für das Längsschneiden bahnförmiger Materialien (Teil 3)," *Coating 5*, 1995, pp. 176 - 179.
- [10] Wingen, P., Haeger, J., "A Primer on Longitudinal Slitting," *Paper, Film & Foil CONVERTER*, July 1987, pp. 43 - 47.
- [11] Bhushan, B., Koinkar, V. N., "Microtribology of metal particle, barium ferrite and metal evaporated magnetic tapes," *Proceedings of the Tenth International Conference on Wear of Materials*. Boston, Mass., USA, 9. - 13 Apr. 1995. Part I, pp. 360 - 370.
- [12] Hombach, T., Sturm, H., "Probleme und Erkenntnisse beim Schneiden bahnförmiger Materialien," *Das Papier*, 29, 1975, 9, pp. 385-392.

- [13] Schable, R., "Axialer und radialer Schlag können Messer beschädigen und die Schnittqualität herabsetzen," *Papier + Kunststoff-Verarbeiter*, 2, 1994, pp. 15-21.
- [14] Friederichs, J. W., "Ultra-fine grained cemented carbide - suitable for tape-slitting knives for magnetic tapes," U.S. Patent No. 5368628-A, 29 Nov.1994.
- [15] Wolf, K., "Ingenieurkeramik: Bearbeitungsverfahren und Anwendungsbeispiele," *KEM*, August 1994, pp. 63-64.
- [16] N. N., "Sliziumnitrid im Vormarsch," *mav* 10, 1995, p. 38.
- [17] Moeller, F., "Zirkonoxid: Weiterentwicklung einer technischen Keramik," *KEM* July 1990, p. 107.
- [18] Kolaska, H., Dreyer, K., "Hartmetalle, Cermets und Keramiken als verschleißbeständige Schneid- und Werkstoffe," Teil 1 und Teil 2, *dima*, 10, 1989, pp. 26-33 and 11, 1989, pp. 51-57.
- [19] Kolaska, H., Dreyer, K., "Harte Angelegenheit," *KEM*, 5, 1991, pp. 119-120.
- [20] Christoffel, K., "Trends in der Schneidstoffentwicklung," *Sonderausgabe Produktions-Automatisierung*, 1995, pp. 36-37.
- [21] N. N., "Ein neuer Stoff - härter als Diamant. Kohlenstoffnitrid: Ein Werkstoff nach Maß," *VDI Nachrichten*, 26 Jan. 1996, p. 12.
- [22] Sigl, L. S., Schwetz, K. A., "TiB₂-Based Cemented Borides: A New Generation of Hardmetals," *pml*, vol. 23, no. 4, 1991, pp. 221-224.
- [23] Kalb, W., "Beschichtungswerkstoffe aus Titanlegierungen für den Verschleißschutz," *Metall*, 43, 1989, 10, pp. 951-953.
- [24] N. N., "Wirtschaftliche Lösung von Reib- und Verschleißproblemen," *Ingenieur-Werkstoffe*, 2, 1990, 1/2, pp. 29-31.
- [25] Esser, S., Lemmer, O., "PVD-Beschichtung für den Verschleißschutz," *Metall-oberfläche*, 42, 1988, 10, pp. 477-479.
- [26] N. N., "Beschichtungsverfahren TriTec löst tribologische Probleme," *Galvano-technik*, 82, 1991, 7, pp. 2361-2362.
- [27] Wild, R., "Stanz- und Umformwerkzeuge mit Hartstoffbeschichtung," *Dünne Schichten*, 1991, 3, pp. 21-29.
- [28] Ballhause, P., "Billard in der Kammer. Gesputterte Hartstoffschichten - Lösung aller tribologischen Probleme?," *KEM*, 1991, September S5, pp. 39-40.

- [29] N. N., "Superharter Stoff," *iam*, November 1992, pp. 12-13.
- [30] Repenning, D., "Korrosions- und reibarme 'diamant-ähnliche' Multilagenschichten," *Der Dünnschichtmarkt*, 5, 1992, pp. 6-8.
- [31] Bonetti, R. S., Tobler, M., "Amorphe, diamantartige Kohlenstoffschichten - Jetzt im industriellen Maßstab machbar," *Technische Rundschau*, 45, 1989, pp. 32-35.
- [32] Reiter, N., "Neue Beschichtungsverfahren erhöhen die Leistungsfähigkeit," *dima*, 3, 1990, pp. 56-60.
- [33] N. N., "Plasma-CVD-Beschichtung," *mav*, 5, 1990, p. 59.
- [34] N. N., "Zäher Kern unter hartem Panzer - Die erste Plasma-CVD-Anlage für Wendeschneidplatten ging in Betrieb," *VDI-Nachrichten*, 13 Apr. 1990, p. 26.
- [35] N. N., "Höhere Standzeit - Erste Plasma-CVD-Anlage in Betrieb," *Industrie-Anzeiger*, 1990, 41, pp. 66-68.
- [36] N. N., "Lokale Laserbeschichtungen gegen Verschleiß und Korrosion," *Galvanotechnik*, 82, 1991, 5, p. 1619.
- [37] Burchards, D., "Belastung bleibt klein. Laserbeschichten von Bauteilen erfordert Flexibilität zum Erreichen der Wirtschaftlichkeit," *Maschinenmarkt*, 98, 1992, 24, pp. 88-93.
- [38] N. N., "Laserbeschichtung erhöht Schutz," *JOT*, 1992, 4, p. 138.
- [39] Werle, P., "Standzeitfrage - Hauchdünner Diamantfilm macht verschleißfest," *iam*, September 1991, pp. 32-34.
- [40] N. N., "Harte und korrosionsbeständige Borierschichten," *Galvanotechnik*, 88, 1997, 10, p. 3381.
- [41] Silman, H., "Konkurrenz für Hartchrom," *Galvanotechnik*, 79, 1988, 4, pp. 1155-1156.
- [42] Kuhn, A. D., "Neue Antihaf-High Tech-Beschichtung," *Galvanotechnik*, 83, 1992, 1, pp. 338-339.
- [43] Mucha, A., Bäther, K.-H., "Ionenstrahltechniken zur Oberflächenmodifizierung," *Dünne Schichten*, 2, 1997, pp. 10 - 18.
- [44] Grischke, M., Dimigen, H., Bewilogua, K., Schäfer, L., "Neue Aspekte bei superharten Schichten und bei der Ionenimplantation," *Schriftenreihe "Praxis-Forum"*, ohne Jahr, pp. 19-33.

- [45] Bartolucci Luyckx, S., Cassuto, Y., Sellschop J. P. F., "Ductile-to-brittle Transition Induced by Nitrogen Ion Implantation into WC Single Crystals," *Materials Science and Engineering*, 90, 1987, pp. 339-341.
- [46] Wolf, G. K., "Ionenstrahlverfahren zur Verbesserung von elektrochemischen Schichten," *Galvanotechnik*, 79, 1988, 11, pp. 3632-3639.
- [47] Anderson, A. D., Loretto, M. H., Dearnaley, G., "Microstructural Study of Ion-Implanted WC-Co," *RM & HM*, 9, 1989, pp. 189-191.
- [48] Kanazawa, K., Chijjiwa, K., Iwaki, M., "Improvement on the Breakage and Chipping of Cutting Tools using N-Ion Implantation," *Bulletin of Japanese Society of Precision Engineering*, 21, 1987, 1, pp. 63-64.
- [49] Ranke, H., Körber, F. J., "Ionenimplantation: Verfahren zur Modifikation technischer Oberflächen - Atome zerstäuben," *KEM*, 8, 1989, pp. 32-36.
- [50] Schwarz, M., "Fremdgänger schaffen Material nach Maß - Beschuß mit Ionenstrahl verändert Oberfläche," *VDI-Nachrichten*, 8 Mar. 1991, p. 39.
- [51] Wolf, G. K., "Neue Anwendungen der Ionenstrahltechnik," *Ingenieur-Werkstoffe*, 3, 1991, 12, pp. 50-52.
- [53] Pöhlandt, K., Lange, K., "Ionenimplantation von Umformwerkzeugen im Vergleich zu herkömmlichen Verschleißschutzbeschichtungen," *VDI-Z Spezial Werkzeuge*, 8, 1992, pp. 26-34.
- [54] König, U., Kolaska, H., Ballhause, P., Wolf, G., "Ionenimplantation von Hartmetallen," Forschungsbericht, Krupp Widia GmbH, Essen, ca. 1992, pp. 6.1-6.35.
- [55] Paterok, L. J., "Thermoimplantieren: Beschichtung für Sägeblätter - Deutlich längere Standzeit," *Industrie Anzeiger*, 1992, 39, pp. 48-51.

Pak L. Ko,¹ Howard M. Hawthorne,² and Jasmin Andiappan³

TRIBOLOGY IN SECONDARY WOOD MACHINING

REFERENCE: Ko, P.L., Hawthorne, H.M., and Andiappan, J., “**Tribology in Secondary Wood Machining,**” *Wear Processes in Manufacturing, ASTM STP 1362*, S. Bahadur and J. Magee, Eds., American Society for Testing and Materials, 1999.

ABSTRACT: Secondary wood manufacturing covers a wide range of products from furniture, cabinets, doors and windows, to musical instruments. Many of these are now mass produced in sophisticated, high speed numerical controlled machines. The performance and the reliability of the tools are key to an efficient and economical manufacturing process as well as to the quality of the finished products. A program concerned with three aspects of tribology of wood machining, namely, tool wear, tool-wood friction characteristics and wood surface quality characterization, was set up in the Integrated Manufacturing Technologies Institute (IMTI) of the National Research Council of Canada. The studies include friction and wear mechanism identification and modelling, wear performance of surface-engineered tool materials, friction-induced vibration and cutting efficiency, and the influence of wear and friction on finished products. This research program underlines the importance of tribology in secondary wood manufacturing and at the same time adds new challenges to tribology research since wood is a complex, heterogeneous, material and its behaviour during machining is highly sensitive to the surrounding environments and to the moisture content in the work piece.

KEYWORDS: wear, friction, surface characterisation, wood, cutting tool, cutting force, carbide, diamond inserts

¹ Senior research officer (NRC) and adjunct professor (UBC), Integrated Manufacturing Technologies Institute-West, National Research Council of Canada, 3250 East Mall, Vancouver, B.C. V6T 1W5, Canada.

² Group leader (NRC) and adjunct professor (UBC), Integrated Manufacturing Technologies Institute-West, National Research Council of Canada, 3250 East Mall, Vancouver, B.C., V6T 1W5, Canada

³ Women in Engineering & Science student, University of Windsor, Ontario, Canada.

As the forest resources of the world become increasingly scarce, intelligent use of forest products is necessary not only to provide economical advantages, but also for sociological reasons. The forest industry occupies a very important sector in the Canadian economy. For example, British Columbia's softwood industry is about seven percent of the world total and B.C. is the world's largest exporter of softwood lumber. Twenty-two percent (or 9,200,000 ha) of productive forest land in B.C. has been harvested in the past 140 years [Forest Renewal B.C. Pamphlet, 1995⁴].

Secondary wood manufacturing, which covers a wide range of products from furniture, cabinets, doors and windows, to musical instruments, is one of the areas in the forest resource chain that can create significant impacts. The emphasis is on high-speed processes and high standard of surface quality. Consequently, many of these products are now mass produced in sophisticated, high speed numerical controlled machines which require the development and use of exceptionally high performance, reliable, wear-resistant tools. In other words, the performance and the reliability of these tools are key to an efficient and economical manufacturing process as well as to the quality of the finished products.

The wood machining tribology program in the National Research Council of Canada (NRCC) deals with applications to the secondary wood industry using expertise gained, and technologies developed, from friction and wear research carried out in the NRC's Tribology Laboratory. Specifically, it deals with the fundamental understanding of tool/wood interaction during cutting, the tool wear processes involved and wood surface quality characterization.

This paper discusses the program in general including a brief literature review, and then presents the results obtained from preliminary studies of tool wear and tool/wood interactions.

Literature Review

The mechanics of wood-cutting have been studied for a long time [1-3]. However, most of these studies involved sawing of primary wood and at relatively low cutting speeds. There are also many early and recent publications on orthogonal metal-cutting and the mechanisms involved in metal-chip formation [4-7]. However, wood is a complex, heterogeneous, material and its behaviour during machining is highly sensitive to the machining direction with respect to the grain direction, the surrounding environments, the material composition and the moisture content in the work piece. These complexities in wood species, together with the current emphasis on high speed machining, demand better understanding of the tool wear mechanisms and tool/wood interactions under various machining conditions.

For many applications, hard materials provide better wear resistance than softer ones. One of the most important prehistoric tool materials was stone, which is relatively hard and wear resistant. Tool materials have evolved from high carbon steel and high

⁴ Forest Renewal B.C. is a Provincial Government Agency of British Columbia

speed steel to cemented tungsten carbide and titanium carbide, and to cubic boron nitride and diamond. As the fundamentals of wear processes and wear mechanisms have become better understood during the past 20 years, many researchers now realize that a simple correlation between hardness and wear resistance may not be valid for all cases, and specifically, in the case of tool wear at high cutting speeds.

It has been recognized in studies of wear of metal-cutting tools that the important wear mechanisms are abrasion, delamination and chemical dissociation and dissolution [8]. One significant difference between metal-cutting and wood-cutting is that in the former the much larger cutting force ensures that workpiece material chips generate very high frictional force and temperature as they move over the tool rake face. This results in severe crater wear near the tool cutting edge, particularly at high cutting speeds. Cook [9,10] considered crater wear to be a thermally activated process. More specifically, the predominant cause of crater wear at high cutting speeds has been considered by some to be diffusion [11,12]; chemical instability of the carbides at high cutting speeds by others [13]; and, more recently, even tool melting [14]. In wood-cutting, although the cutting forces involved are usually much lower, the cutting speeds are much higher. Furthermore, wood cutting tools are much thinner than metal cutting tools. Therefore, high frictional heat and hence high tool tip temperatures can still be generated during wood-cutting.

A wood-cutting tool usually consists of a cutting edge at the intersection of a rake face and a clearance face with a cutting angle between 30 and 50 degrees, depending upon the tool tip material, formed by these two faces. A fairly comprehensive review of wood-cutting tool wear was published by Klamecki in 1979 [15]. This review and many other publications on wear of wood-cutting tools [16,17] are concerned primarily with tool damage and tool life rather than with the actual wear mechanisms involved. Tool wear in wood-cutting is classified generally in terms of abrasive wear and chemical wear on the one hand, and impact and brittle failure on the other hand [18,19]. The latter results usually in chipping, gapping or crumbling of the tool edge. The sharp cutting edge and the relatively small cutting angle of a steel wood-cutting tool make it more susceptible to gross plastic deformation and blunting. Many solid wood products and, in particular, the commonly used medium-density fibreboards (MDF) are very abrasive, which can quickly wear down a soft tool. On the other hand, knots and variations in growth ring patterns, together with the impact nature of some of the machining processes, can cause fracture of hard, brittle tool materials, which can quickly render such tools unusable. Thus, the basic requirements for a wood-cutting tool appear to be (1) wear resistance; (2) fracture resistance; and (3) resistance to gross plastic deformation.

By utilizing tools that are more resistant to cutting edge wear, tool sharpening down time can be reduced while producing cleaner, smoother contours.

Tungsten carbide tools are now mostly used for machining solid wood as well as particleboard. The machining process usually involves high temperatures and pressures in the cutting zone and near the tool edge. The role of corrosion in the deterioration of woodcutting edges of cemented carbides was found to be very significant in several studies [20-25]. They showed that the organic acids and phenolic compounds contained in green wood are capable of promoting corrosion of steel. Stewart [26] found that high-temperature corrosion/oxidation is a major contributor to the wear of tungsten carbide when machining MDF. He suggested that tool wear can be reduced by selecting tool

materials, coatings, or treatments that are relatively chemically inert at high temperatures and/or can conduct heat away from the cutting zone. Thus, wear mechanisms other than abrasion need to be considered when machining MDF.

Sheikh-Ahmad et al. [27] reported preferential chemical wear of the cobalt matrix in coated tungsten carbide tools during continuous machining of particleboard. The resulting loss of matrix caused the carbide grains to break loose from the composite tool material. The tool wear increased with increases in grain size and cobalt binder content. It was also found that the tool tip temperature did not appear to be high enough to cause oxidation of the tungsten carbide grains, but might be high enough for oxidation and softening of the cobalt binder, which in turn could lead to an increase in abrasive wear.

Cubic boron nitride (cBN) is the hardest material known next to diamond, and has excellent abrasion resistance. Micron sized cBN crystals are randomly oriented and strongly bonded to each other to provide uniformly high hardness and wear resistance. These tools are manufactured by bonding a layer of cubic boron nitride crystals to a tungsten carbide substrate.

Polycrystalline diamond (PCD) has a very high thermal conductivity and conducts heat twice as well as copper and five times better than tungsten carbide. It is also relatively inert at high temperatures. PCD tipped tools are capable of high material removal rates in production boring, turning and milling operations of metals. PCD tool blanks are manufactured using fine particles of man-made diamond crystals, which are grown together and integrally bonded to a cemented tungsten carbide substrate. Thus PCD has significant potential to replace tungsten carbide or high-speed steel as the primary cutting tool material for MDF because of its ability to resist chemical attack at higher temperatures and dissipate heat away from the cutting zone [28].

For machining MDF, Stewart [29] found good correlation between cutting forces and edge recession on steel tools with different rake angles. His results indicate that moderate rake angles between 10 and 30 degrees are optimum for steel tools.

Besides being an important indicator of product quality, the finished wood surface also provides a good means of evaluating optimum cutting parameters and tool life. There are highly sophisticated instruments for characterisation of surface topography, such as stylus or laser profilometers and surface analyser instruments using optical interferometry. For wood surfaces, however, the cell and fibre structures on and below the surface, give rise to pores, protruding fibres and small grooves (from fibre tearout) and detection of these can be missed by the stylus and/or the optical devices. Lemaster and Stewart [30] developed a "laser line" (rather than a "laser spot") technique so that the optical profilometer is less sensitive to such surface features. The method works like a front end filter for the system and makes the surface waviness much more prominent.

Wood Machining Tribology

The wood machining tribology program is part of a new initiative of the NRCC to deal with the machining and manufacturing processes of secondary wood products. The overall aim is to develop a model of manufacturing processes for intelligent wood machining, which includes machine parameter optimisation, optimum cutting tools and on-line sensors. The tribology group is involved in four major areas, namely, tool wear, tool/wood interaction, wood surface quality characterisation, and parametric studies that

include optimum machining parameters, tool geometry, tool materials and several chosen wood species. In tool wear studies, the wear performance of surface engineered tool materials will be evaluated. The studies of tool/wood interaction include friction and wear mechanism identification, cutting forces and tool dynamics. Wood surface quality characterisation will first entail identifying surface parameters that best characterise wood surfaces and then the influence of tool wear, tool geometry and tool/wood friction on finished product surfaces will be studied.

The machines and equipment for wood-machining studies at NRCC include metallographic and surface examination instruments, such as, Scanning electron microscopy, 3-D surface measurement systems and imaging analysers; and several newly acquired machining equipment. These include a 5-axis and a 3-axis computer-numerically-controlled (CNC) router, a CNC lathe and two other standard lathes. These machines are instrumented with force and vibration sensors. A specially designed tool dynamometer with two tri-axial force transducers sandwiched between a stationary platform and a top platform that supports the tool holder, is used in lathe machining studies. For the routers, commercial force tables capable of measuring forces and moments in three directions are used to support the wood specimens. A modified reciprocating test rig with a linear drive capable of up to 10 cm amplitude and 5 Hz is available for friction studies of various combinations of tool materials and wood species. The stationary platform that holds the wood specimens is supported on a tri-axial force transducer enabling instantaneous measurement of friction and normal forces.

Test Program for Tool Wear Studies

Test Series

Two series of orthogonal machining tests were carried out. The first one involves machining the disc surface of solid wood and medium density fibreboard (MDF) specimens using HSS, carbide and diamond tipped tools. The tool edge is at various angles to the grain (for the tests with solid wood) as the disc rotates (varying between 0 and 90 degrees), and is travelling at 90 degrees to the grain. The other series involves machining the side of a MDF disc using a tungsten carbide tool. Almost all the results presented in this paper are from the first series of tests.

Wood Specimens

The medium density fibreboard has become increasingly popular for products ranging from furniture to mobile homes to hardwood floors. In addition, MDF can be made from 100% recycled dry waste and produced from some materials, which normally would be dumped into landfills. Thus, it is important to find the most effective and cost efficient tool for machining this fairly abrasive material. MDF also provides a more homogeneous specimen for fundamental machining studies, so it is chosen as the primary wood material used in the present program. For the first series of single-point machining tests, the MDF specimens were circular disks, 28cm in diameter prepared from 2cm thick sheets that have an average density of 0.77 g/cm^3 and 6 to 7% moisture content.

Several solid wood specimens including some hardwood and some softwood were also tested. These wood specimens were prepared from 2.5cm to 3cm thick boards and made to the shape of a circular disc for use on a lathe.

Wood-Cutting Tools

In the first series, a large number of tests were carried out to evaluate the effectiveness of the polycrystalline diamond tipped and cubic boron nitride tipped tools in cutting MDF compared to steel tools. Two grades of PCD tipped tools, PCD 1500, PCD 1600, and two grades of cBN tipped tools, BZN 6000 and BZN 8200 were tested. The PCD number refers to the diamond particle size, where 1500 is a more coarse grain (25 μm) than 1600 (4 μm). The BZN 6000 insert consists of a layer of about 90 volume-% Borazon cBN particles integrally bonded to the tungsten carbide, while the BZN 8200 insert consists of a layer of about 65 volume-% cBN mixed with TiN.

These bits were bonded to standard square bar-shaped steel shanks measuring 49 mm in length, 5 mm in height and width at the base of the tool. The width of the cutting edge is 4 mm and is tapered to a width of 3 mm neck, Figure 1(a). The tool has a clearance angle of 12 degrees and a rake angle of 48 degrees, and a radial clearance angle of 4 degrees. Similar shaped tools made from D2 steel blanks and heat-treated to 56 Rockwell C were also used. These latter tools were ground and lapped to an angle of 30 degrees using 30 μm and 6 μm diamond paste. The sharpening is such that at a magnification of 200 times, the tip has no discernible radius. After sharpening, the standard deviation of the angle of the blade from 30 degrees is 0.626 degrees.

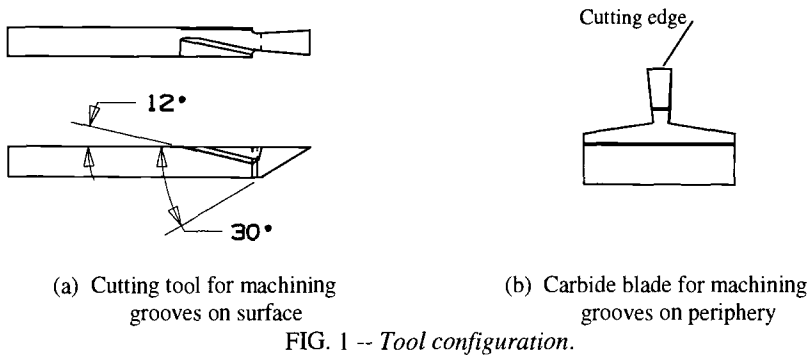
The second type of cutting tool was prepared from tungsten-carbide blades that were reshaped by grinding the cutting edge down to 4 mm from its full 30 mm width, Figure 1(b). These blades were used in the second series of tests involving machining into and then across the periphery (the thickness) of the MDF discs. The aim was to correlate the cutting force to the density of the MDF, which varies across the thickness of the sheet from both faces.

Test Procedures

In this paper, only the results from single-point machining tests and sliding friction tests are presented.

During each test, cuts were made on the flat face of the disk to form concentric machined grooves, 2 mm apart, using a standard metal lathe. The rotational speed of the disk was maintained at a constant 539 rpm, while the linear velocity varied from 5.36 to 7.61 m/s for cutting circles of 19 to 27 cm diameter, respectively. In later tests, a CNC lathe will be used to maintain a constant linear velocity. The cutting tool was fed normal to the disk face at 0.05 mm/rev. (chip thickness) to a depth of 4 mm, the nominal depth of the dense outer layer of the MDF. Using both sides, each disc provided a cumulative length of cut of approximately 1 km.

In the second series of tests, the tool was fed normal to the axis of the disc at 0.05 mm/rev and to a depth of 2 mm. Five grooves were cut. The cutting force results were used to verify the trend of force variation obtained from machining the disc surface at various depths.



The cutting tool was held on the specially designed dynamometer described earlier, Figure 2. It has been shown that the lower the cutting force, the longer the tool life [31], and that tool wear affects the normal force component more than the parallel force component [29]. The parallel force is defined as the cutting force tangent to the tool path arc (Z-direction). The normal force is the feed force and is defined as the force perpendicular to the surface of the wood specimen (defined as X-direction in the 1st series of tests and Y in the 2nd series). The cutting forces in both the parallel and normal directions as well as the tool wear were recorded at regular intervals and analysed. The data acquisition software is capable of sampling at up to 10^5 data points/sec.

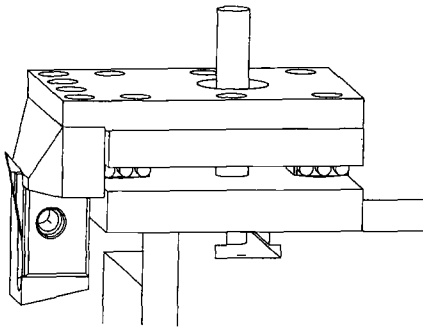


FIG. 2 -- Tool holder and force transducer assembly.

Tool tip images were taken at specific intervals of cutting and stored for later analysis using Optimas 6.0 image analysis software, to determine the recession of the tip. The image of the original, unworn edge could be retrieved and superimposed on subsequent images for accurate measurement of edge wear and wear on the clearance and rake faces of the tool.

The effect of temperature on tool wear is being studied with a third series of tests which is designed to vary and control the bulk temperature of the tool tip up to 500°C. The results will be presented in a later paper.

The force data can be plotted in either rectilinear coordinates or polar coordinates. In the latter format, the force diagram can be superimposed onto the surface of the machined disc providing a convenient way of displaying the correlation between the cutting force and the grain structure in solid wood machining, Fig. 3.

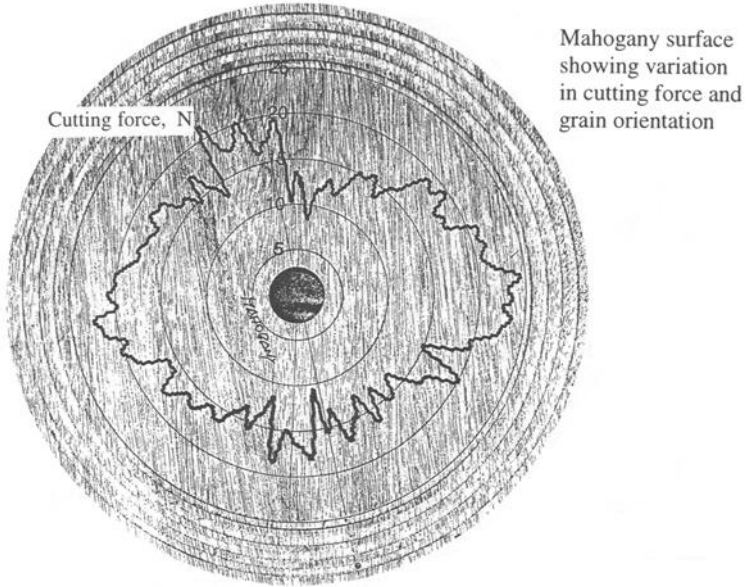


FIG. 3 -- Example of polar cutting forces superimposed on a machined surface.

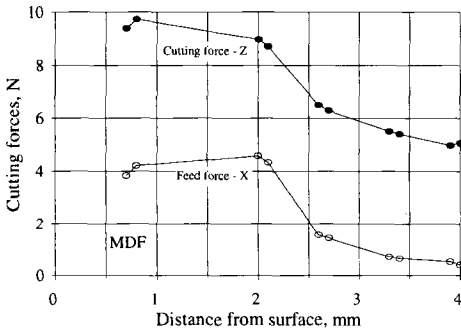
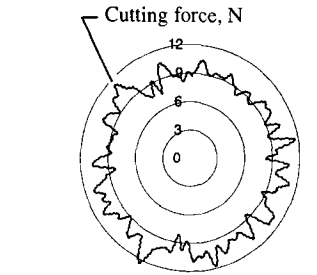
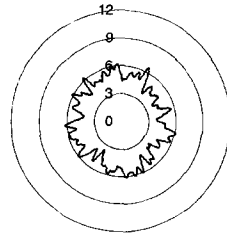


FIG. 4 -- Cutting-force variation through thickness of MDF.



(a) Machining on MDF surface



(b) Machining at 3mm from surface

FIG. 5 – Polar Cutting forces

Results and Discussion

Cutting Forces – MDF Density

MDF is manufactured in such a manner that the face layers of each board are of a higher density than the core layer. Figure 4 shows the cutting-force profiles from the near-surface to a depth of 4mm of a MDF specimen. The results clearly show that the cutting forces in the face layers were nearly double the forces in the inner part of the MDF and on average, this pattern extends to about 2.15 mm on one face and 1.82 mm on the other. Thus, the high density layers are about 2 mm thick. Beyond the 2mm layer, the density decreases gradually until it levels off at about 4 mm. Figures 5 shows examples of two polar-plots of the average cutting forces obtained on the disc surface and at a depth of 3 mm. Again, the forces are about twice as much on the surface as at 3 mm depth. This observation is confirmed by cutting force results from the second series of tests.

Tool Tip Wear – Recession

Figures 6 and 7 show images of the worn tips of the four tipped tools and the high-speed steel tool. The corresponding graphs of recession vs. length of cut for these tools are presented in Figure 8.

The results clearly show that the D2 steel tool has the largest recession; three to four times higher than those of the special tool tips. Among the diamond and cBN tool tips, BZN 8200 appears to have a higher recession rate than the other three. It was observed that the tip of BZN 8200 chipped badly after the first kilometre of cutting.

It is noted that, in general, the recession rate decreases with the length of cutting. This trend is more pronounced with the tipped tools whose recession rates decreased rapidly to near zero after the first 4 km. This observation may provide a useful reference during later studies. As all tools would become somewhat blunted or chipped after machining, the sharper the edge the sooner these would occur. A new series of tests is planned to correlate cutting forces and surface finishes with tools of different geometry and sharpness.

Examination of images of the worn tools, reveals the variation in recession of the different types of tool insert materials (Figures 6 & 7). The PCD 1500 tipped tool (Figures 6(a)) shows that the insert has chipped on the left-hand side face, which occurred after 8 km of cutting. The recession on the clearance face is 373 μm , while on the rake face it is 343 μm . The figures of 6(b) show the PCD 1600 tipped tool before and after wear. The recession from both faces remains very small, and the radius of curvature of the worn tip is 20.6 μm . The chip on the BZN 6000 tipped blade (Figures 6(c)) measured 294 μm on the clearance face and 237 μm on the rake face. This chip occurred after only 2 km of cutting, although it was very slight. The figures of 6(d) clearly show that the BZN 8200 tipped tool has worn and/or chipped severely in comparison with the other three tipped tools. The recession on the clearance face is 383 μm and 717 μm on the rake face.

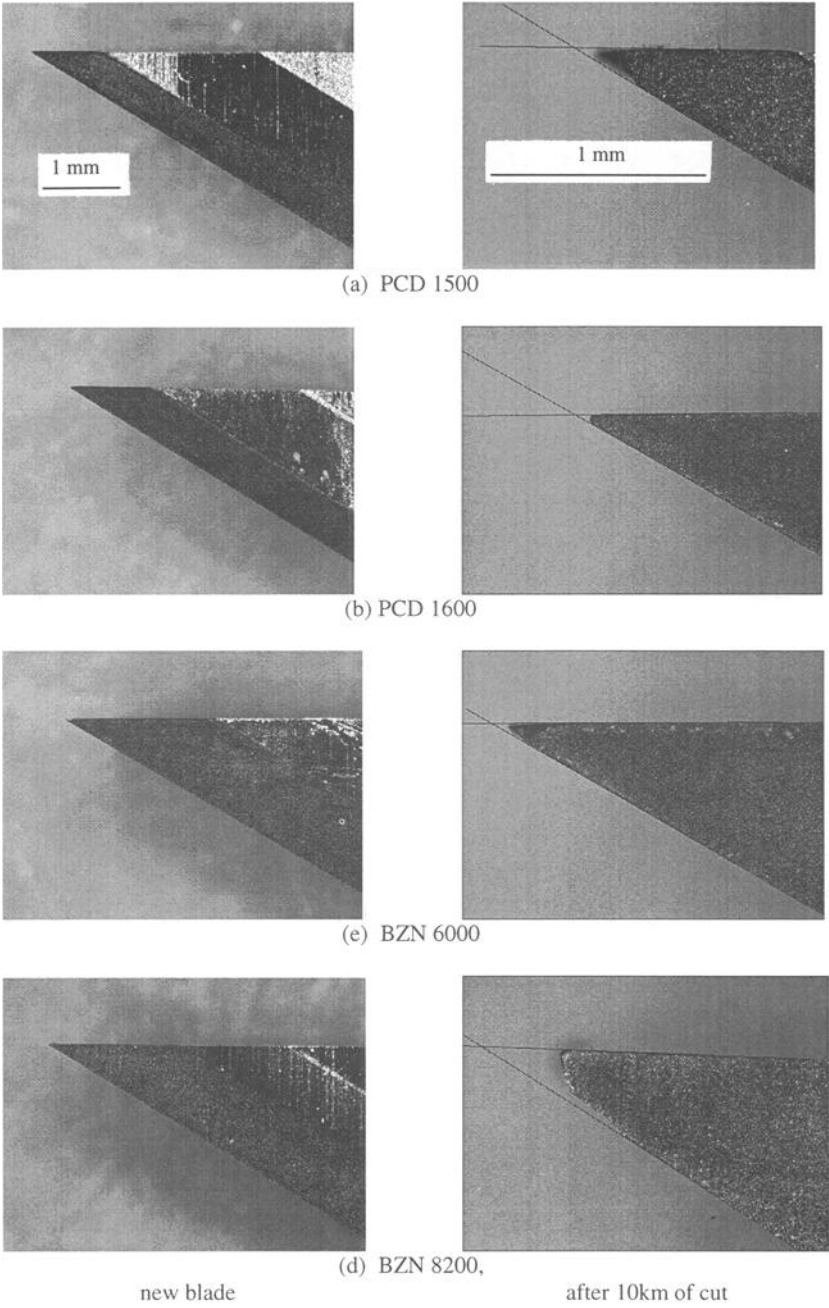


FIG. 6 -- Left-hand side images showing tip recession after 10 km length of cut.

By comparison, the wear of a D-2 steel tool reached 1554 μm on the clearance face and 805 μm on the rake face after 6 km. After 10 km, the recession had increased correspondingly to 1910 μm and 1321 μm . The images in Figure 7 show that the wear on the tool tip is associated with severe plastic flow rather than chipping and wear as observed in the previous images.

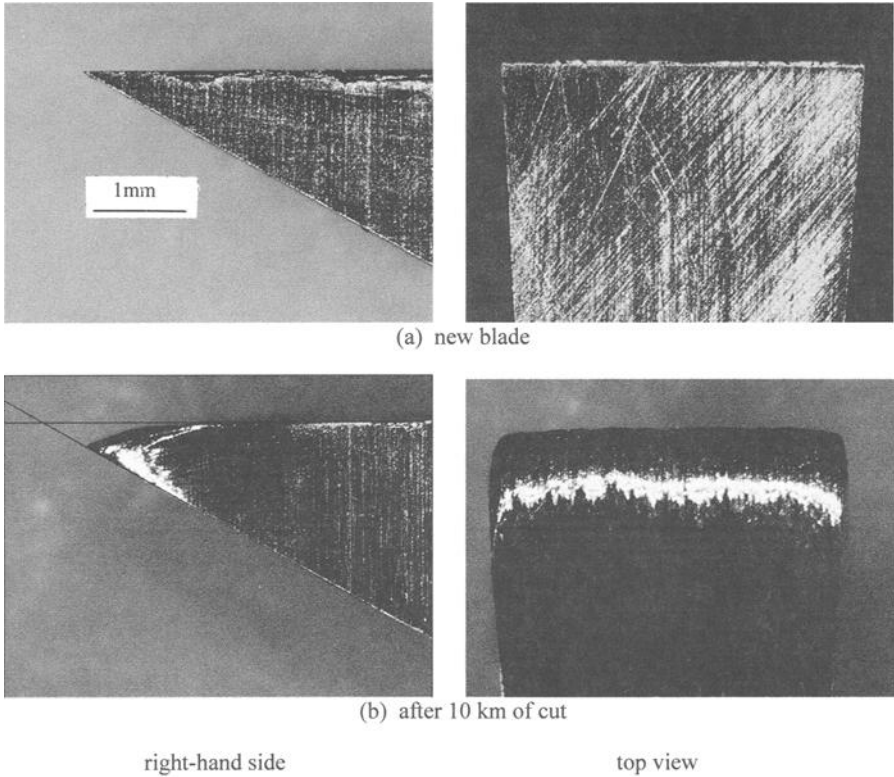


FIG. 7 -- Images of high-speed steel (D2) cutting tool, 50x magnification.

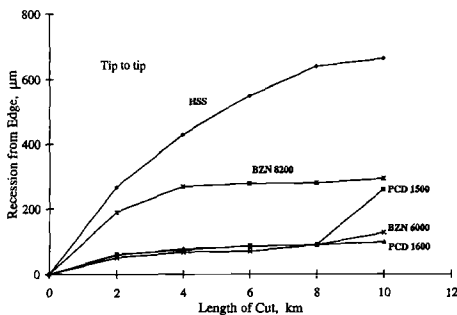


FIG. 8 -- Tool tip recession vs. length of cut.

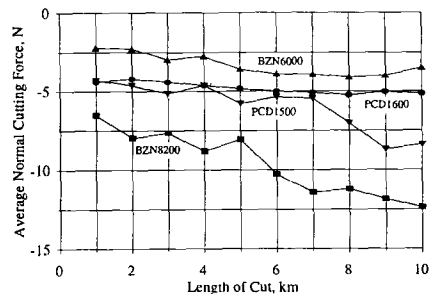


FIG. 9 -- Cutting forces vs. length of cut.

Tool/Wood Interactions – Cutting Forces

There is a strong correlation between the recorded cutting forces and tool tip wear or the sharpness of the edge. The results show that the average cutting forces in both X-normal (Figure 9) and Z (tangential to cutting, not shown) directions are the lowest with BZN 6000 tipped tool, followed by the PCD 1600. Similar trends are found with the corresponding maximum and minimum values of these two forces. The cutting forces using the steel blade were significantly higher than the diamond tipped and cubic boron nitride tipped blades by a factor of around 2, in the Z direction, to more than 10, in the X direction. This finding agrees with the observations made by Stewart [29] that tool wear affects the normal force (X-direction) component more than the parallel (Z-direction) force component. The results from the cBN and PCD tools, with the exception of cBN 8200, also show that the cutting forces, following the trend of the recession shown in Figure 6, cease to increase after the first 4-6 km. The sudden increase in cutting forces of the PCD 1500 tool after about 8 km is likely due to the occurrence of the chip on the left-hand-side face. Similarly, based on the cutting force results, one can infer that the BZN 8200 tip had chipped earlier at the 4-5 km point, hence the appearance of a continuous increase in cutting forces.

Tool/Wood Interactions – Friction Forces

To gain fundamental understanding of the wood cutting processes and the mechanics involved, some knowledge of the friction between the tool and wood materials is needed. A short series of tests was carried out with MDF and several solid wood species rubbing against five tool steels and a carbide tool material on the reciprocating test rig. For the solid wood species, both along-grain and across-grain directions were tested. All tests were carried out with a 50N normal load acting on a tool material specimen, 1cm in diameter and 2cm long. The tool specimen was oriented with a generator parallel to the wood surface and perpendicular to the direction of sliding simulating a rounded cutting edge. Two sliding speeds, 1.4 cm/sec and 4.2 cm/sec, were used. The wood surface was machined and then polished with the same grade of sandpaper after each test.

The results of friction tests revealed that there are significant variations in the coefficients of friction for different wood species. Red Cedar, a softwood species, consistently showed high friction against various types of tool materials; whereas, Fir and Spruce, two other softwood species, consistently showed low friction values that are less than one-half of those of the Cedar and some hard wood species. Figure 10(a) shows the coefficients of friction for carbide tool material vs. wood species and for the average of several tool steel materials vs. wood species taken along the wood grain direction. It shows that all wood species sliding against carbide material exhibited about 35% higher friction than against tool steels. Similar friction plots for sliding across the wood grain direction are shown in Figure 10(b). In general, the friction values are slightly lower than those from the along-grain sliding. This trend appears to hold for all the friction pairs.

Three wood materials (Fir, Yellow Cedar and MDF) were chosen for further tests to study the effect of varying the normal load from 21N to 50N in four steps. The results of MDF in Figure 11(a) show that there are small fluctuations when the coefficient of

friction was plotted against normal load, however, there is no discernable trend. The variation may be attributed to experimental statistics. Similar plots were obtained for Yellow Cedar and Fir but not presented in order to limit the number of graphs in this paper. Nevertheless, the results of both show that normal loads up to 50N on a 1cm diameter rod specimen have no effect on the coefficient of friction. On the other hand, there are definite effects of sliding speed and tool material on the coefficient of friction, and the results are fairly consistent. These are clearly illustrated in the graphs of Figure 11(b). They show that the coefficient of friction is always slightly higher with higher sliding speed, and the coefficient is also higher when wood species are slid against carbide material than against tool steels.

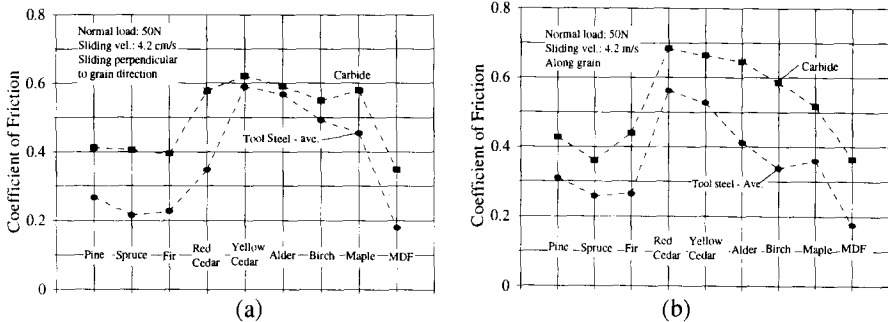


FIG. 10 -- Coefficients of friction of tool materials vs. wood species.

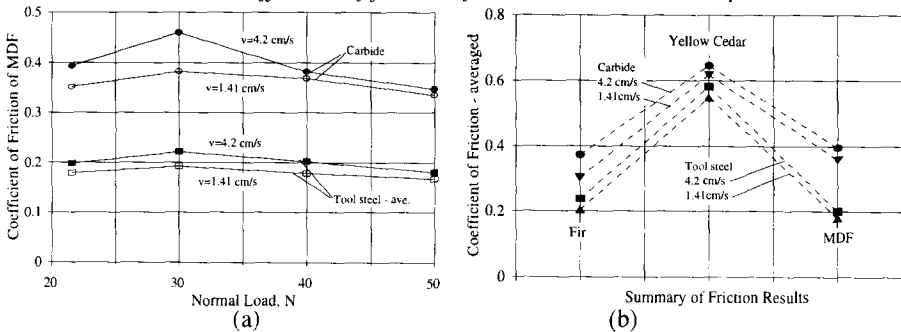


FIG. 11 -- Effects of normal load and sliding speed on tool/wood friction.

Metallography of Worn Tools

Figure 12 shows SEM micrographs of a worn diamond PCD 1600 tip and a cBN BZN8200 tip. The cBN tip has worn substantially more than the PCD tip. However, unlike the tool steels (Fig. 7), the primary wear mechanism in both cases appears to be a degradation of the surface structure resulting from localized high temperature generated at the interface during cutting. In the case of cubic boron nitrided tungsten carbide, the binder material might become softened from the frictional heat and allowed the carbide grains to come loose from the surface. The PCD is known to have much better heat dissipation capability so it would be less affected. Still, the micrographs in Fig. 12(a) show that the voids on the surface of the PCD tip are about the size of the diamond grains

(approx. 5 μm) suggesting that some diamond grains did come off the surface. A crack that appears on the micrograph is likely formed from a series of adjacent voids. The formation of this crack would signal the beginning of a chip breaking away from the tool tip. There is no evidence of abrasive wear, whereas the images of a worn steel blade, Fig. 7, showed severe plastic deformation and some degree of abrasion.

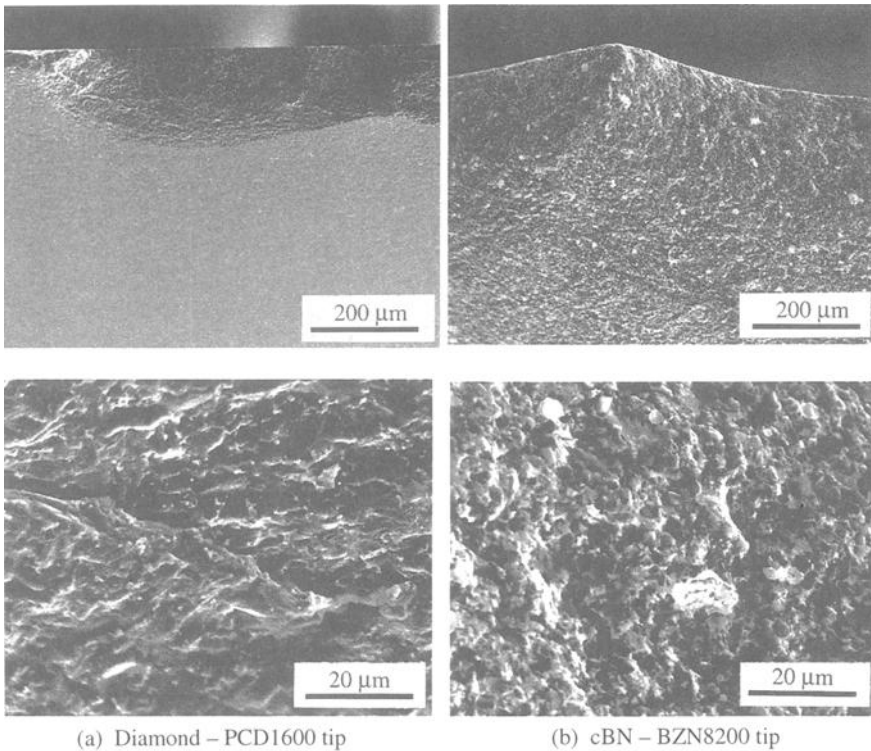


FIG. 12 -- SEM micrographs of worn tool tips.

General Discussion and Summary

The polycrystalline diamond-tipped tools and cBN-tipped tools were much superior in terms of tool wear and cutting forces than the D-2 steel tools. The latter displayed high tip temperatures from cutting, with discolouration of their tips, and severe plastic deformation. As expected, the PCD and cBN tipped tools showed no temperature discolouration and no massive tool-tip deformation. Of the tipped tools, it was found that the PCD 1600 tipped blade showed the least recession of tool material due to cutting, while the BZN 8200 tipped blade chipped and showed signs of wear more quickly than the others. Through examination of the cutting forces, it was found that the BZN 6000 tipped blade recorded the lowest cutting force values, while the BZN 8200 tipped tool showed the highest cutting force values.

These preliminary findings indicate that there is good potential for using polycrystalline diamond or cubic boron nitride tipped tools, in particular, tools with a PCD grade of 1600 or finer and inserts with 90% or greater Borazon cBN particles. The metallographic examination of these special tool inserts revealed that the primary wear mechanism is a breakdown of the grain structures which is probably a consequence of localised high temperature generated during machining. A comprehensive test program is planned to study the effects of tool sharpness, tool geometry, tool tip temperature and other machining parameters.

Since the cuts in the first series of tests were made to a depth of 4mm, the lower density in the core of the MDF would have affected the absolute relationship between tool wear (tip recession rate) and length of cut shown in Figure 8. However, this effect would be common to all the tool materials tested and would not significantly affect the overall evaluation of the tool materials. In future tests, cuts will be limited to the 2.5mm depth in a series of tests. Later, the specimens can be reused for other series of tests using only the core section of the disc.

The large variation in friction values among various wood species indicates that this should have a profound effect on chip formation and finished surface quality when cutting solid wood as the chip slides along the tool rake face during cutting.

The present paper has not dealt with the topic of surface characterisation and quality of surface finish. The latter is the most important indicator of tool wear and tool performance.

Acknowledgements

The authors wish to thank Darren Hass, a co-op student from the University of British Columbia, for carrying out the machining tests and for collecting and analysing the force data. They also wish to acknowledge the assistance provided by Mark Robertson of the National Research Council.

References

- [1] Kivimaa, Eero, 1950, "Cutting Force in Wood-Working," Finland State Institute for Technical Research, Ph.D. thesis.
- [2] Franz, N.C., 1958, *Analysis of Wood-Cutting Process*, Univ. of Michigan Press, Ann Arbor, Michigan.
- [3] McKenzie, W.M., 1961, "Fundamental Analysis of the Wood-Cutting Process," University of Michigan, Department of Wood Technology, Ph.D. thesis.
- [4] Clack, V.W. and Brewer, R.C., 1966, "New Technique for Shear Zone Thickness Determination in Orthogonal Metal Cutting," *Proc. Inst. of Mech. Eng.*, U.K., Vol. 181(I-25), pp. 667-686.
- [5] Barlow, P.L., 1966, "Influence of Free Surface Environment on the Shear Zone in Metal Cutting," *Proc. Inst. of Mech. Eng.*, U.K., Vol. 181(I-26), pp. 687-705.
- [6] Ramalingam, S. and Black, J.T., 1973, "An Electron Microscopy Study of Chip Formation,"

Metall. Trans. Vol. 4, p. 103.

- [7] Wright, P.K. and Robinson, J.L., 1977, "Material Behaviour in Deformation Zones of Machining Operation," *Metal Technology*, May, p. 240.
- [8] Suh, N.P., 1980, "New Theories of Wear and Their Implications for Tool Materials," *Wear*, Vol. 62, pp. 1-20.
- [9] Cook, N.H., 1966, *Manufacturing Analysis*, Addison-Wesley, Reading, Mass.
- [10] Cook, N.H., 1973, "Tool Wear and Tool Life," *Trans. ASME*, Vol. 95, p. 931.
- [11] Suh, N.P., 1975, "Surface-Treatment and Coating Techniques for Cemented Carbide Tools," *Proceedings, North American Metalworking Research Conf.*, Dearborn, Michigan, pp. 35-47.
- [12] Akasawa, T. and Hashiguti, Y., 1980, "Crater Wear Mechanism of WC-Co Tools at High Cutting Speeds," *Wear*, Vol. 65, pp. 141-150.
- [13] Kramer, B.M., 1979, "Tool Wear," Ph.D. thesis, MIT, Cambridge, Mass.
- [14] Farhat, Z., Altintas, Y. and Troczynski, T., 1997, "Melt Wear of WC-TiC-Co Cutting Tool in High Speed Machining of P 20 Mold Steel," submitted to *Int. J. Mach. Tool & Manuf.*
- [15] Klamecki, B. E., 1979, "A Review of Wood Cutting Tool Wear Literature," *Holz als Roh- und Werkstoff*, Vol 37, pp. 265-276.
- [16] Huber, H., 1985, "Tool Wear Influences by the Contents of Particleboard," *Proceedings, 8th International Wood Machining Seminar*, pp. 72-85.
- [17] Porankiewicz, B., Ziomek-Moroz, M. and Wagner, K., 1995, "Study of Wearing Process of Cemented Carbide Cutting Edge When Milling Secondary Wood Products," *Proceedings, 12th Int. Wood Machining Seminar*, Kyoto University, Japan, pp. 272-281.
- [18] McKenzie, W.M., 1993, "Wood is Easy to Cut – or is it?" *Proceedings, 11th International Wood Machining Seminar*, Oslo, pp. 27-39.
- [19] Sugihara, H., Okumura, S. Haoka, M. and Makino, Y., 1979, "Wear of Tungsten Carbide Tipped Circular Saws in Cutting Particleboard: Effect of Carbide Grain Size on Wear Characteristics," *Wood Science and Technology*, Vol.13, pp. 283-299.
- [20] Mohan, G.D. and Klamecki, B.E., 1981, "The Susceptibility of Wood-Cutting Tools to Corrosive Wear," *Wear*, Vol. 74, pp. 85-92.
- [21] Bailey, J.A., Bayoumi, A. and Stewart, J.S., 1983, "Wear of Some Cemented Tungsten Carbide Tools in Machining Oak," *Wear*, Vol. 85, pp. 69-79.
- [22] Bayoumi, A., Bailey, J.A. and Stewart, J.S., 1983, "Comparison of the Wear Resistance of Various Grades of Cemented Carbides That May Find Application in Wood Machining," *Wear*, Vol. 89, pp. 185-200.

- [23] Bayoumi, A.E. and Bailey, J.A., 1985, "Comparison of the Wear Resistance of Selected Steels and Cemented Carbide Cutting Tool Materials in Machining Wood," *Wear*, Vol. 105, pp. 131-144.
- [24] Porankiewicz, B. and Wagner, K., 1993, "The Chemical Corrosion of Carbide Cutting Edge when Milling Melamine Coated Particle Board," *Proceedings, 11th International Wood Machining Seminar*, Oslo, pp. 137-145.
- [25] McKenzie, W.M. and Hillis, W.E., 1965, "Evidence of Chemical Acceleration of Wear in Cutting Plant Materials," *Wear*, Vol. 8, pp. 238-243.
- [26] Stewart, H.A., Shatynski, S.K. and Rabin, B., 1986, "High Temperature Corrosion of Tungsten Carbide from Machining Medium-Density Fibreboard," *Carbide and Tool Journal*, Vol. 18(1), pp. 2-7.
- [27] Sheikh-Ahmad, J.Y., Stewart, J.S. and Bailey, J.A., 1995, "Performance of Different PVD Coated Tungsten Carbide Tools in the Continuous Machining of Particleboard," *Proceedings, 12th Int. Wood Machining Seminar*, Japan, pp. 282-291.
- [28] Stewart, H.A., 1991, "A comparison of Tool Materials, Coatings, and Treatments Related to Tool Wear During Wood Machining," *Forest Products Journal*, Vol. 41(9), pp. 61-64.
- [29] Stewart, H.A., and Drawer, P.O., 1989, "Analysis of Tool Forces and Edge Recession after Cutting Medium-Density Fibreboard," *Proceedings, 9th Int. Wood Machining Seminar*, California, pp. 320-341.
- [30] Lemaster, R.L. and Stewart, J.S., 1995, "Progress in Evaluating Surface Quality Using Optical Profilometer Techniques," *Proceedings, 12th Int. Wood Machining Seminar*, Kyoto, Japan.
- [31] Tanaka, C., 1987, "Tool Wear of Wood Cutting Tools Made of Five Different Materials," *Proceedings, 8th Wood Machining Seminar*, Japan, pp. 86-98.

Friction in Vibratory Conveyor

Jerry Z. Raski¹

CHAOTIC BEHAVIOR ON IN-PHASE VIBRATORY CONVEYORS

REFERENCE: Raski, J.Z., "Chaotic Behavior on In-Phase Vibratory Conveyors," *Wear Processes in Manufacturing*, ASTM STP 1362, S. Bahadur and J. Magee, Eds., American Society for Testing and Materials, 1999.

ABSTRACT: One of the basic building blocks of IBM's computer technology is the thin-film interstitial metallized ceramic (IMC) substrate. The packaging of these substrates employs small input/output (IO) pins to provide both mechanical and electrical connection to the printed circuit board. In the automated manufacturing of the substrate, the input and output pins are individually conveyed by in-line vibratory conveyors. However, a non-periodic motion of these pins is observed at certain angles of conveyor table tilt that cannot be explained by classical models of friction. This paper models the motion of a single I/O pin on an in-phase, linearly oscillating conveyor using the classical model of friction and compares that result with experimental observations. It is shown here, analytically and experimentally, that when the vibratory conveyor table amplitude and the coefficient of friction between the pin and the table are sufficiently large, the pin is conveyed forward with some velocity. If the conveyor table's angle of tilt is sufficiently large and the coefficient of friction is sufficiently low, the pin may slip backwards just as fast as the conveyor table drives it forward, resulting in a net pin velocity of zero. Surrounding the condition at which the net velocity of the pin is zero is a chaotic basin of attraction in which the pin motion is non-periodic. This basin of attraction was experimentally determined to be bracketed within a range of values of the coefficient of friction. The implications of these theoretical and experimental results are discussed in terms of the practical application of in-phase vibratory conveyors in manufacturing.

KEYWORDS: vibratory conveyor(s), vibratory feeders, chaotic pin motion, coefficient of friction, boundary film(s), lubricants, table amplitude, table tilt angle, pin groove angle

One of the basic building blocks of IBM's computer technology is the thin-film interstitial metallized ceramic (IMC) substrate. The packaging of these substrates employs small pins to provide both mechanical and electrical connection to the printed circuit board. In the automated manufacturing of the substrate the input and output pins are individually conveyed by vibratory conveyors.

¹Advisory engineer, IBM Printing Systems Company, IBM, 6300 Diagonal Highway, Boulder, CO 80301.

In his tutorial paper, Colijn [1] provides a general classification of vibratory conveyors. He makes the distinction between vibratory conveyances in which the material must be trajectoryed from the conveying surface during transport (out-of-phase) and reciprocating conveying in which the material does not lose contact with the conveying surface (in-phase). Colijn recommends an empirical approach for determining conveying rates and is critical of the analytical approaches taken to date.

Booth and McCallion [2] performed an analytical analysis of a point mass on an in-phase vibratory conveyor. By assuming that the coefficient of friction (COF) between the mass and the conveying surface is constant, they found an approximate linear relation between the amplitude of vibration of the conveyor and the mean conveying velocity. Experimental measurements were made with various materials at various conveyor throw angles and tilt angles to confirm the analysis.

Harding and Nedderman [3,4] examined optimizing the design of an in-phase vibratory conveyor in terms of the conveyor's throw angle, tilt angle, amplitude, and frequency. They also made the distinction between the static and dynamic values of the COF. Harding and Nedderman concluded that the fastest conveying velocity takes place near the table amplitude at which the particle is trajectoryed. The conveyor, they conclude, should be operated with as low a frequency and as high an amplitude as possible to obtain the optimum conveying velocity. They found the optimum values of throw angle to be a function of the tilt of the conveyor and the values of the static and dynamic COF.

Redford and Boothroyd [5] were the first to analyze out-of-phase conveyors and compare them to in-phase conveyors. They found that they could achieve high conveying velocities for a wide range of COF's using out-of-phase conveyance. With in-phase conveyors they found that the mass cannot be conveyed up steep tilt angles if the COF is low.

Hota and Karmakar [6] optimized the design of in-phase and out-of-phase vibratory conveyors. For in-phase conveyors, increasing the COF increases the conveying velocity, but that velocity decreases with increasing values of table tilt. The conveying velocity is also increased by a large table amplitude and a small throw angle. The optimum velocity of out-of-phase conveying is independent of the COF.

In the feeding of IMC input/output pins day-to-day variations are reported. Breathing moist air onto the track can arrest the motion of the pins. "Sticky" pins and pins with irregular motion are observed. How to feed pins in a consistent manner was not understood. This work sets out to explain the vibratory feeding of IMC pins using the following approach:

1. The motion of a single pin on an in-phase vibratory conveyor is modeled with the COF treated as a constant. This provides a useful physical insight into the motion of the pins.
2. Experimental observations and measurements of single pin motion are presented and compared to the simple analytical model.
3. The practical implications of the results are discussed in terms of the use of vibratory feeders in manufacturing.

Theoretical

Figure 1 is a schematic diagram of the table of an in-phase vibratory conveyor. The table oscillates in the $+s$ direction according to $s = -a \cos(\omega t)$ where a is the amplitude and ω is the frequency of vibration. The direction of vibration is at an angle ϕ , called the throw angle. The pin sits in a grooved slot of inclusive angle ψ and the entire table can be tilted through the angle ζ . The forces acting on the pin are the pin's reaction force to the table's vertical acceleration, the force due to gravity, and the frictional force that opposes the motion of the pin.

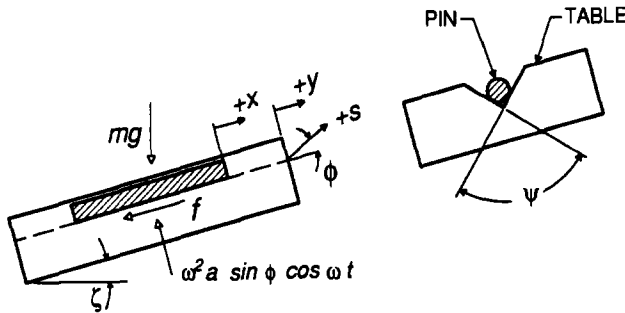


FIG. 1 -- Schematic of a vibratory conveyor.

If the table's vertical acceleration exceeds the acceleration due to gravity, the pin loses contact with the table and is *thrown* forward. However it is possible to achieve forward motion of the pin without it having to lose contact with the table. Writing Newton's second law of motion for the pin describes the motion of the pin by a second order differential equation,

$$m\ddot{x} + f = -mg \sin \zeta \tag{1}$$

where m is the mass of the pin, x is the displacement of the pin, and f is the frictional force. Here the pin is modeled as rigid point mass. The justification for this is two-fold. First, the average velocity of pins of various lengths was observed on the vibratory feed table and no length effect was observed. Second, the table's frequency of vibration is significantly lower than the natural frequency of vibration of the pin. Note that Equation (1) is true as long as the pin maintains contact with the table.

Making the substitution, $z = x - y$, where y is the displacement of the table, Equation (1) becomes,

$$m\ddot{z} + f = -mg \sin \zeta - m\omega^2 a \cos \phi \cos(\omega t) \tag{2}$$

where z is the relative position of the pin on the table.

Classically the frictional force is proportional to the normal force and opposes the relative motion.

$$f = \text{sgn}(\dot{z}) \mu N(t) \tag{3}$$

where $\text{sgn}(\dot{z})$ is the sign function, μ is the constant of proportionality, and the normal force is,

$$N(t) = m \csc \frac{\psi}{2} \left[g \cos \zeta + \omega^2 a \sin \phi \cos(\omega t) \right] \tag{4}$$

In nondimensional terms, combining (2), (3), and (4) produces,

$$\ddot{Z} + \text{sgn}(\dot{Z}) \mu \csc \frac{\psi}{2} (1 + A \cos \tau) = -\tan \zeta - A \cot \phi \cos \tau \tag{5}$$

where $\ddot{Z} = \ddot{z} / g \cos \zeta$ is the dimensionless relative acceleration, $\dot{Z} = \omega \dot{z} / g \cos \zeta$ is the dimensionless relative velocity, $A = \omega^2 a \sin \phi / g \cos \zeta$ is the dimensionless table amplitude, and $\tau = \omega t$ is dimensionless time. Notice that at a dimensionless table amplitude of $A < 1$, the vertical acceleration of the table is less than the acceleration due to gravity and the pin maintains contact with the table.

The COF in Equation (5), μ , may depend on a number of variables such as relative velocity [7,8], the rate of application of tangential force [9], the plastic deformation of asperities [10,11], boundary lubrication [12], and adsorbed moisture [13]. Nevertheless, we begin by considering the situation where the COF is a simple constant to illustrate the general behavior of the motion of the pin. The solution of Equation (5) can then be found by integrating piecewise.

When the table acceleration overcomes the frictional force, relative motion occurs. At low table amplitudes, when the pin just begins to slip, the relative velocity is zero for more than two instances during the cycle. At large table amplitudes the relative velocity passes through zero twice over the period. Suppose the relative velocity is negative from $\tau = -\Phi$ to Ψ . Then the velocity during this time is,

$$\begin{aligned} \dot{Z}_-(\tau) &= \int_{-\Phi}^{\tau} \ddot{Z}(\tau') d\tau' \\ &= (\mu \csc \frac{\psi}{2} - \tan \zeta)(\Phi + \tau) + A(\mu \csc \frac{\psi}{2} - \cot \phi)(\sin \Phi + \sin \tau) \end{aligned} \tag{6}$$

which is valid from $\tau = -\Phi$ to Ψ . Likewise when the relative velocity is positive,

$$\begin{aligned} \dot{Z}_+(\tau) &= \int_{\Psi}^{\tau} \ddot{Z}(\tau') d\tau' \\ &= (\mu \csc \frac{\psi}{2} + \tan \zeta)(\Psi - \tau) + A(\mu \csc \frac{\psi}{2} + \cot \phi)(\sin \Psi - \sin \tau) \end{aligned} \tag{7}$$

for $\tau = \Psi$ to $2\pi - \Phi$. The length of time over which the relative velocity is negative, $\Psi + \Phi$, can be found by marching each of these piecewise solutions out in time. Dividing Equation (6) by (7) the length of time over which the relative velocity is negative, $K = \Psi + \Phi$, can be found,

$$K = \frac{2\pi R}{(R - 1)} \tag{8}$$

where,

$$R = \frac{(\mu \csc \frac{\psi}{2} - \cot \phi) (\mu \csc \frac{\psi}{2} + \tan \zeta)}{(\mu \csc \frac{\psi}{2} + \cot \phi) (\mu \csc \frac{\psi}{2} - \tan \zeta)} \tag{9}$$

The time at which the velocity first turns negative, Φ , is given by the root of the following nonlinear equation obtained from (6).

$$(\mu \csc \frac{\psi}{2} - \tan \zeta) K + A(\mu \csc \frac{\psi}{2} - \cot \phi)(\sin \Phi + \sin(K - \Phi)) = 0 \tag{10}$$

Under steady state conditions, the relative velocity of the pin reaches a constant average value. The average dimensionless relative velocity of the pin, V , is,

$$V = \frac{1}{2\pi} \left[\int_{-\Phi}^{\Psi} \dot{Z}_-(\tau') d\tau' + \int_{\Psi}^{2\pi-\Phi} \dot{Z}_+(\tau') d\tau' \right]$$

Substituting (6) and (7) provides,

$$\begin{aligned} V = \frac{1}{2\pi} \left[\frac{K^2}{2} (\mu \csc \frac{\psi}{2} - \tan \zeta) - \frac{(2\pi - K)^2}{2} (\mu \csc \frac{\psi}{2} + \tan \zeta) \right. \\ \left. + A(\mu \csc \frac{\psi}{2} - \cot \phi) [K \sin \Phi + \cos \Phi - \cos \Psi] \right. \\ \left. + A(\mu \csc \frac{\psi}{2} + \cot \phi) [(2\pi - K) \sin \Psi + \cos \Phi - \cos \Psi] \right] \tag{11} \end{aligned}$$

Equation 11 provides the average relative velocity of the pin in terms of the geometry of the table, the dimensionless table amplitude, the COF, and the times at which the relative velocity passes through zero.

Figure 2 illustrates the theoretical behavior of the pin described in (11). Here the dimensionless average velocity, V , is varied as a function of dimensionless table amplitude, A , for various angles of table tilt and various COF's. Figure 2a shows the effect of varying the COF at 0° table tilt. At small table amplitudes the pin does not slip and there is no relative motion. As the table amplitude increases, the pin begins to move and the average relative velocity of the pin increases. The larger the COF, the larger the increase in average velocity for a given change in table amplitude. The pin will always move forward if the COF is greater than zero. These results are consistent with previous analysis [1-6].

Figure 2b is similar to 2a, but at a table tilt angle of +5°, the pin is being conveyed uphill. Here the average velocity is positive at large values of COF, passes through zero as the COF decreases, and becomes negative for small values of COF. Figures 2c and 2d show that the value of COF at which the average velocity is zero varies with the angle of tilt of the table.

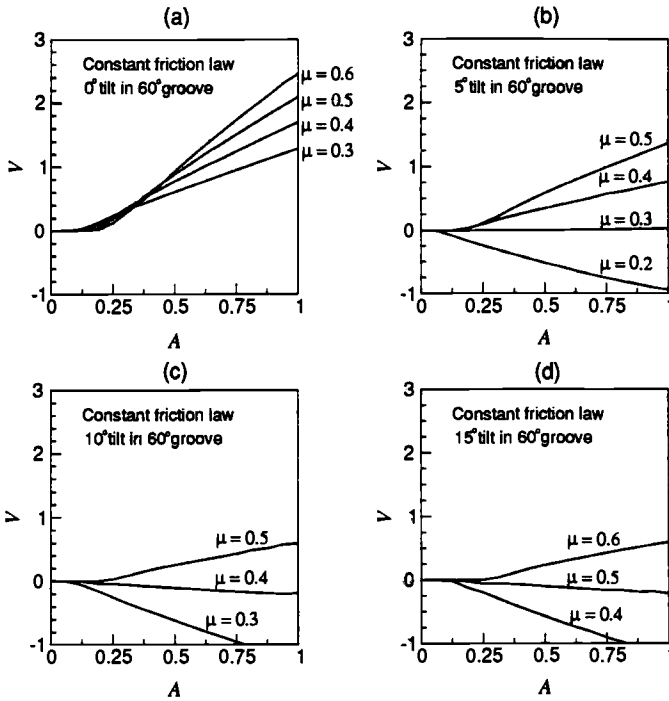


FIG. 2 -- Average velocity for various μ , amplitudes, and tilt angles.

Of practical interest are the values of COF at which the average relative velocity is zero. This brackets the values of tilt and groove angles at which the vibratory feeder can convey pins uphill. There are two physically realizable situations at which the average velocity is zero.

1. The table amplitude is sufficiently small and/or the COF is sufficiently large that the pin does not slip on the table.
2. The COF and the table tilt angle are such that the pin, on the average, slips backward as fast as the table drives the pin forward.

In the first situation, the horizontal table acceleration must overcome the frictional force in order for any relative motion to occur. At small table amplitudes no sliding occurs because $f < \mu N$ and $Z = Z = 0$. From (5) no sliding occurs when,

$$\mu \csc \frac{\psi}{2} (1 - A) \geq -\tan \zeta + A \cot \phi$$

at $\cos \tau = -1$. The converse of this inequality is also true: for relative motion to occur,

$$A > \frac{(\tan \zeta + \mu \csc \frac{\psi}{2})}{(\cot \phi + \mu \csc \frac{\psi}{2})} \tag{12}$$

Figure 3 illustrates the values of table amplitude required to initiate motion as predicted by (12). At a 0° tilt angle, a 60° groove angle, and a COF of 0.50, the dimensionless table amplitude must be greater than 0.15 for motion to begin.

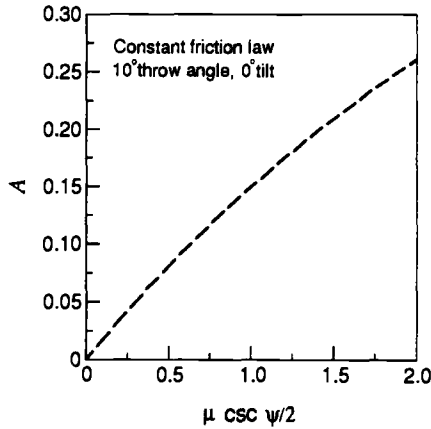


FIG. 3 -- The initiation of sliding.

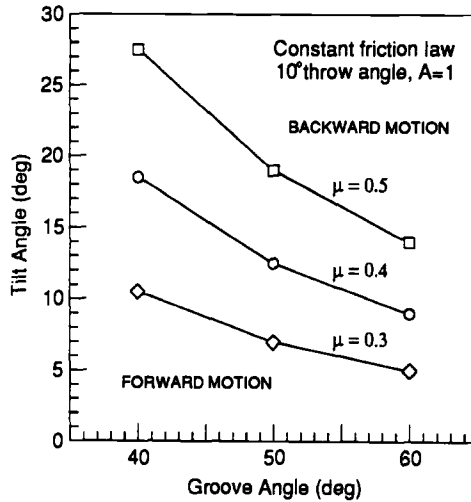


FIG. 4 -- Tilt and groove angles for zero average velocity.

The second situation is illustrated in Figure 4 where groove angle is plotted against tilt angle for various values of COF at which the average relative velocity is zero. In Figure 4, with a value of COF of 0.3 and a 60° grooved table, the table could be tilted up to 5° and the pin would move uphill. If the table were tilted to an angle of greater than 5°, the pin would move backward. However, increasing the COF to 0.5 under the same circumstances would allow the table to be tilted to as much as 15° with continued uphill

forward motion. Decreasing the groove angle has a similar effect to increasing the COF, i.e., it increases the angle to which the table can be tilted while maintaining its uphill forward motion.

Experimental Procedure

Measurements of average pin velocity were made to determine their motion on a vibratory conveyor. The vibratory in-phase linear feeder used was a commercially available device like that used in the manufacture of IMC substrates. The device is a resonant, twin-mass conveyor with a 10° throw angle. The two masses consist of the table of the conveyor, which conveys the pins, and the reaction mass, which counters the excitation of the base of the conveyor. The resonant frequency of the two mass system was found at 31.4Hz and the table design doubles this frequency at the table to 62.8Hz. The conveyor employs an electromagnetic exciter to drive the vibration of the table. In these experiments, the conveyor's electromagnetic exciter was driven by an electrical current, in the form of a sine wave, generated by a frequency generator and amplified by an audio amplifier. An accelerometer was mounted to the conveyor's table to measure the accelerations in the primary direction of motion, $+s$ in Figure 1. The vertical acceleration of the conveyor table, $\omega^2 a$, was determined from the accelerometer measurement and knowledge of the throw angle.

The grooves which carried the pins were machined into a 440C stainless steel plate, hardened to $R_c 56$, and rigidly fastened to the trough of the conveyor. The grooves' inclusive angles were manufactured by dressing a grinding wheel to the groove angle, with a tolerance of ± 30 minutes, and grinding the grooves into the plate. Prior to use, the plate was cleaned in laboratory detergent and water. After drying in clean nitrogen, the plate was vapor degreased in methyl chloroform for 30 minutes and allowed to dry. During testing, a commercial duster, a pressurized halogenated hydrocarbon, was used to remove any dust particles. Prior to making measurements, the track was "conditioned" by allowing multiple pins to be conveyed along the track. These controls are consistent with the use of the vibratory conveyors used in a manufacturing environment.

Two similar types of pins were used in this experiment. The first type of pin was made from a particular copper. The second was this particular copper pin flash gold plated. These pins represent the two standard types of IC pins used in manufacturing ceramic substrates. The copper used was an oxygen-free copper with zirconium in the C15000 composition range developed for high electrical conductivity and strength retention at high temperatures. Both pins have a nominal diameter of 0.4mm and are nominally 8.3mm long.

Measurements of average pin velocity on the conveyor were made by laying out a 150mm long track on the grooved plate, driving the vibration of the table to a known vertical acceleration, and measuring the amount of time the pins took to traverse this distance. The pins were placed some 10 to 20mm away from the start of the 150mm distance in order to allow the motion to reach steady state.

Experimental Results and Discussion

Figure 5 shows a variety of average velocity measurements on the copper and gold pins. These measurements were taken at three different groove angles and four different tilt angles. Each data point in Figure 5 represents the average of nine velocity measurements on nine different copper or gold pins. The standard deviations of these measurements was on the order of 0.1 dimensionless velocity.

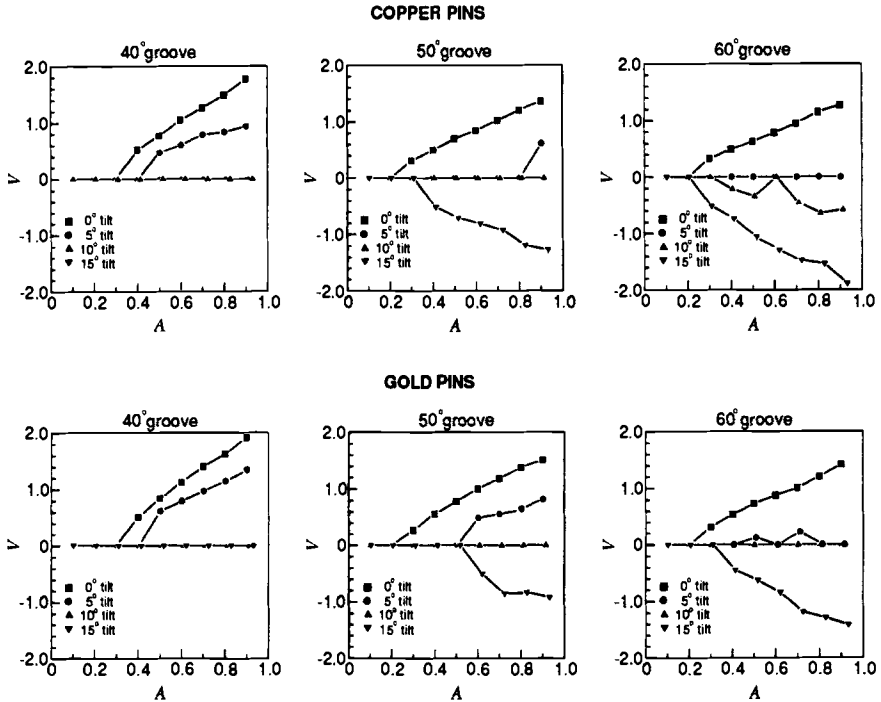


FIG. 5 -- Measured average pin velocities at various table amplitudes.

Qualitatively, the experimental measurements in Figure 5 are similar to the theoretical predictions shown in Figure 2. At low values of dimensionless table amplitude the pin does not move. As the angle of tilt increases, the average velocity of pins decreases, passing through zero, and becomes negative. Yet, in several ways the observed motion differed from the theoretical model. At the start of motion, for low values of dimensionless table amplitude, the pins were often observed to reach a positive velocity and then stop. This arresting of pin motion could not be attributed to groove defects. In some cases the pin would stop at a particular location along the grooved track, and in other cases the pin would not repeatedly stop at a particular location. This starting and stopping of relative motion manifests itself in Figure 5 as an abrupt jump to some relative velocity from no relative motion. At larger values of table amplitude the pins often displayed a non-systematic variation in velocity as they moved along the grooved track.

Two interesting effects were observed when the table of the conveyor was tilted upward.

1. No Motion: No relative motion of the pin could be observed. This behavior would be consistent with the COF and tilt angle being such that a zero average velocity would be predicted. (See Figure 4.) However, if the pin were slightly displaced, it could begin to display the non-periodic motion described in the next item.
2. Non-Periodic Motion: Small amplitude (on the order of several millimeters), non-periodic motion of the pins was observed. This non-periodic motion only occurred when the table of the conveyor was tilted. The non-periodicity was confirmed through observation of the pins under a strobe light at 50X magnification.

This non-periodic motion manifests itself in Figure 5 as a zero average velocity for both the 10° and 15° tilt angles in a 40° groove and as a lack of systematic variation of velocity with tilt angle.

When the conveyor table is tilted, multiple zeros in the average velocity and erratic motion would be expected if the COF significantly varies as a function of one or more uncontrolled parameters. Consider Figure 2c. If the COF varied from 0.5 to 0.4 along the track, the expected average motion would be forward and then backward, effectively trapping the pin at a "friction hill." Like the rock of Sisyphus [14], the pin would be driven forward by the high COF until it encountered the low COF. Once the COF was low enough to result in backward motion, the pin would move backward until the COF became large enough to produce forward motion.

The lower values could be due to the presence of organic films acting as a boundary lubricant. If organic lubricants are present on the surface, even in contaminate amounts of molecular dimension, they may serve to lower the COF between the surfaces. Bowden and Tabor [12] have shown that the reduction of the COF due to a boundary layer of lubricant depends on the molecular weight of the lubricant; the higher the weight the lower the COF. They also showed that a single molecular layer of film produces the same reduction in COF as a thicker film. However, the thinner film is worn away more rapidly on repeated sliding than thicker films: the wear life of the film depending on its thickness.

Chaotic behavior would be expected if the COF varied non-linearly in this manner. The ingredients sufficient for chaos are an energy source and a non-linearity [15]. In the case of vibratory conveyance, the negative frictional damping provides the source of energy and the non-linearity from the variation in the COF due to the wearing away of organic boundary layer films. This system is similar to chaotic systems obtainable from multiple potential wells.

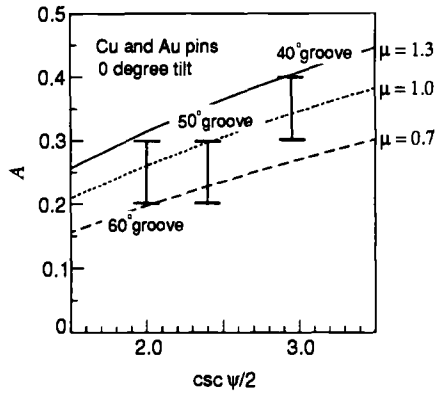


FIG. 6 -- Experimental start of motion for 0° tilt.

Figure 6 shows the experimentally measured values of dimensionless table amplitude at which relative motion is initiated. The solid error bars indicate the range over which motion began at 0° tilt for the copper and gold pins at three different groove angles. Also shown in Figure 6 are the theoretical values of the COF required to delay motion. Figure 6 implies that the static COF reached over 1.0 in these experiments.

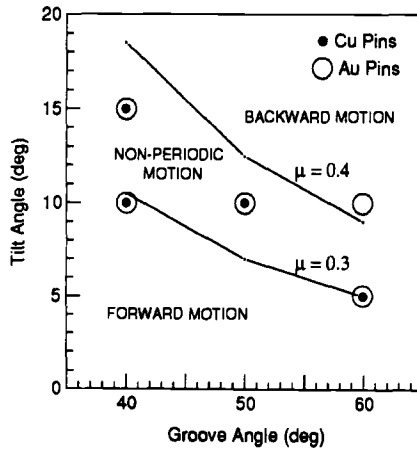


FIG. 7 -- Basin of chaotic attraction.

Figure 7 shows the basin of attraction for chaotic behavior. The solid dots in this figure represent the combination of groove and tilt angles at which non-periodic behavior of the copper pins was observed. The open circles are for the gold plated pins. There was no difference in effect between the copper and gold pins. Also shown in Figure 7 are the values of COF at which the constant friction model would predict zero relative velocity (see Figure 4). Figure 7 brackets the values of the dynamic COF between 0.3 and 0.4.

To summarize the practical implications of the experimental results, high values of COF are desirable to achieve high conveying rates and to convey the pins uphill. However, relatively large conveyor table amplitudes will be required to initiate pin motion at these large values of COF. The groove angle can also be decreased in order to better convey the pins uphill. This is equivalent to increasing the value of COF between the pins and the track. However, the groove angle cannot be made so small as the pins can become wedged in the grooves. Contamination of the track must be avoided since this tends to lower the COF between the pins and the track and attracts the pins toward chaotic behavior.

Conclusions

A single IMC input/output pin on an in-phase linear vibratory pin conveyor was modeled as a single degree of freedom system. Forward motion of the pin can be achieved without the pin leaving the table. Two sets of circumstances were found for which the average velocity of the pin is zero. First, the COF is sufficiently large and/or the conveyor amplitude is sufficiently small that the conveyor table does not slide out from under the pin. Second, the conveyor table tilt angle and the coefficient of friction (COF) are such that they cause the pin to slip backwards just as fast as the table drives it forward.

Experimental measurements of two types of IMC input/output pins on a linear pin vibratory conveyor qualitatively agree with a constant COF model. However, comparison of the model to the experimental results leads to the conclusion that the COF varies significantly between 0.3 to 1.0 due to organic contaminants. There was no difference in effect between the copper and gold pins. Chaotic motion of the pins was observed on tilted conveyor feed tables due to these contaminants alone. This chaotic motion was attributed to a "friction hill," i.e., a gradient of COF encompassing values of the COF that could drive the pin backwards as well as forwards. The basin of attraction to chaotic motion is experimentally defined.

The practical design and use of in-phase vibratory conveyors for use in IMC manufacture requires that small pin groove angles are used to increase the frictional force. Any organic coating or film on the pin or track effectively reduces the COF and may lead to chaotic behavior. Small angles of feed table tilt are also desirable to avoid chaos.

References

- [1] Colijn, H., "Include Vibratory Conveyors to Meet Bulk-Handling Demands," *Chemical Engineering Progress*, Vol. 87, No. 1, Jan. 1991, pp. 54-59.
- [2] Booth, J.H. and McCallion, H., "On Predicting the Mean Conveying Velocity of a Vibratory Conveyor," *Proceedings of the Institute of Mechanical Engineers*, Vol. 178, Pt. 1, No. 20, 1963-64, pp. 521-538.
- [3] Nedderman, R.M. and Harding, G.H.L., "The Free-Flight Vibrating Conveyor: Part 1. Basic Theory and Performance Analysis," *Transactions of the Institute of Chemical Engineers*, Vol. 68, Part A, March 1990, pp. 123-130.

- [4] Harding, G.H.L. and Nedderman, R.M., "The Free-Flight Vibrating Conveyor: Part 2. Stability Analysis and Criteria for Optimal Design," *Transactions of the Institute of Chemical Engineers*, Vol. 68, Part A, March 1990, pp. 131-138.
- [5] Redford, A.H. and Boothroyd, G., "Vibratory Feeding," *Proceedings of the Institute of Mechanical Engineers*, Vol. 182, Pt. 1, No. 6, 1967-68, pp. 135-152.
- [6] Hota, S.P. and Karmakar, R., "Optimisation Studies on Vibratory Conveyors," *Bulk Solids Handling*, Vol. 8, No. 6, December 1988, pp. 715-717.
- [7] Tolstoi, D.M., "Significance of the Normal Degree of Freedom and Natural Normal Vibrations in Contact Friction," *Wear*, Vol. 10, 1967, pp. 199-213.
- [8] Popp, K. and Stelter, P., "Stick-Slip Vibrations and Chaos," *Philosophical Transactions of the Royal Society of London A*, Vol. 332, No. 1624, July 1990, pp. 89-105.
- [9] Richardson, R.S.H. and Nolle, H., "Surface Friction under Time-Dependent Loads," *Wear*, Vol. 37, 1976, pp. 87-101.
- [10] Oden, J.T. and Martins, J.A.C., "Models and Computational Methods for Dynamic Friction Phenomena," *Computer Methods in Applied Mechanics and Engineering*, Vol. 52, 1985, pp. 527-634.
- [11] Burwell, J.T. and Rabinowicz, E., "The Nature of the Coefficient of Friction," *Journal of Applied Physics*, Vol. 24, No. 2, February 1953, pp. 136-139.
- [12] Bowden, F.P. and Tabor, D., "The Friction and Lubrication of Solids," Clarendon Press, Oxford, 1986, pp. 176-199.
- [13] Gao, C., Kuhlmann-Wisldorf, D., and Makel, D.D., "Moisture Effects Including Stiction Resulting from Absorbed Water Films," *Journal of Tribology*, Vol. 114, January 1992, pp. 174-180.
- [14] "Bulfinch's Mythology," Doubleday, New York, 1948, p. 292.
- [15] Thompson, J.M.T. and Stewart, H.B., "Nonlinear Dynamics and Chaos," John Wiley and Sons, New York, 1986, pp. 235-236.

Erosion in Manufacturing

Alberto J. Pérez-Unzueta,¹ Dora Martínez,¹ Marco A. Flores,² R. Arroyave,² A. Velasco,² and R. Viramontes²

Erosion and Corrosion Mechanisms in Pneumatic Conveying of Direct Reduced Iron Pellets

REFERENCE: Pérez-Unzueta, A. J., Martínez, D., Flores, M. A., Arroyave, R., Velasco, A., and Viramontes, R., “**Erosion and Corrosion Mechanisms in Pneumatic Conveying of Direct Reduced Iron Pellets,**” *Wear Processes in Manufacturing, ASTM STP 1362*, S. Bahadur, and J. Magee, Eds., American Society for Testing and Materials, 1999.

ABSTRACT: Samples of steel pipe segments and hard coatings were separately tested for hot gas corrosion resistance and hot erosion resistance by multiple impacts of direct reduced iron (DRI) pellets in a hot erosion testing device and in a pilot plant. Material loss and microscopic observations were used to evaluate both the corrosion and erosion mechanisms. This will help to evaluate the main mechanisms of pipe damage as the conditions for high temperature pneumatic transport of direct reduced iron pellets become more stringent. Corrosion tests were performed in a laboratory reactor with atmospheres composed of hydrogen and carbon monoxide mixtures in order to simulate conditions at the pilot plant. Results from the corrosion tests provided an indication of the suitability of these materials to be used as pipes. Laboratory tests provide useful information on the behavior of different materials at different temperatures ranging from room temperature up to 600 °C, and at different impact angles.

KEYWORDS: high temperature erosion wear, high temperature corrosion, pneumatic transport, steel, alloys

Direct reduced iron (DRI) is obtained by the reduction of iron ores in reactors with a hydrogen (H) and carbon monoxide (CO) based atmosphere. Spherical particles of iron ores up to 12 mm in diameter are loaded into the reactors. After most of the oxygen (O) is removed the spherical particles become porous and they are called sponge iron. Typical composition of DRI is 90% minimum of iron (Fe). The rest is formed by residuals such as silicon dioxide (SiO₂), calcium oxide (CaO) and carbon (C). Particle density is around 3200 kg/m³. At the present, most of the DRI needs to be transported from the direct

¹Professor and research student, respectively, Universidad Autónoma de Nuevo León, FIME, A.P. 74F, 66450 San Nicolás, N.L., México.

²Invited researchers, Universidad Autónoma de Nuevo León, San Nicolás, N.L., México.

reduction (DR) reactors to the steel melting furnaces. This transportation can be done by train, truck or conveying belts. One alternative is the pneumatic transportation of the still hot particles straight to the steel making furnaces. This will save time and energy otherwise spend waiting for the particles to cold down and to be transported, and then heat up them in the steel furnaces. In order to make this process interesting in terms of energy savings, the transportation should be done at temperatures of around 400 to 800 °C. Particles to be conveyed are formed by the sponge iron pellets up to 12 mm in diameter and dust particles down to 2 µm. Transport rate is expected to be in the order of 100 to 400 tons per hour, and the transport distances are from 60 to 600 meters [1,2].

Pneumatic transportation of direct reduced iron (DRI) at high temperatures and under reducing atmospheres is a challenging task. Pipes are subject to high thermal stresses, corrosion attack, abrasive and erosive wear [3,4]. Free carbon and iron carbide tend to react with air, generating heat in an exothermic reaction where temperatures can reach above 1600 °C. Thus, the need for an inert or reducing atmosphere, to avoid such reactions [5]. The main transport requirement is not only to convey between two points but, to preserve the intrinsic value associated to metallic content, temperature and particle size of the DRI.

Materials to be selected to build up the pneumatic line should stand, first at all, the high corrosion by the conveying gas. Also, materials should stand the erosion produced by the particles, and the thermal stresses associated with temperature changes. There is a limited number of alloys that can be used for a such design. In this work, the authors present the experimental work performed in three different steels and a hard facing alloy. Corrosion tests have been performed on a specially designed reactor for testing under hot corrosion atmospheres based on H₂-CO mixtures. Hot erosion testing was performed on a specially designed laboratory rig, which can convey fine particles under a H₂-CO or other atmospheres and it can impinge the sample targets at different angles (from zero to 90°). Also, a pilot plant for the high temperature pneumatic transportation of DRI under H₂-CO atmosphere has been just commissioned and is being used at the present to test different real size pipes.

Experimental Method

Materials

The materials used for this work were a carbon steel ASTM Seamless Carbon Steel Pipe for High Temperature Service (A106 grade B), a low alloy steel ASTM Seamless Ferritic Alloy Steel Pipe for High Temperature Service (A335 grade P22), and a stainless steel (ss) type AISI 304. The hard facing alloy is a proprietary Cr-Ni-Mo-C alloy which was applied on carbon steel plates. Chemical composition of the alloys are shown in table 1. For the hot corrosion tests and for the hot erosion tests, samples were cut from pipes. The testing surfaces were prepared with emery paper from grit size 320 to size 800. For the hot conveying pilot plant, segments of 1 m long pipes were installed as a part of the conveying pipeline.

TABLE 1 -- *Chemical composition of steels pipes (wt. %).*

Alloys	Mn	C	Si	P	S	Cr	Ni	Mo	Fe
A106 gr. B	0.30	0.049	0.11	0.016	0.035	0.035	0.027	-	balance
A335 gr. P22	0.47	0.127	0.398	0.020	0.012	2.5	0.039	0.52	balance
AISI 304	1.73	0.07	0.293	0.022	0.003	18.09	10.18	-	balance
Cr-Ni-Mo-C Hard facing alloy	3.00	3.00	0.63	-	-	24.00	3.00	2.50	balance

Erosive Material

The erosive particles used in this work are DRI pellets. A typical composition (wt.%) of DRI pellets is 90% Fe minimum, 5% SiO₂, 2% C and 1.5% CaO. For the hot erosion machine, pellets of DRI were ground to +1/16 to -1/8 mesh size to be impacted on the steel samples. For the pilot plant, the particles to be conveyed were pellets from normal production and the size was variable between 6 and 12 mm in diameter.

Corrosion at High Temperature

Corrosion tests were performed in a horizontal reactor under a H₂-CO atmospheres similar to the ones found inside a DRI reactor, heater or conveying line and is called reformed gas (R-gas). Typical components of R-gas are 71% H₂, 16% CO, 8% CO₂, 3% CH₄, 1% N₂, and 1% H₂O. R-gas is heated within a stainless steel pipe inside a silicon carbide resistance furnace. A set of 8.0 x 15.0 x 4.0 mm steel samples and blanks of carbon steel plates coated with metallic overlays of hard facing alloy are inserted inside the pipe. Table 2 shows the test conditions:

TABLE 2 -- *High temperature corrosion test conditions.*

Temperature (°C)	700 ± 10
Testing time (h)	150
Pressure (MPa)	0.15
Atmosphere	R-gas
Gas density (kg/m ³)	350

Hot Erosion Machine

The wear test facility is essentially a shot blast machine with a heater. In fact the only difference is the design requirement for the operation with different atmospheres, such as an inert atmospheres, R-gas with different contents of H₂, or a nitrogen (N₂) based atmosphere. In this facility, different materials were subject to erosive attack. Samples can be positioned at different angles of impingement. Samples were cut to a predetermined size 40.0 x 25.0 x 6.0 mm. The test surface was machined with a diamond disk to achieve a flat face and then it was polished to an average 50 µm roughness Ra.

The samples were weighed and the roughness was measured with a digital roughness meter. The samples were then installed in the target holder and subject to a 2.5 cm diameter stream of ground DRI pellets at an approximate velocity of 10 m/s carried by a hot inert atmosphere (N_2) at temperature of 560°C. Table 3 shows the test conditions.

TABLE 3 -- *Test conditions for the hot erosion machine.*

Temperature (°C)	560 ± 10
Conveying material	Crushed pellets of DRI
Particle size (mm)	from 1.6 to 3.2
Load conveying (tons)	4.3 (for mild steel and 304 ss.) 11.16 (for hard facing alloy)
Load flow rate (kg/s)	0.0166
Atmosphere	Nitrogen (N_2)
Particle velocity (m/s)	10
Gas flow (m^3/h)	75

Pilot Plant Testing Facility

A local steel manufacturer has built a pilot plant for an experimental high temperature pneumatic transport of DRI. Part of this pilot plant consists of a pneumatic loop to convey the DRI pellets produced from the DR reactors to the steel melting furnaces. Segments of 4 inches of diameter test pipes were installed to monitor the loss of thickness on horizontal sections. Here, the impingement angle is zero. Testing pipes were of carbon steel ASTM A106 gr. B, low alloy steel ASTM A335 grade P22, stainless steel AISI 304 and a carbon steel coated with layers of a hard facing proprietary alloy Cr-Ni-Mo-C. From the nearest bend, thermocouples were welded to the pipe surface on each of the test sections. Also, a microphone listening station was installed before the test section to help assess the phase density. Pressure sensors were installed every 10 m. Facilities for installation and removal of testing pipes were also implemented. Before testing, the wall thickness of the testing pipe segments were measured with an ultrasonic gauge at four different positions each at 90°. The measurement positions and the direction of the flow were carefully identified. Table 4 shows the test conditions for the pilot plant.

TABLE 4 -- *Test conditions for the pilot plant.*

Temperature (°C)	580 ± 10
Pressure (MPa)	68.95
Conveying material	pellets of DRI
Particle size (mm)	from 6.5 to 12.0
Load conveying (ton)	600
Load flow rate (ton/h)	1.0
Atmosphere	reducing $H_2 + CO_2$
Gas velocity (m/s)	29.37.
Gas density (kg/m^3)	350

Results

Corrosion at High Temperature

Table number 5 shows the results of samples tested in the laboratory rig for corrosion at 700°C.

TABLE 5 -- *Results from the hot corrosion tests.*

Alloy	Mass change by unit area (mg/cm ²)	Carburization depth (mm)
A106 grade B	-14.9	1.0
A335 grade P-22	-14.9	1.0
Ss AISI 304	-7.4	0.75
Hard facing alloy	0.0	0.00

Figure 1 shows an optical microscope photograph of a sample of hard facing alloy on a mild steel base after the hot corrosion test. The sample shows the surface under attack. There is no evidence of surface damage, metal dusting, carburization or any other kind of damage, on the hard facing alloy (right hand side). However, the bare mild steel shows a layer of metal dusting of around 60 µm depth (left-hand side). Similar observation were obtained in the P-22 steel and, in a lesser degree, in the 304 stainless steel.

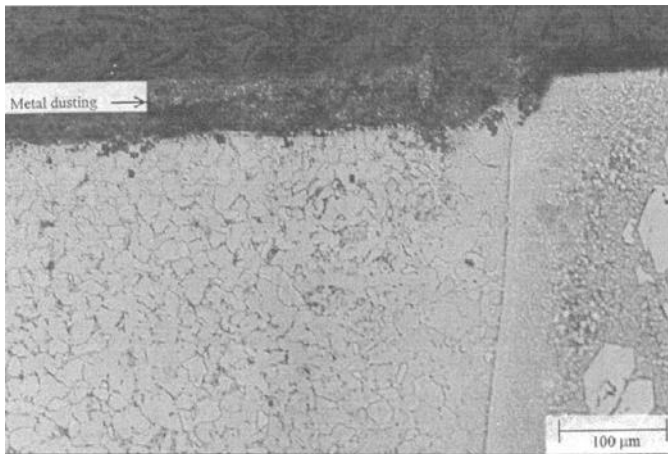


FIG. 1 -- *Optical microscope photograph of a sample of hard facing alloy on carbon steel base after the hot corrosion test. X200 nominal. Left is bared carbon steel showing metal dusting. Right is the hard facing alloy.*

Hot Erosion Machine

Results obtained in the hot erosion device are shown in Table 6. Samples were cut from pipes or were custom made on plates. This table also shows the dimensionless erosion coefficient (K), as described by Hutchings [6].

TABLE 6 -- Results from the hot erosion machine.

Alloy	Impingement angle	Erosion Coefficient K (10^{-3})
AISI 304	parallel to flow	15.3
AISI 304	30°	400.0
Hard facing alloy	parallel to flow	5.2
Hard facing alloy	30°	60.0

Figure 2 shows a stainless steel 304 positioned parallel to the flow after 2800 kg of impact particles. The impact produced ploughing on the surface. The direction of flow and ploughing is from top to bottom. There is a clear evidence of plastic deformation at the front of the ploughing mark and that material has been removed. In the bottom of the impact scratch marks can be observed. Figure 3 shows a stainless steel 304 positioned at 30° after 2800 kg of impact particles. The damage on the surface seems to be higher than that of the same steel in a parallel position. There are more plastic deformation that overshadow the scratching marks. Figure 4 shows a sample of hard facing material, parallel to the flow after 11,160 kg of impact particles. Very little damage was observed and it was only present on the matrix. Primary carbides effectively protect the surface from damage. Figure 5 shows a sample of hard facing material at 30° after 11,160 kg. Higher damage to the surface is observed. It is clear that the erosive particles erode the “softer” matrix leaving the primary carbide loose, until they became detached.

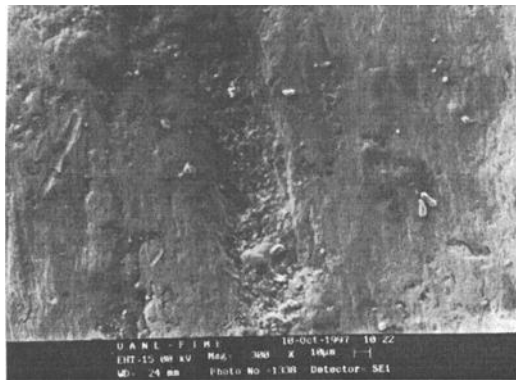


FIG. 2 -- SEM photograph of the surface of 304 stainless steel positioned parallel to the flow, after 2800 kg of impact particles in the hot erosion machine. X300 nominal.

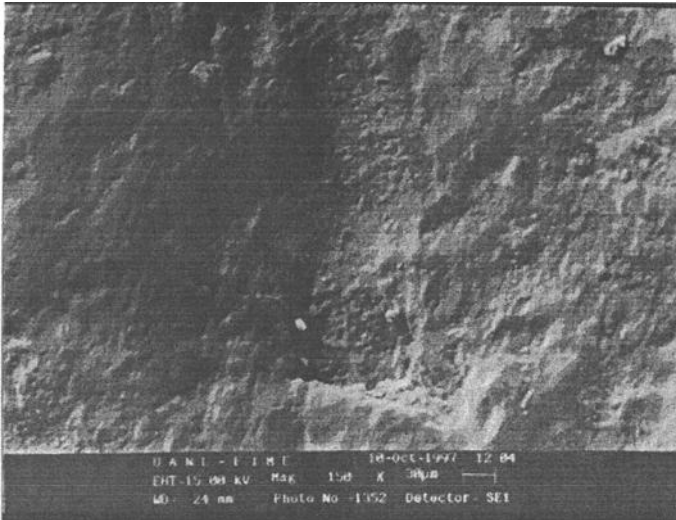


FIG. 3 -- SEM photograph of the surface of 304 stainless steel positioned at 30°, after 2800 kg of impact particles in the hot erosion machine. X150 nominal.

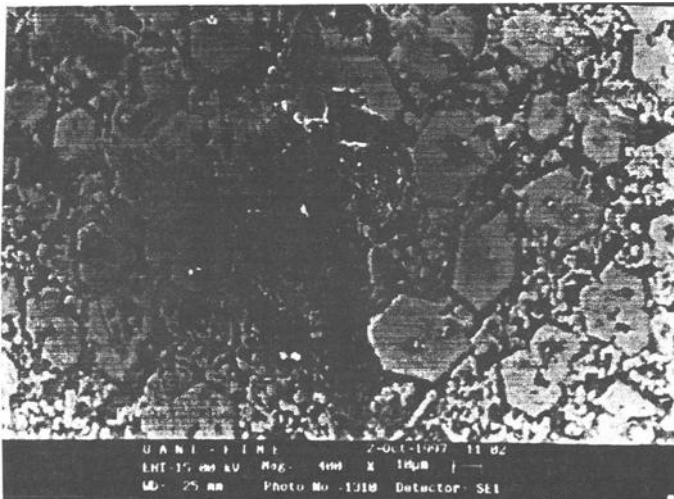


FIG. 4 -- SEM photograph of the surface of the hard facing alloy positioned parallel to the flow, after 11,160 kg of impact particles in the hot erosion machine. Very few damage is observed. X400 nominal.

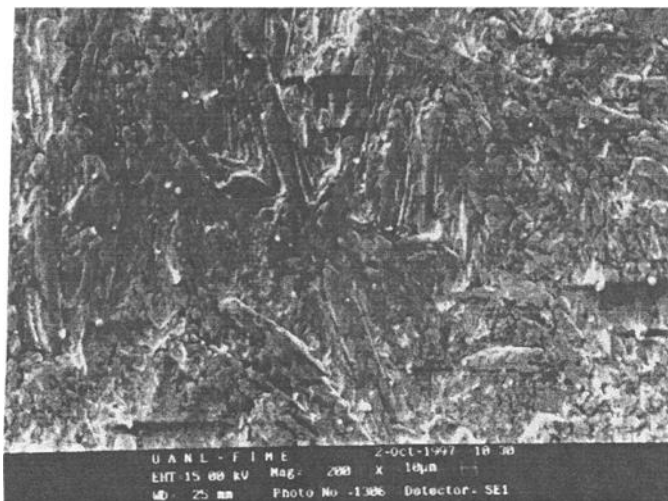


FIG. 5 -- SEM photograph of the surface of the hard facing alloy positioned at 30°, after 11,160 kg of impact particles in the hot erosion machine. Higher damage to the surface is observed. X200 nominal.

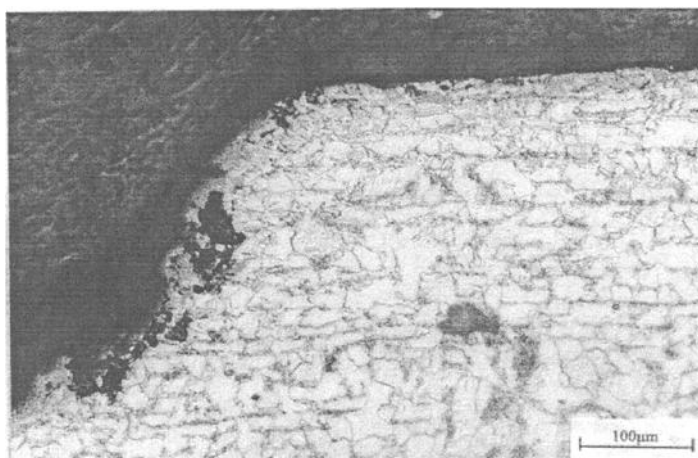


FIG. 6 -- Optical microscope photograph of A106-B carbon steel surface after 600 tons of DRI pellets transported by the pilot plant. On the left there is a pit of hot gas corrosion. The layer of oxide on the surface was between 10 to 20 µm. X200 nominal.

Pilot Plant Testing Facility

The hot pneumatic transport pilot plant is equipped with a 100 m experimental loop for erosion-corrosion test at industrial pilot plant conditions. Three segments of 4 inch diameter pipes were carefully monitored to observe the damage by erosion and corrosion. Table 7 shows the results for the pilot plant tests for carbon steel A106 gr. B, low alloy steel A335 gr. P22, and AISI 304 stainless steel.

TABLE 7 -- *Results from the pilot plant tests.*

Material	Position	Thickness loss (mm)	Surface features
A106 gr. B	Upper:	0.37	High damage by hot gas corrosion pitting.
	Right:	0.11	
	Left:	0.12	
	Bottom:	0.40	
A335 gr. P 22	Upper:	0.48	High damage by hot gas corrosion pitting.
	Right:	0.64	
	Left:	0.53	
	Bottom:	0.20	
AISI 304	Upper:	0.14	No apparent damage by hot gas corrosion, but some plastic deformation.
	Right:	0.17	
	Left:	0.23	
	Bottom:	0.03	

Figure 6 shows a carbon steel A106-B after 600 tons of DRI pellets transported by the pilot plant. It can be seen that there is a layer of oxide on the surface. This oxide layer is not uniform along the surface. However, it was possible to measure a thickness between 10 to 20 μm . Pits of hot gas corrosion can be seen. There is no evidence of plastic deformation. Similar observations were made on steel A335-P 22. Figure 7 shows a SEM photograph of AISI 304 steel after the pilot plant test. The surface does not show signs of chemical attack. However, it can be observed that a layer of 12 μm on the surface. By means of a micro-chemical analysis performed on the surface, it was possible to identify that this layer was made of DRI adhered to the surface of the AISI 304 stainless steel. The internal surface of the carbon steel and P 22 steel pipes showed evidence of ploughing and plastic deformation, see Figure 8. Stainless steel 304 showed less evidence of ploughing or plastic deformation.

Discussion*Corrosion at High Temperature*

Results from the hot gas corrosion laboratory test were as expected. Carbon steel A106 gr. B, and low alloy steel A335 gr. P22 showed a higher loss of material, mostly

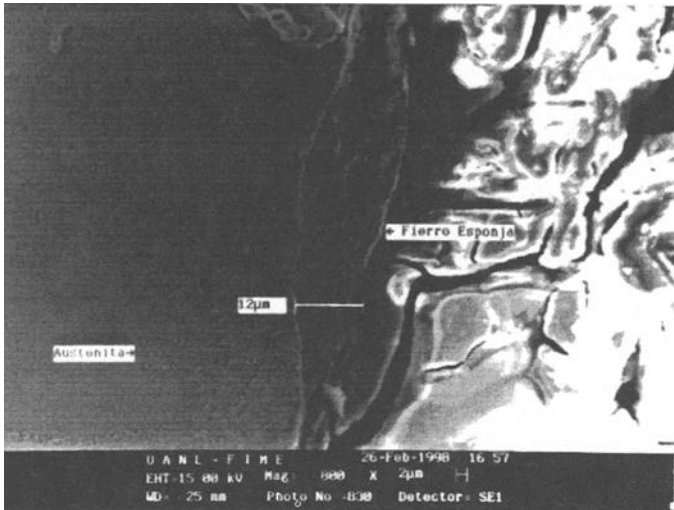


FIG. 7 -- SEM photograph of a 304 stainless steel after 600 tons of DRI transported in the pilot plant test. The surface does not show signs of chemical attack. A layer of 12 µm can be observed. This layer was identified as adhered DRI. X800 nominal.

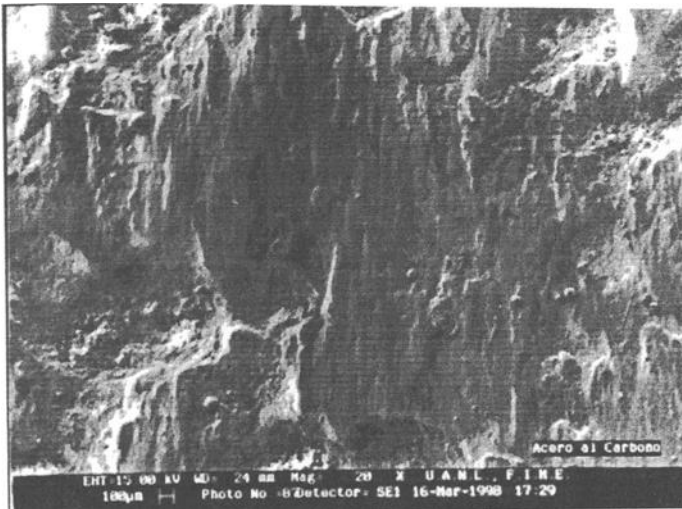


FIG. 8 -- SEM photograph of A106-B carbon steel after 600 tons of DRI transported in the pilot plant test. Extensive damage by ploughing and plastic deformation can be observed. X20 nominal.

by the metal dusting mechanism [7]. Stainless steel AISI 304 showed less damage, almost half of that of mild and P22 steels. The hard facing alloy did not show loss of material at all, see Table 5.

Hot Erosion Machine

The main attribute of this device is that it can perform tests at different impingement angles. It has been accepted that erosion is a function of the impingement angle [6]. For ductile metals, the higher erosion rate can be found in angles near to 30° . Smaller angles or angles leaning to 90° show less erosion. Figures 2 and 3 showed this difference. At 30° (Fig. 3) the surface damage is higher than at 0° . In both cases, ploughing, plastic deformation and material loss occurs but, at 30° it is higher. Table 6 shows that at impingement angles of 30° , the erosion constant K is more than one order of magnitude higher than for an impingement angle of zero.

Pilot Plant Testing Facility.

Carbon steel A106 gr. B, and low alloy steel A335 gr. P22, showed extensive damage, mostly by hot gas corrosion pitting. This damage could have “erased” some of the mechanical damage produced by the particles, such as ploughing, plastic deformation and cutting. As Figure 6 shows, also there is a layer of oxide on the surface, making it difficult to estimate the real loss of thickness of the pipe walls by ultrasonic measurements. At this point, it can be considered that the main damage to the pipes is due to hot gas corrosion. The values shown in Table 7 do not account for the oxide layer formation, and as the layer is not uniform, as shown in Figure 6, it would be speculation to assume the real loss of thickness from an arithmetical subtraction. However, it is clear that the 304 stainless steel suffered less damage, although the numbers on Table 7 do not show a significant difference.

304 stainless steel shows some plastic deformation at the surface. As no corrosion damage was observed, all mechanical damage, i.e. erosion, is still present and can be assumed as the leading damage mechanism.

In the case of carbon steel and P 22 steel, it is still possible that the deformed steel grains undergo a recuperation and/or recrystallization at the temperature used in this work (580°C). Mild steel recrystallization temperature is 540°C [8]. Some very small grains observed at the surface can be related to the recrystallization process, see Figure 6.

Erosion testing at high temperature still needs to deal with changes in hardness in both, pipe material and particles. More efforts to deal with this situation are needed to understand the erosion process at high temperature. Equations which take into account the hardness at high temperature or, even more, the relative hardness between particles and surface are much needed [9].

Conclusions

1. High temperature corrosion tests showed that a Cr-Ni-Mo-C hard facing alloy is more resistant than 304 stainless steels, A335-P 22 steel and A106-B carbon steel, in that hierarchy order, when tested under DR reactor gas.

2. The hot erosion machine allows performing comparative tests for different materials at different impingement angles. Results obtained in this study showed that impingement angles of 30° generate erosion coefficients of nearly one order of magnitude higher than zero degrees. Also, Cr-Ni-Mo-C hard facing alloy is 3 times more resistant than AISI 304 stainless steel at 0° and 7 times more resistant at 30°.

3. The pilot plant testing loop showed that after 600 tons of conveyed load at 580°C, A106-B carbon steel and A335-P 22 steel undergo considerable damage due to hot gas corrosion pitting. Stainless steel 304 showed minimum corrosion, and erosion was the main damage mechanism. Cr-Ni-Mo-C pipes are still under test.

Acknowledgments

The authors would like to thank Dr. Raul Quintero, president of the Technology Division at HYLSA for permission to publish this work. The authors would also like to thank CONACyT.

References

- [1] HYLSA. "Pneumatic Transport of DRI," Internal Report (in Spanish), HYLSA, Monterrey, Mexico, 1997.
- [2] Deaquino, E., Martínez, D., Pérez-Unzueta, A., Velasco, A., Flores, M., and Viramontes, R., "Wear in Pneumatic Transport Under Hot Reducing Atmospheres," *Powder Technology*, Vol. 95 (1998), pp. 55-60.
- [3] Marcus, R., Leung, L., Klinzing, G., and Rizk, F. "Pneumatic Conveying of Solids. A Theoretical and Practical Approach," Chapman and Hall, London, 1990.
- [4] Burnett, A., "Wear in Pneumatic Conveying Pipelines," *Powder Handling and Processing*, Vol. 5 (1993).
- [5] Flores, M. and Soriano, A., "Pneumatic Transport of Hot Sponge Iron," *Proceedings of the IFPS 8 Meeting*, Pittsburgh, PA, 1995.
- [6] Hutchings, I., "Tribology, Friction and Wear of Engineering Materials," Edward Arnold, London, 1992.
- [7] Grapke, H., "Metal Dusting of Low and High Alloy Steels," *Corrosion Science*, Vol. 51, No. 9, 1995, pp. 711-719.

- [8] Guy, A., "Elements of Physical Metallurgy," 2nd ed., Addison Wesley, MA, 1959.
- [9] Perez-Unzueta, A. and Martinez, D., "A New Erosion Model for High Temperature," (in Spanish), Universidad Autónoma de Nuevo León, Internal Report, San Nicolás, Mexico, April 1998.

Lucien H. Chincholle¹

CHARACTERIZATION OF THE WEAR PROCESSES DUE TO THE MATERIAL EROSION MECHANISMS

REFERENCE: Chincholle, L. H., "Characterization of the Wear Processes due to the Material Erosion Mechanisms, *Wear Processes In Manufacturing, ASTM STP 1362* S. Bahadur and J. Magee, Eds., American Society for Testing and Materials, 1999.

ABSTRACT: A device to measure the instantaneous erosion rate has been perfected. It is available for all types of erosion such as those involving corrosion, abrasion, erosion by shock and cavitation. The calibration being made, it gives a quantitative value of the erosion and moreover, on certain cases, it is possible to deduce the erosion type. A wide range of applications is possible for using this device. This paper presents some experiments carried out in the wear domain. The first results obtained in a specific conditions for the fretting erosion are interesting. It can be seen that the evolution of the instantaneous *erosion* behavior varies with some parameters such as the applied force, frequency, friction coefficient and time. By way of a better knowledge of the oxide formation, this new tool gives new insights to help analyze the complicated instantaneous processes of wear, by means of current density measurement.

KEYWORDS: Wear, erosion measurement, corrosion, abrasion, cavitation, shock, friction coefficient, electrochemical measurement

Nomenclature

<i>Erosion:</i>	Sum of all removed material
C%	Sediment concentration
D (mm)	Sand diameter
ΔP (bar)	Drop in head
e (mg/h)	Erosion rate
i (μA)	Corrosion current, given by the Decaver
j ($\mu A/mm^2$)	Current density
k	Proportional to...
P (bar)	Pressure
ρ	Specific mass
s (mm^2)	Eroded surface
T°C	Temperature
t (s)	Time
V (m/s)	Velocity (liquid or sand)

¹ Emeritus Professor, Laboratoire Génie Electrique Paris, Paris-South University, Orsay, 91190, France.

Wear is difficult to understand and predict in actual systems. The problems are various, complicated and often many influences work together. The fundamental encountered parameters are not well characterized in nature, size and time. First we have to define the importance of each one and, eventually, the synergistic effects. For example, fretting involves adhesive wear combined with corrosion, abrasion by debris and fatigue cracks leading to failure. Moreover, in some cases, there is the lack of a good method for wear rate measurement. A new technique such as that described here can stimulate new research.

Here we present a good method able to give another view of erosive wear analysis. In our laboratory, we study the "erosion" in aqueous media. For us the term *erosion* includes all types of techniques giving a metal removal such as corrosion, abrasion, jet with or without sediment, cavitation, etc. It can be a nano-scale erosion or a very large-scale big erosion. We have developed this study during many years and designed an apparatus called a Decaver to make the instantaneous erosion rate measurements. By a single reading of the device the total erosion rate can be deduced. To make this measurement, it is not necessary to know the erosion type. By analyzing the instantaneous erosion rate, the type of erosion can be identified.

Looking at papers concerning erosion, we see that people try to answer some of the following questions about various problems caused by cavitation and sedimentation:

Is there erosion just now?

How serious will it be?

How to measure it?

Where will it occur?

What type of erosion is it?

Will there be cavitation or not?

What can be done to avoid or to reduce the erosion?

How to choose the right material to resist erosion?

How to make rapid and efficient repairs?

Is there a relationship between the friction coefficient and the rate of material removal?

No pertinent answers can be made due to the complexity of each erosion type and the great number of parameters. Their diversity shows that, generally speaking, there is not yet a clear view of the erosion processes. For example, the cavitation cloud behind a cylinder and the possibility to have an erosion appears as a double complexity.

Our objective is to try, with our experience relative to *erosion* measurement, to give aid in wear mechanism identification. The difficulties that we encounter to make this transfer of knowledge from a simple *erosion* to the wear are both due to two factors. On the one hand we pass from water to air. On the other hand the *erosion* develops between two surfaces.

1. Background

1.1. Erosion Definition

Erosion Definition. - For us, *erosion* is the sum of electrochemical corrosion, mechanical abrasion, cavitation erosion and synergistic effects between them. We have developed a number of tests in various fields such as abrasion, cavitation, water jets and corrosion in an aqueous medium. We write *erosion* in this form to distinguish our specific studies from the erosion considered in the usual classifications of wear types, including the ASTM definition for erosion.

Electrochemical Corrosion. - This case is simple. We have only to apply Faraday's law: 96 500 Coulombs set a gram atomic weight free. For example, for titanium, 1 mA corresponds to an erosion rate (corrosion) equal to 1.79 mg/h and we have:

$$e = k j \quad (1)$$

Mechanical Erosion - This study is complicated because the erosion depends on many parameters. We shall distinguish successively, the erosion by abrasion and the erosion by shock. Many experiments have been conducted, particularly with a grindstone, with cavitation, with sand or with a rubber sponge ball inside a condenser tube. *By Grindstone*. A grindstone works as a gouge. The material removal process depends on the grindstone characteristics such as hardness, general texture, velocity, pressure on the sample, elasticity, special working conditions. For example, if the grindstone removes only the passive layer, we write the same relation as corrosion erosion: $e = k j$. But, if the abrasion is important, we have to consider that, *only the surface* of the torn off material ribbon is oxidized. As all the removed matter is not oxidized, we have to find another relation as a function of the current density:

$$\text{erosion rate (mg/h)} = f(j) \quad (2)$$

Due to the complexity of the parameters, we see that a specific calibration is necessary. After that, a stochastic analysis allows a clear idea of the role of various parameters needed to calibrate our instrument, called the Decaver [1].

By sand. At times, the sand erosion process can resemble the preceding one: $e = k j$, such as when the sand is carried by a discharge of water. Then, it induces a friction and sometimes an erosion. But, it can also be very different when it impacts this surface and induces a shock wave.

Shock

By sand - When a shock wave is produced in the material, the erosion develops in two stages. First, the sand particle hammering makes the material harder and then, this layer can be divided from dislocations and microfractures, into particles that are ejected in the flow. Their large diameter is a function of the shock intensity. Sometimes the shock impact beats the metal flat making a sort of tongue that is also divided into particles. These particles can be considered as spherical particles with mean diameter (D). It results in:

$$e = f(j) \quad (3)$$

By cavitation erosion - In this case the material is removed by imploding cavity' shocks. As we have shown [4], shock erosion depends on various hydraulic parameters.

By jet with or without sand - A water jet without sand and with a small velocity is not erosive. When the velocity increases, cavitation appears and also erosion. Thus, the jet erodes by cavitation. In the case of jet with sand, abrasion exists even with low velocity. When this increases, cavitation also starts and we have to add two erosion types. The erosion rate shall be equal to the sum of (1) and (3):

$$e = k j + f(j). \quad (4)$$

Finally, *erosion* is due to corrosion, mechanical abrasion and cavitation. As a consequence, we have to calibrate the device in order to have a relation giving, in all experimental conditions, the instantaneous erosion rate versus the Decaver signal:

$$\text{erosion rate} = f(j) \quad (5)$$

When all the removed metal is not oxidized, we suppose that it is in a spherical form with a mean diameter D. This mass is proportional to D^3 and the surface area proportional to D^2 just as is the current. So we can write the total removed material as

$$: m = f(j) + f(j^{1.5}). \quad (6)$$

Later on we shall see the difficulties in transferring this view to the wear domain.

1.2. Device

Principle - The Decaver is a new electrochemical detector based on a particular property of the passive layer [2]. Some metals are covered, particularly in an aqueous medium, with an oxide layer characterized by a semiconductor aspect. When this layer is destroyed in any erosion process, it is instantaneously reconstructed. This process sets electrons free and the device collects the corresponding current. As this is a function of the erosion rate, it can be used to measure the physical phenomenon of the erosion. In fact, it measures a corrosion current. We shall write that the erosion rate is a function of the electric current density: erosion rate (mg/h) = f (j)

Characteristics of the Device - The device gives a current value, i μA (A: Coulomb by second), corresponding to an erosion rate value: e (mg/s or mm/year).

This measurement being instantaneous, we know the erosion rate at any moment. As regards the erosion, we can see the influence of each physical parameter.

The current is proportional to the eroded surface: i (μA) = $k e$ (mg/h) = $k S$.

By integration of the electric current signal, we obtain a quantity of electricity It (C)]

equal to: $\int_{t_1}^{t_2} i dt$. This value corresponds to the accumulated erosion as well as the mean

penetration depth when we know the eroded surface. On the device, a counter assumes this task.

The device is very sensitive. We can easily detect about 0.01 μA , because we have demonstrated that the current, coming from the corrosion region, is of a current-source type [2].

Industrial Device - Laboratory prototypes, built twelve years ago, work satisfactorily. Today, industrial devices are available. The characteristics of the device output signal are interesting.

1.3. Using the Decaver

The Decaver can be used when there is a material removal in a liquid medium and that it is necessary to improve a working part of a machine. We note some uses where there is an *erosion* problem to work out. For example:

- to know the instantaneous erosion rate of a hydraulic machine,
- to improve material specific properties,
- to make fast repairs,
- to choose the working point in view of the erosion,
- to study the wear with permanent information on the removed material (*erosion*),
- to study sediment (concentration, diameter, velocity) and the usings.

2. Calibration - Experimental Devices and Results

Calibration procedures permit us to see the device working in various wear situations with its advantages and disadvantages. Calibration involves both for each wear type physical and experimental considerations.

2.1. Sediment Calibration

Apparatus to Study the Sediment Erosion - Sediment Loop

The experimental device is a simple loop including a pipe (8 mm diameter, 212 cm³ water volume), a motor-pump, a sensor and the reference electrode. A manometer gives the drop in head between two points of the hydraulic circuit and permits us to deduce the flow velocity at any moment. The sensor is placed along the cross section of the pipe. The sediment, injected into the circuit, moves inside it and strikes the sensor. The electric signal goes from the probe to the device.

Our working technique consists first in choosing one well-defined sediment, for example Rugos 2000 and varying the velocity. The velocity rate is measured for each run. 300 runs correspond to all combinations of 5 diameters, 5 concentrations and 12 velocities [3] .

- Physical Analysis - We write successively:
- the volume of the total flow flux: sV
 - the sediment flux: sCV
 - the mean impact of the energy density for one grain: kDV²
 - the mean impact energy flux density, per second: kps CDV³

More generally, it can be said that the erosion generated by sand shocks depends on the following sand parameters: specific density, diameter, velocity and concentration. We can foresee a correlation between the electric current and the physical parameters in the form of the relation: $k C D V^3 = f(j)$. This will be specify by way of a stochastic analysis of the experimental results.

When we have a very small abrasion, all the metal removed is oxidized (analog to the corrosion) and we have $m = kj$. With a great abrasion (or an *erosion* by shock), the

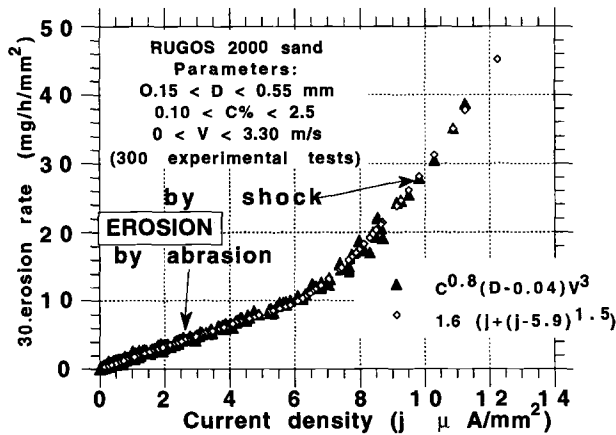


FIG. 1 - Decaver calibration with sediment on an experimental loop.
 We see a superposition of two curves as a function of the electric current density. The first one concerns the mechanical values of the flow (shock energy density). The second one is relative to the electric current density provided by the device. This last relation shows that, with sand, there are two types of erosion: a mechanical abrasion (straight line) and a shock erosion (curve $j^{1.5}$)

metal removed can be approximated by spherical particles and we have:

$$m = k(j^{1.5}) \quad (7)$$

Comparison Between Theoretical and Experimental Results - To establish a mechanical relation between the kinetic energy and the device signal, we make a stochastic analysis of the experimental results. We have deduced the following mechanical relation: $C^{0.8} (D-0.04) V^3 = f(j)$

At the same time, considering that we have both an abrasion erosion (kj) and a shock erosion ($kj^{1.5}$), we can write an electric value: $f(j) = j + k(j^{1.5})$

From these two relations, we deduce a new well defined relation. It is the sediment general relation between the mechanical parameters and the electric current density:

$$C^{0.8} (D-0.04) V^3 = k (j + j^{1.5}) \quad (8)$$

2.2. Cavitation Calibration - Experimental Results with Cavitation Erosion.

Apparatus to Study the Cavitation Erosion - Tests have been made successively with a vibratory device, cavitation channel and hydraulic turbine.

° *Ultrasonic cavitation device*. It is a normal type: piezoelectric transducer, 20 kHz, vertical axis ending in a cone. The temperature as well as the distance between the cone and the sample are constant.

° *Cavitation channel*. The testing channel ($20 \times 20 \text{ mm}^2$) includes a cylinder on which cavitation can be easily generated by the flow. This cylinder constitutes also the probe of the Decaver. Thus, we detect the total cylinder erosion. It is a rather simple test facility but it is sufficient to make our experiments. Its main interest is to permit changes easily. Moreover, we can regulate parameters that seem important to us: pressure (P bar), drop in head (ΔP), velocity (V m/s) (or flow rate Q), temperature (T °C), dissolved gases, etc..

The loop is connected to the general water supply that gives an initial pressure of about 4 bars. Then, by drip leakage, this pressure decreases to 3 or 2 bars. We have the possibility to degas by an auxiliary circuit. The flow varies from 15 to 19 m^3/h and the temperature stays constant or rises freely. The test time is about four minutes and it is easy to repeat it. During the test the device polarizes the probe (constant potential) and gives a current i (μA) in relation to the loss of weight [4].

° *Hydraulic turbine cavitation tests* [5]. The experiments were carried out on Electricité de France equipment with a Kaplan wheel (12 m head, 2 MW power). The static belt of the turbine was chosen according to the ease with the probe setting and especially the fact that the belt, abraded by cavitation, was replaced by a new one. Thus, we knew, by examining the old belt, the exact place where cavitation erosion existed as well as the erosion rate. The device gave variations in erosion instantly. Thus we were able to verify the correct working of the Decaver on an industrial site as well as testing its calibration.

Physical Analysis - Today we are not yet able to present a complete physical study which defines directly a relation between the erosion rate and the electric signal. This work is in progress. We have already establish in our research the fundamental parameters ruling the cavitation erosion on a cavitation channel. Now, we analyse the kinetic energy that induces the erosion rate. Let us summarize some experimental results which helped us in this study.

° *Series with 64 runs - Only the pressure varies* - We allow that, during each test (4 mn), the temperature stayed constant. The aim of these experiments was to drawn the evolution of the cavitation erosion measured by the Decaver signal (i μA) when one parameter varied slowly. Figure 2 shows one test extracted from a series of 64 runs,

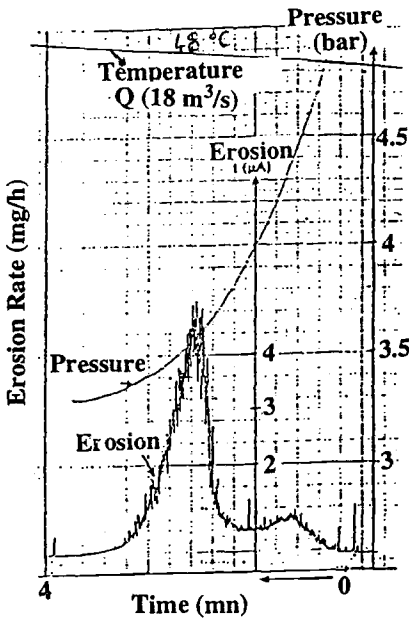


FIG. - 2 *Characteristic curve of the cavitation erosion. This curve visualizes the erosion inside an hydraulic machine. As an identity card, it characterizes a machine in a specific environment..*

This curve has been recorded on a cavitation channel with a constant flow rate. The temperature evolves weakly. The pressure variation permits to vary the cavitation erosion. When the pressure decreases the erosion rate ($j \mu A/mm^2$) evolves. There are two thresholds. At the beginning ($t=0$) there is no erosion because there is no cavitation due to the high pressure. At the end of test ($t=4$), we have no erosion on the sensor, with a big cavitation. We see an erosion maximum value. This is a characteristic point used to study the fundamental parameters of cavitation erosion.

when the pressure decreased from 6 to 3 bars, with a constant flow rate on the cavitation channel. Each cavitation erosion curve presented two peaks and two thresholds. For high pressures, there was no cavitation and no erosion. For low pressures, the cavitation was very developed but there was no erosion on the cylinder [5].

* *Series with 230 runs - All parameters vary.* On the cavitation channel, during these last few years, we have obtained a total series of 230 runs giving 230 curves corresponding to very different tests with all parameters varying. They are *cavitation erosion characteristic curves*. These curves are of great importance because they provide a certain amount of information. Firstly we know the continuous erosion rate and where to choose the right working point for a hydraulic machine in terms of erosion. Secondly we dispose of 230 maximum erosion points which are characteristic points. By considering successively the three following parameters: P, T and ΔP (proportional to V^2), we deduce the erosion variations in relation to each one of them. Finally, we can generalize this relation by one specific coefficient relative to the maximum erosion rate whatever the parameter values.

$$\sigma_c = \frac{P}{\Delta P} + \frac{1}{T} - 0.00565 T \quad (9)$$

This experimental and physical relation between the maximum erosion current and the fundamental parameters enabled us to carry out the physical cavitation erosion analysis. The *fundamental parameters* are temperature, pressure and drop in head. They characterize one working point. Afterwards, *secondary parameters* govern the erosion intensity for a given working point. They are the pressure, the gas content, etc..

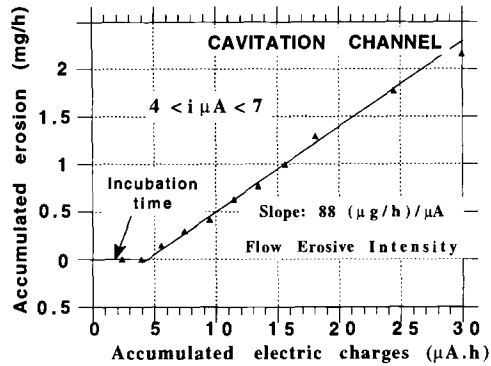


FIG. 3 - Accumulated cavitation erosion in the channel.
 The erosion is obtained by weighings. We vary the flow rate and the pressure in order that the device gives a signal value in the range 4 to 7 μA . We observe that the slope (88 $\mu\text{g/h per } \mu\text{A}$) is a constant value that we name Flow Erosive Intensity.

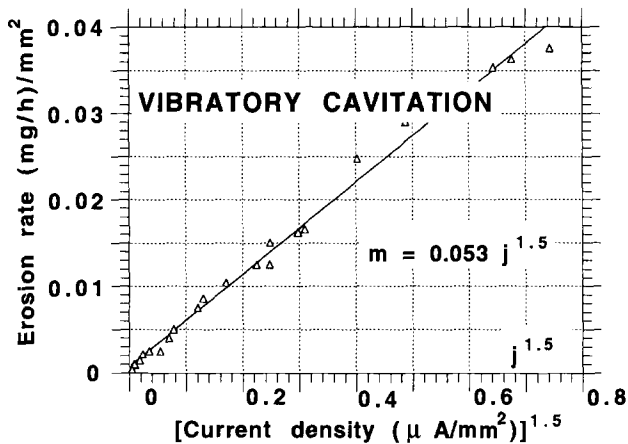


FIG. 4 - Decaver calibration on a cavitation vibratory equipment.
 The erosion was measured by weighing the probe. We can see that the erosion rate (mg/h per mm²) is proportional to $j^{1.5}$ as we foresaw with the physical analysis.

Experimental Results with Cavitation Erosion

* Experimental results obtained by weighings the probe on the cavitation channel [5]

Figure 3 shows the evolution of the accumulated cavitation erosion in relation to the accumulated electric charges. Although it is difficult to have a constant measured

current (in the range 4-7 μA), the information obtained is twofold. When we have a current without removed material, the device detects firstly the incubation time corresponding to the surface deformation. Secondly, the erosion slope characterizes the Flow Erosive Intensity (F.E.I.) measured by the mean current density. This is the mean erosion rate and we can use it to define the ability of the liquid to cause an erosion.

* *Experimental results obtained by weighing the probe on the vibratory device* [5]
By weighing the probe, we obtained a relation between the erosion rate and the electric measurement (Figure 4).

The Decaver gives a current i (j is the electric current density). This current depends on the erosion rate by the relation: f ($j^{1.5}$).

$$\text{Erosion rate (mg/h)} = k j^{1.5} \quad (= 0.053 j^{1.5}) \quad (10)$$

Thus we had a *second relation (cavitation)* between experimental weighing and the electric current density

2.3. Decaver Calibration - Generalization of these physical and experimental results

2.3.1. Correlation Between the Decaver Signal and the Experimental Results with Sediment and Cavitation Successively - To summarize:

° With sediment we have made, conjointly, a physical study and an experimental analysis (Decaver signal) to obtain a first relation:

$$C^{0.8}(D-0.04)V^3 = k [j + k j^{1.5}] \quad (11)$$

° With cavitation, we have made conjointly, weighings and experimental analysis with the Decaver signal to obtain a second relation:

$$\text{mass} = k (j^{1.5}).$$

When we look at these relations, a similarity becomes evident. As regards the electric current density, we see that these relations have two classes of terms: j and $j^{1.5}$. By comparing of these two relations we can present a general view giving the erosion by sediment and by cavitation:

° With sediment: $C^{0.8}(D-0.04)V^3 = k [j + k j^{1.5}]$

° With cavitation: $f(P, \Delta P, T) = f(j)$ and erosion rate: $m = k j^{1.5}$

2.3.2. Correlation Between the Decaver Signal and the Physical Analysis - These results have led us to clarify the erosion mechanism.

The term kj characterizes the corrosion and also, the wear abrasion of only the passive layer. The term $kj^{1.5}$ characterizes the removed material by shock (cavitation, sand jet) or by abrasion when a metal ribbon is torn off. A mechanical analysis shows that the shock energy due to the kinetic energy induces dislocations inside the material. With these results, it is possible to deduce from the Decaver signal the number of particles and their sizes.

The term $k [(j+k (j^{1.5}))]$ characterizes the total erosion that is to say the sum of each erosion type (by corrosion, by abrasion, by shock, by cavitation), including the synergistic effects.

Finally we can compare all successive results to establish a synthesis of all relations to have a generalization of all erosion types;

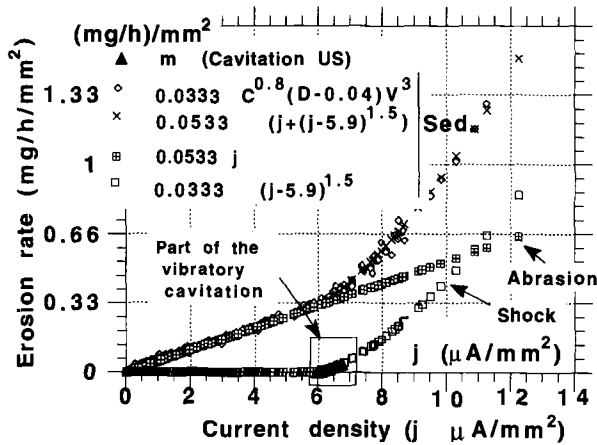


FIG. 5 - Decaver Calibration Generalization.

The upper curve represents both the shock energy density ($C^{0.8}(D-0.04)V^3$ for sediment,) and an electric relation $(j+(j-5.9)^{1.5})$ as a function of the Decaver signal. This curve corresponds to the sum of the erosion by abrasion and by shock. It resumes the physical analysis results for all types of metal removal. If we look below at the window there is the cavitation erosion curve that permits to calibrate the vertical axis.

2.3.3. Generalization of These Results - Calibration of the Decaver. When we analyse successively each erosion type (n types), we take into consideration three aspects for each one.

- a - the removed mass rate: -----> a = removed mass rate (mg/h)
- b - the physical basis of the erosion: ---->b = f (fundamental parameters)
- c - the electric measurement value: ----> c = f (j $\mu A/mm^2$)

A complete research work should give three relations for each erosion type :

$$a^1 = b^1 = c^1 \quad a^2 = b^2 = b^3 \quad \dots \quad a^n = b^n = c^n$$

We have considered four types of erosion: corrosion, abrasion, cavitation, shock. These studies are in progress but we are able to propose a generalization of the erosion measurement by a general simplified relation:

$$a = b = c$$

Mass loss rate (mg/h) = mechanical relation = electric measurement relation

Whatever the erosion type, the removed metal mass is a function both of a specific mechanical phenomena with its parameters and of the measurement given by the device. For each erosion type, mechanical parameters are specific but the electric relation is the same.

- In Figure 5 we see the corresponding calibration curve:
- the linear part corresponds to an erosion where only the passive layer is removed.
 - the "parabolic part" characterizes an erosion where removed particles are not wholly oxidized.

Figure 5 shows that the "parabolic" part is the sum of two curves, a straight line kj and the f curve $j^{1.5}$:

$$\text{Removed mass rate} = f(\text{electric signal}) = \frac{f(\text{kinetic energy})}{I}$$

$$\text{Erosion rate (mg/h)} = k[j + (j-5.9)^{1.5}] = k[C^{0.8} (D-0.04) V^3] = f(P, \Delta P, T) \quad (12)$$

In a word, we can say that this relation characterizes the sum of many wear types:

- with j , we have the corrosion or a small abrasion

- with $(j-5.9)^{1.5}$, we have the shock erosion or a big abrasion. The term $(j-5.9)$ shows that this *erosion* type occurs with a certain value of the current density corresponding to one threshold value of the shock pressure.

In order to control the results concerning the erosion rate, we have weighed the probes in various erosion cases such as erosion by a grindstone. The removed mass rate matches the value provided by the previous relation. We can deduce that this defines each type of erosion corresponding to a corrosion, to a shock erosion or to both.

3. Application of the *Erosion* Results to the Wear Domain

3.1. Difficulties Encountered in Transferring the *Erosion* Results to the Domain of Wear

The study of wear is much more complicated than that of *erosion*. However, it can be said that in any case, wear includes an *erosion*. For us *erosion* can be considered as one basic element in the study of the wear to which we have to add various phenomena. Our aim is to show that the Decaver can help to analyze the wear process. We do not have a great deal of experience in this domain. We have just made some rapid tests to see the response of the device in the case of the fretting erosion. We have obtained some curves giving relations between several parameters. Much remains to be done to interpret this information correctly.

First difficulty due to the wear complexity - To present the possible role of the device in the study of the wear, let us examine the case of fretting erosion in water. Many remarks are to be made as regards the reduced volume between the two pieces, the applied forces and the various materials together. As a consequence, we can observe an *erosion*, a material shifting or the existence of a third body that works as a gouge and finally the formation of an evolving mixture.

When there is a removed material, we say that we have an *erosion*. More generally, the device detects this *erosion* whatever its type. It responds to different phenomena each time that there is an oxidation (corrosion) such as when the material is torn off or shifted with its oxide because the new passive surface is regenerated.

Second Difficulty Due to the Device - The problem is the necessity to work in an aqueous medium and with only one metal in contact with insulating material. According to the fundamental principle of the device, we measure a corrosion current.

Consequently, this forms a loop through the sensor material, then the ionised liquid and finally the passivated layer. As a consequence, liquid with ions is necessary. For example the use of oil or air is not satisfactory.

In some cases, we think that it is convenient to work first in a liquid in order to prepare a general study with a better understanding of certain parameters. However, according to the great pressure on the contact points, the mechanical role of the water being reduced, we think that this technique can be used. Also the oxidation becomes difficult. When all metal is not oxidized at once, it will be oxidized later. Another difficulty can be the working on an industrial site. The sensor can have any form, even to be the whole piece if this is insulated from the electric mass.

In order to classify the abrasion resistance of reading glasses, we have tested this material successively in water and in air. The same classification was satisfactory for 80% of the cases. Only this test can give an idea of the resistance value but a great advantage is the rapid and quantified measurement.

We see that there are many remarks to be made and questions to be answered. The best solution is to test this method and to analyze the possibilities of the device.

3.2. First Experimental Results

Description of the Experimental Wear Facility to Test the Device - To show the possibilities of our measuring device in the domain of wear we have carried out some fretting tests on an apparatus built at the Institut National de Sciences Appliquées of Lyon (INSA). This device comprises a fixed sample of stainless steel and a mobil piece of PMMA (Polymethylmethacrylate). The effects of some parameters have been investigated: applied normal force in the range (30-100N) for a surface about 7.5 mm², constant shifting speed and variable frequency (0.5-5 Hz). The sample constitutes the probe of the Decaver. Consequently, every time there is an oxidation of the stainless steel we detect it. For example we can see, with a high sensitivity, the following cases:

- a particle is pulled out of the sample
- an abrasive debris scratches its surface
- the great pressure of the PMMA piece shifts the material with its oxide. This is reconstituted.

Working Technique - Our working technique consists in collecting a lot of information in order to define the fundamental parameters by a stochastic analysis of the experimental results. The great advantage of the device is to give these results rapidly. This technique has been used in cases of sediment and cavitation. The aim of subsequent research work is to make use both of our device and a visualisation facility so as to observe at the same time the *erosion rate*, the various materials and the friction coefficient.

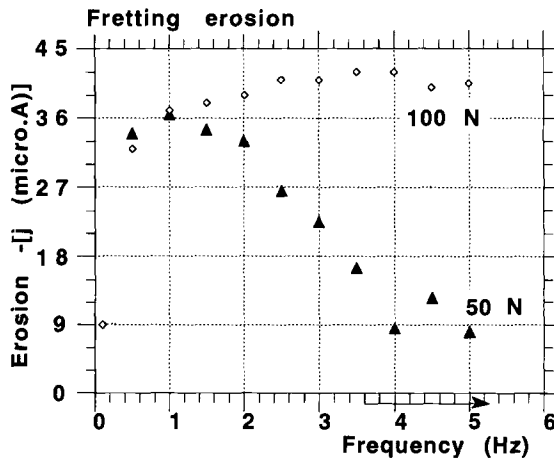


FIG. 6 - Test of fretting erosion with a constant charge
 These curves concern two tests, successively with 50 N and 100 N.
 Variations seems rational

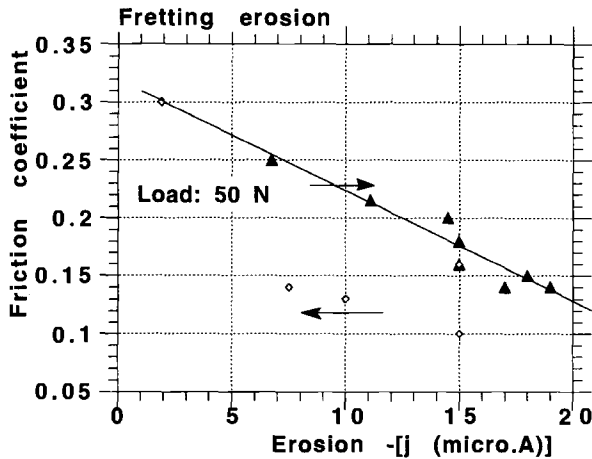


FIG. 7 - Relation between friction coefficient and erosion rate .
 Tests have been made with a constant charge and an increasing frequency. This curve seems to us interesting because it presents a linear relation between the friction coefficient and the erosion. The existence of this relation shows that it can be useful to develop this type of research.

Experimental Results - Figures 6, 7 shows experimental results obtained at the INSA with the laboratory apparatus. The first result concerns variations of the device signal in relation to the frequency both there and back (the force is successively 50 and 100 Newton at the starting point). Figure 7 represents the variations of the friction coefficient in relation to the signal (50 N constant strength and variable frequency).

When, with a titanium probe, we have an electric signal we say that there is a corrosion current coming from a corrosion zone. What can this zone be? If we consider that these results recur we could try to use them to solve some wear problems.

3.3. Some Ideas on Wear Analysis by Using Erosion Measurements - Applications

Attempt to Interpret a Test Result - When the signal increases, it corresponds to an increasing eroded zone. If the signal is zero, there is no more erosion (or corrosion). A peak of the signal can correspond to a short erosion for example to one torn off particle. A short time signal could be a debris scratching the metallic surface. So wear analysis should be possible by way of curves working as a scanner to recognize different types of erosion as well as the role of layer debris. Our objective is both diagnosing and solving practical problems.

Also we want compare the working signal and the camera views through the PMMA. So, we think that it is possible to extrapolate the erosion results obtained in the water to those obtained in the air.

At the moment, no serious conclusions can be deduced. Before studying the role of parameters, it is necessary first to see in what conditions the results recur. At the moment, an interesting fact that we have observed is a relation between the Decaver signal that characterizes an erosion and the friction coefficient.

Various Domains for Using the Wear Testing Device - Choice of the right material to resist *erosion* or which is well adapted to one type of wear.

- Development of a new material or of a new surface treatment.
- Study of the sediment or the powder that can work by abrasion or by shock. The device detects the intensity of these operations. It permits to choose the right abrasive product in accordance with the type of work needed (cleaning or machining). Moreover we can detect the cleaning efficiency as also the powder wear itself.
- At the present time our objective is to study the wear of bio-implants.
- Possibility to make easy repairs thanks to a good and rapid control.

Research - The great interest of the Decaver is to help to prepare the way for new research with a better understanding of wear. Here are some possible topics for research:

- Sliding friction study.
- Analysis of the coefficient of friction with regard to *erosion* on a PMMA-stainless steel device for example.
- Wear measuring of a cutting tool. As the *erosion* can be made by abrasion and by shock it is possible to adapt both the material and the technique.

The main advantage of this new device is to be a good tool which allows the user to "see" with accuracy the *erosion* in a wear zone. Although this requires an understanding of the specific conditions for use, it is not a sophisticated surface measuring instrument.

Conclusion

We have explained an attempt to apply a new measurement technique to the domain of the wear. A new device gives the instantaneous value of the *erosion* rate (material removal rate) whatever it may be. We have demonstrated that each encountered *erosion* can be classified into one of the following types: (1) corrosion type, only the passive layer is reconstructed (corrosion, small abrasion), (2) shock type: only a part of the removed material is oxidized (big abrasion, shock, cavitation).

We have made some initial tests on a fretting facility with one stainless steel surface. The device seems convenient to study both the series of the fretting physical phenomena and the influence of the physical parameters such as the applied force, the frequency, the friction coefficient and the time.

The *erosion* generated by the wear is well described by the Decaver signal. The main interest of the device is to show wear in a new light. It permits, as a scanner, to visualize the *erosion* between two surfaces. Although some relations have been obtained between the device signal and the wear parameters, the principal part remains to be done.

References

- [1] - Chincholle, L., "Procédé de détection et de mesure de la cavitation érosive, Decaver", Patent ANVAR, 7809255, 1978.
- [2] - Chincholle, L., "Répartition du courant à la surface d'une électrode dans un milieu aqueux, lorsque cette surface est partiellement abrasée", *CRAS, Electrochimie*, T.296, 1983.
- [3] - Chincholle, L., "How a single relation can define the erosion rate versus the decaver signal, whatever the erosion type in a liquid", *International Conference on Fluid Engineering*, 1997, Tokyo, Japan.
- [4] - Chincholle, L., "Etude de l'érosion instantanée de cavitation en fonction du débit, de la pression et de la température", *Journal of Hydraulic Research*. Vol. 26 1988, (1), pp.67 - 82.
- [5] - Chincholle, L., "New views of cavitation erosion by using an instantaneous erosion measurement device", *1st ASME JSME Fluids Engineering Conference*, 1991, Portland, Oregon.

ISBN 0-8031-2603-4